School of Engineering and Science

Experimental Study of a Compartmented Fluidized Bed Gasifier for Fuel Gas Production from Oil Palm Shell Biomass

Chok Vui Soon

This thesis is presented for the Degree of
Doctor of Philosophy
of
Curtin University

November 2011

Declaration

To the best of my knowledge and belief this thesis contains no material previously published by any other person except where due acknowledgement has been made.

This thesis contains no material which has been accepted for the award of any other degree or diploma in any university.

Signature : _____

Date : _____

ABSTRACT

Both experimental study of pilot plant scale cold flow model and pilot plant performance testing were carried out in this research with particular reference to palm shell as a biomass feedstock. The reactor was based on the concept of compartmented fluidized bed gasifier (CFBG). Sand was used as second fluidizing material.

From the cold flow model, the single component (sand) system characteristic fluidization velocities for the gasifier are larger than those observed in the combustor. These differences can be minimized by utilizing larger sand size. The existing correlations are modified for the sand. For the binary mixture, the characteristic fluidization velocities showed the tendency to increase with the increase in the palm shell size and weight percent. The concept of critical loading is introduced to characterize the palm shell content in the binary mixture where the characteristic fluidization velocities for the binary mixture are determined principally by the sand. The critical loading increases with the sand size, but decreases with the increase of palm shell size. The correlations developed for the sand can be used for the binary mixture within the critical loading.

Despite of the local variation on the palm shell vertical and lateral distribution, the overall good mixing quality can be established in both the compartments. The overall mixing quality is enhanced with the decrease in the palm shell size and the increase in the palm shell weight percent. Bigger bed diameter also improves the overall mixing quality while bed height did not contribute significantly.

Solid circulation rate (SCR) increases with the increase in the bed height while the main bed aeration does not affect the SCR. Based on statistical approach, the V-valve and riser aerations are simultaneously adjusted to determine the optimum SCR. Optimum SCR value increases with the increase in the sand size.

The pilot plant designed by using the findings from the cold flow model has demonstrated CFBG as a prospective technology for palm shell gasification for the production of medium calorific value fuel gas. The conceptual model of the palm shell gasification process was proposed.

ACKNOWLEDGEMENTS

I would like to give my sincere acknowledgements to my supervisor, Professor Dr Alexander Gorin, who gave his expertise, understanding, and patience to my study. During the period of my PhD candidature, he has not only made many valuable comments at each step of my studies but also directed the overall blueprint of the research. More importantly, the knowledge and philosophy I learned from him are precious treasures throughout my life.

My special thanks goes to all members in our research group for their support and advice throughout my candidature. In particular, I would like to thank Dr. Yan Hong Ming, Dr. Chua Han Bing and Dr. Chandrasekar Srinivasakannan and all the research students for their help and valuable feedback on my studies.

I would like to thank the Ministry of Science, Technology and Innovation (MOSTI) and Malaysia Palm Oil Board (MPOB) for the project funding.

The basic but essential helps and supports from all the staffs in Curtin University, Sarawak Campus is gratefully acknowledged.

Lastly, I would like to dedicate this thesis to my parents and wife for all of their love, support and encouragement in all that I set out to achieve.

Thank you all.

Chok Vui Soon

LIST OF PUBLICATIONS

Journal papers

1. **Chok, V. S.**, Gorin, A. & Chua, H. B. (2010). Minimum and Complete Fluidization Velocity for Sand-Palm Shell Mixtures, Part I: Fluidization behaviour and Characteristic Velocities, *American Journal of Applied Sciences*, 7 (6), 763-772.

2. **Chok, V. S.**, Gorin, A. & Chua, H. B. (2010). Minimum and Complete Fluidization Velocity for Sand-Palm Shell Mixtures, Part II: Characteristic Velocities Profiles, Critical Loading and Binary Correlations, *American Journal of Applied Sciences*, 7 (6), 773-779.

3. Khan, Z., Yusup, S., **Chok, V. S.** & Uemura, Y. (2010). Review of Hydrogen Production Technologies in Malaysia, *International Journal of Engineering and Technology*, 10 (2), 111-118.

4. Wee, S. K., **Chok, V. S.**, Gorin, A., Chua, H. B. & Yan, H. M. (2009). The Effect of Effective Diameter on Fluidization Quality in Compartmented Fluidized Bed Gasifier, *Pertanika Journal of Science & Technology*, 17(2), 343-350.

5. Wee, S. K., **Chok, V. S.**, Srinivasakannan, C., Chua, H. B. & Yan, H. M. (2008). Fluidization Quality Study in Compartmented Fluidized Bed Gasifier, *Energy & Fuels*, 22 (1), 61-66.

Contribution in Book

1. Khan, Z., Yusup, S., Ahmad, M. M., Uemura, Y., **Chok, V. S.**, Rashid, Umer & Inayat, Abrar (2011). *Kinetic Study on Palm Oil Wastes Decomposition.* In: Biofuels. InTech Open Access Publishers, Croatia. ISBN 978-953-307-480-1 (In Press).

Conference Papers

1. **Chok, V. S.,** S. Yusup & M. Z., Gorin, A. (2009). Palm Shell Gasification in Pilot Scale Compartmented Fluidized Bed Gasifier: Preliminary High Temperature Performance and Challenges, *PIPOC International Palm Oil Congress: Chemistry, Processing Technology & Bio Energy Conference*, Kuala Lumpur, Malaysia.

2. **Chok, V. S.**, Wee, S. K., M. Z., Gorin, A. & Chua, H. B. (2009). Effect of Particle and Bed Diameter on Characteristic Velocities in Compartmented Fluidized Bed Gasifier, *2nd CUTSE International Conference: Progress in Science & Engineering for Sustainable Development*, Miri, Malaysia.

3. **Chok, V. S.,** Wee, S. K., Mohd Ariffin, M. Z., Gorin, A., Chua, H. B. & Yan, H. M. (2008). Optimization of Solid Circulation Rate in Compartmented Fluidized Bed Gasifier for Power Generation, *International Conference on Power Control and Optimization: Innovation in Power Control for Optimal Industry. AIP Conference Proceedings*, 1052, 301-304, Chiang Mai, Thailand.

4. Gorin, A., **Chok, V. S.**, Wee, S. K., Chua, H. B. & Yan, H. M. (2008). Hydrodynamics of binary mixture fluidization in a compartmented fluidized bed, *18th International Congress of Chemical and Process Engineering: CHISA 2008*, Prague, Czech Republic.

5. Wee, S. K., **Chok, V. S.**, Srinivasakannan, C., Chua, H. B. & Yan, H. M. (2007). Cold Flow Model Hydrodynamics Study of Compartmented Fluidized Bed Gasifier (CFBG), *Heat Transfer in Components and Systems for Sustainable Energy Technologies: Heat-SET 2007,* Chambery, France.

6. **Chok, V. S.**, Wee, S. K., Srinivasakannan, C., Chua, H. B. & Yan, H. M. (2007). *Fluidized Bed Biomass Gasification Technology: Review, Proceeding in BIOENERGY Outlook 2007*, Singapore.

7. **Chok, V. S.**, Chin, L. F. B., Wee, S. K., Tang, W. W. & Gorin, A. (2007). Hydrodynamics studies of sand/palm shells binary mixtures in Compartmented Fluidized Bed Gasifier (CFBG). *Proceeding of the 1st Engineering Conference on Energy and Environment, UNIMAS,* Kuching, Malaysia, 301-306.

8. **Chok, V. S.**, Wee, S. K., Srinivasakannan, C., Chua, H. B. & Yan, H. M. (2005), A novel compartment fluidized bed gasifier for synthesis gas production and power generation from palm waste, *2nd International Conference on Chemical and Bioprocess Engineering in conjunction with 19th Symposium Malaysian Chemical Engineers: ICCBPE 2005,* Kota Kinabalu, Malaysia.

TABLE OF CONTENTS

NOMENCLATURES

Ar	Archimedes number	-
Ar_M	Archimedes number for mixture as defined by Mourad et al. (1994)	-
A_b	Bed cross sectional area	(m^2)
C_1, C_2	Constants in Wen & Yu (1966) and Noda et al. (1986) correlations	-
C1, C2, C3	Imaginary columns in the combustor and gasifier	-
d_p	Mean particle size	(μm)
d_{pi}	Mean sieve size	(μm)
d_F , d_P	Fluid and packed particle diameter as defined by Goosens et al. (1971)	(m)
d_m	Effective mixture diameter as defined by Goosens et al. (1971)	(m)
d_M	Effective mixture diameter as defined by Rao and Ram Bheemarasetti (2001)	(m)
D_e	Effective column diameter	(m)
f	Sum of square over mean square error	-
F	Standard reference value in the F distribution	-
g	Gravitational acceleration	(m/s^2)
H_b	Static bed height	(m)
k	Constant as defined by Rao and Ram Bheemarasetti (2001)	-
k_1, k_2, k_3	Constants for the determination of solid circulation rate	-
K	Constant as defined in Equation (5-1)	-
m_s	Solid mass	-
m	Local mixing quality	-
M	Overall mixing quality	-
M	Mixing index as defined by Nienow et al. (1978)	-
n	Sampling locations	-
ΔP_b	Bed pressure drop	(cmWg)
Q	Fluidization quality	-

Q_b, Q_v, Q_r	Dimensionless aerations to bed, V-valve and riser	(U/U_{mf})
R1, R2, R3	Imaginary rows in the combustor and gasifier	-
Re_{mf} , Re_{cf}	Reynolds number at minimum and complete fluidization velocity respectively	-
Re_C	Reynolds number at complete fluidization velocity as defined by Mourad et al. (1994)	-
t	Time	(s)
U	Operating superficial velocity	(m/s)
U_{mf}	Minimum fluidization velocity	(m/s)
U_{cf}	Complete fluidization velocity	(m/s)
V_b	Bed volume	(m^3)
w_F , w_P	Weight fraction of fluid and packed particle	(wt%)
x, X	Local and average weight fraction	(wt%)
x_j, X_j	Local and average jetsam weight fraction	(wt%)
x_i	Weight fraction of each sieve interval	(wt%)

Greek Symbols

ϕ_s	Solid Sphericity	-
ε, ε_{mf}	Porosity at fixed bed and at the minimum fluidized bed	-
ε_b	Porosity at bubbling fluidized bed	-
μ	Viscosity	(kg/ms)
ρ_f , ρ_p	Fluid and particle density as defined by Goosens et al. (1971)	(kg/m^3)
ρ_F , ρ_P	Fluid and packed particle density	(kg/m^3)
ρ_b , ρ_s	Bulk and solid particle density	(kg/m^3)
ρ_m	Effective mixture density as defined by Goosens et al. (1971)	(kg/m^3)
ρ_M	Effective mixture density as defined by Rao and Ram Bheemarasetti (2001)	(kg/m^3)

Abbreviation

ANOVA	Analysis of variance
BFB	Bubbling fluidized bed
BIGCC	Biomass integrated gasification and combined cycle
CAL	Calculated
CFBG	Compartmented Fluidized Bed Gasifier
DFB	Dual/twin fluidized bed
DPT	Differential pressure transmitter
EXP	Experimental
FT	Flow transmitters
GHG	Green house gases
HHV_d	Higher heating value for dry fuel gas
HHV_w	Higher heating value for wet fuel gas
ID	Internal column diameter
P & ID	Piping and instrumentation diagram
SCR	Solid circulation rate
TT	Temperature transmitter

LIST OF FIGURES

LIST OF TABLES

CHAPTER 1

INTRODUCTION

The use of biomass as a potential source of alternative energy to cope up with the depleting resources of fossil fuel and to reduce the emission of greenhouse gases (GHG) is in serious consideration globally. Due to the abundance supply and wide spread availability of biomass, bioenergy has received great interest from academics and industries, and every country is working on a mission to increase the energy contribution from biomass. However, the viability of an energy-supply strategy based on biomass depends on a number of factors related to technological development, economic incentives and effective policies to facilitate public and private initiatives, among others.

Fluidized bed biomass gasification offers one of the most promising conversion technologies that can strategically enable the biomass feedstock to supplement the diverse energy needs; specifically, biomass gasification enables the production and co-production of hydrogen, electricity, fuels and chemicals. Moreover, fluidized bed gasifier is well-known for its ability to handle a wide range of biomass fuels with minimal pre-processing, making it a preferred technology for many biomass applications because of the diversity of the biomass feedstock.

Biomass is generally heterogeneous in nature with significant variation in morphology and physical characteristic. Due to its peculiar properties, most biomass including the present feedstock (palm shell) cannot be fluidized on its own, thus utilization of a second fluidizable material is necessary to facilitate fluidization. Accordingly, the basic operating parameters for the fluidized bed, namely minimum and complete fluidization velocities are to be determined for the binary mixtures. Besides that, fluidization of two dissimilar materials can lead to poor mixing unless the fluidized bed is operated at a sufficiently larger superficial velocity than the characteristic fluidization velocities.

Conventional biomass gasifier combines both the combustion and gasification zones in a single reactor. Although it offers a simple and economical design, it can only generate a low calorific value fuel gas when air or air-steam mixtures are used as the gasifying agents.

It is widely acknowledged that biomass gasification with steam can generate hydrogen rich, nitrogen free and medium calorific value fuel gas, but it is highly endothermic. To meet its energy demand, a possible technological solution is to couple the endothermic steam gasifier with a separate combustor that burns biomass and/or residual chars with air and interconnect the two reactors using solid transfer lines for mass and heat exchange. However, the use of interconnecting transfer lines complicates the design and operation of biomass gasification which often leads to solid breakage and energy lost.

A single compartmented vessel could potentially exhibit both the benefits of the conventional and dual reactors gasification system. It is compact, low cost and does not require a separate transfer lines when used as an interconnected dual fluidized bed. This concept, hereafter referred to as Compartmented Fluidized Bed Gasifier (CFBG) offers a prospective technology for biomass gasification with steam. But until now, limited laboratory studies were performed and coal was the only feedstock.

1.1 SCOPE OF THE STUDY

The scope of this study is to investigate the fluidization behavior, hydrodynamic and solid circulation rate in a pilot plant scale cold flow model with particular reference to palm shell as a biomass feedstock. This constitutes as a part of this work.

By using the research findings, the subsequent work is to design and operate CFBG pilot plant for palm shell gasification and to realize compartmented reactor system for biomass gasification for the production of medium calorific value fuel gas suitable for syngas and power generation.

1.2 THESIS OUTLINE

The thesis can be considered as consisting of two parts: the first part of the thesis is focused on experimental study on sand and palm shell fluidization performed in the cold flow model of a pilot plant scale while in the second part, palm shell gasification is performed in the CFBG pilot plant. The structure of the thesis is organized into seven chapters.

Chapter 1 gives the introduction to the problem statement, objectives of the research and the scope of the study.

Chapter 2 provides the background knowledge on gas-solid fluidization and mixing behavior for a single and multi-component system, particularly sand-biomass binary mixtures. It presents the fundamental principle for the determination of minimum fluidization velocity (U_{mf}) developed from a single component system of uniform size and its subsequent adaption to a multi-component/binary system of different particle size and/or density. This also includes the identification of complete fluidization velocity (U_{cf}), a characteristic fluidization velocity observed in the latter system. Then, it continues to discuss on the importance and quantification of local (m) and overall mixing quality (M) when fluidizing dissimilar components.

This chapter reviews as well the various working principles of fluidized bed biomass gasification technologies and shows the advantages of compartmented fluidized bed gasifier (CFBG). It describes the features of CFBG with two compartments, namely the combustor and the gasifier with their ability to internally circulate solid between compartments. The methodologies of measuring the solid circulation rate (SCR) are also discussed in this chapter.

The literature review concludes by summarizing these findings, identifies the research perspective and presents the specific objectives for the present work.

Chapter 3 investigates the fluidization behavior of sand-palm shell mixtures and determines the U_{mf} and U_{cf} for different mixtures of sand and palm shell size and weight percent in the respective compartments of CFBG. It also introduces the concept of critical loading as a parameter to characterize the state when the

characteristic fluidization velocities of the binary mixture remain nearly unchanged from its pure sand values. In addition, this chapter gives the comparison of the experimental U_{mf} and U_{cf} values with various published correlations.

Chapter 4 studies the local mixing behavior of sand-palm shell mixtures and determines the operative superficial velocity that promotes good local mixing quality in the different bed sections. It also elucidates the dependency of the overall mixing quality (M) on the bed material properties and geometrical parameters.

Chapter 5 presents the investigation of the solid circulation rate (SCR) between the combustor and gasifier under different operating conditions and the determination of the optimum SCR value from the statistical analysis.

Chapter 6 gives the description of the CFBG pilot plant designed and operated based on the findings from the previous chapters. The specification of the main equipment, instrumentation and gas analyzers, the process flow, piping and instrumentation diagrams are included. This chapter serves to prove the concept of CFBG as a prospective technology for palm shell gasification to produce medium calorific value fuel gas suitable for syngas and power generation.

Chapter 7 gives the summary and conclusions of this work as well as the recommendations for future work.

CHAPTER 2

LITERATURE REVIEW

Fluidization is a phenomenon where a bed of solid particles is transformed into a liquid-like behavior through suspension in gas or liquid (Kunni & Levenspiel, 1991). This unique behaviour has attracted various industrial applications of fluidized bed e.g. in biomass gasification and has also spurred research interests in fluidization engineering. Many theories and concepts have been proposed to explain what affects hydrodynamics of a fluidized bed. Although the literature covers a variety of such theories and findings, this review will focus on three major areas namely the characteristic fluidization velocities and mixing/segregation in binary system as well as the working principles of fluidized bed biomass gasification technologies.

The introduction will start from kinematics of gas-solid fluidization due to the common interest and general application in any fluidized bed technology.

The first section of the literature review begins with a discussion of the main parameters in gas-solid fluidization process developed and accepted for single component system and adapted for the binary system. The second section gives a critical review on the binary mixing/segregation phenomenon including a guideline that can be used to identify the tendencies of sinking and floating of a component in a binary system. Literature on sand-biomass mixtures are discussed in both sections due to their special relevancy to the present research. The next section provides an overview on the working principle of the conventional and novel fluidized bed biomass gasification technologies, in which the preferred option, namely Compartmented Fluidized Bed Gasifier (CFBG) is described. The literature review continues by highlighting the significant findings, the lessons learnt and the key operating parameters during its pioneering stage. It also includes the discussion on

the solid circulation rate (SCR), one of the leading parameters for a steady gasification to be realized in CFBG.

The review summarizes the literature in each section to establish the research perspectives for the development of sand-palm shell mixtures in a pilot plant scale fluidized bed. This will facilitate the use of the biomass as gasification feedstock in CFBG pilot plant for the production of medium calorific value fuel gas suitable for syngas production and power generation.

2.1 FLUIDIZATION

Several key parameters affecting hydrodynamics of a fluidized bed are discussed in the following section, namely minimum and/or complete fluidization velocity (U_{mf} and U_{cf}) in a single and binary component system, fluidization quality (Q), and mixing quality (M). Various U_{mf} and U_{cf} correlations are reviewed particularly those developed from the sand-biomass mixtures. Meanwhile, different fluidized bed biomass gasification technologies are also presented. As shown later, a single partitioned reactor with the ability to circulate solid between compartments, known as Compartmented Fluidized Bed Gasifier (CFBG) exhibit both the features found in the complex dual fluidized beds system and the conventional gasifier. Correspondingly, one of the critical operating parameters for a steady gasification in CFBG, i.e. solid circulation rate (SCR) is discussed.

2.2 CHARACTERISTIC FLUIDIZATION VELOCITY

2.2.1 SINGLE COMPONENT SYSTEM

Minimum fluidization velocity, U_{mf} is one of the most basic parameters to design and operate any fluidized bed system. It is known that the fundamental understanding of U_{mf} developed from the single component system provides the basis for the extension to the multicomponent system (Formisani et al., 2001).

U_{mf} occurs at the transition point between the fixed and fluidized states. Hence, at the transition point, it is possible to derive an equation for U_{mf}, by equating the

expression for pressure drop across the packed bed with the expression for pressure drop in a fluidized bed.

Ergun (as cited in Kunni & Levenspiel, 1991) proposed a generalized equation for pressure drop across the packed bed as

$$\frac{\Delta P_b}{H_b} = 150\frac{(1-\varepsilon)^2}{\varepsilon^3}\frac{\mu U}{(\phi_s d_p)^2} + 1.75\frac{(1-\varepsilon)}{\varepsilon^3}\frac{\rho_f U^2}{\phi_s d_p} \tag{2-1}$$

that combines both the viscous and kinetic effect to cover any flow condition. It is developed based on a single size of isotropic solids.

Under fully laminar condition where the first term (viscous effect) dominates, Equation (2-1) can be reduced to Carman-Kozeny equation (Carman & Kozeny, 1937 as cited in Rhodes, 2008),

$$\frac{\Delta P_b}{H_b} = 180\frac{(1-\varepsilon)^2}{\varepsilon^3}\frac{\mu U}{(\phi_s d_p)^2} \tag{2-2}$$

but with the constant of 180 instead of 150.

At the point of fluidization (i.e. achieving U_{mf}), the bed pressure drop can be represented as

$$\frac{\Delta P_b}{H_b} = (1-\varepsilon)(\rho_p - \rho_f)g \tag{2-3}$$

From Equations (2-1) and (2-3), it follows that

$$Ar = \frac{150(1-\varepsilon_{mf})}{\phi_s^2 \varepsilon_{mf}^3}\mathrm{Re}_{mf} + \frac{1.75}{\phi_s \varepsilon_{mf}^3}\mathrm{Re}_{mf}^2 \tag{2-4}$$

where ε_{mf}, $Ar = \frac{d_p^3 \rho_f (\rho_p - \rho_f) g}{\mu^2}$ and $\mathrm{Re}_{mf} = \frac{d_p \rho_f U_{mf}}{\mu}$ are voidage, Archimedes and Reynolds number respectively with U_{mf} as the characteristic velocity.

If all fluid and particle properties needed are available, Equation (2-4) can then be solved to find Re_{mf} and subsequently U_{mf} value.

Although classical equations such as Ergun (1952) or Carman-Kozeny (1937) are comprehensive and versatile, both the sphericity (ϕ_s) and voidage (ε_{mf}) used in the correlations are only concepts, which may only be imperfectly determined in a given real system. In practice, both parameters are not mutually independent (S.Y. Wu, (1991)).

Alternatively, Wen and Yu (1966) found that the sphericity-voidage functions in Equation (2-4), namely $\frac{1-\varepsilon_{mf}}{\phi_s^2 \varepsilon_{mf}^3}$ and $\frac{1}{\phi_s \varepsilon_{mf}^3}$ can be approximated as 11 and 14 respectively for a wide range of flow condition, fluid properties, particles sizes and densities. Their correlation is applicable for $0.001 < \mathrm{Re}_{mf} < 4{,}000$. Using this approximation, Equation (2-4) is reduced to

$$\mathrm{Re}_{mf} = \left(C_1^2 + C_2 \cdot Ar\right)^{0.5} - C_1 \qquad (2\text{-}5)$$

where C_1 and C_2 is 33.7 and 0.0408 respectively.

Equation (2-5) is commonly referred to as the Wen and Yu correlation. It became the generic form for many other U_{mf} correlations differing only in terms of the constant C_1 and C_2 (Adanez & Abanades, 1991; Delebarre, 2004).

It is worthy to mention that the voidage is almost independent of fluidization velocity, bed height and even temperature (Saxena & Rao, 1993).

Gauthier et al. (1999) tested the Wen and Yu correlation and other similar ones namely the correlations from Bourgeois and Grenier (1968)

$$\mathrm{Re}_{mf} = \left(25.46^2 + 0.0382 \cdot Ar\right)^{0.5} - 25.46 \qquad (2\text{-}6)$$

and Lucas et al. (1986)

$$\mathrm{Re}_{mf} = \left(29.5^2 + 0.0357 \cdot Ar\right)^{0.5} - 29.5 \qquad (2\text{-}7)$$

Gauthier et al. (1999) found that these correlations gave the closest U_{mf} prediction for wide size distribution sand. They observed that the transition from fixed bed to fluidized state is not defined by one single point. At U_{mf}, the bed is only partially fluidized; it achieves full fluidization at complete fluidization velocity, U_{cf}. They proposed U_{cf} correlation

$$\mathrm{Re}_{cf} = \left(5.2 \cdot 10^{-3} \cdot Ar\right)^{0.777} \tag{2-8}$$

where $\mathrm{Re}_{cf} = \dfrac{d_p \rho_f U_{cf}}{\mu}$ and is applicable for 1.35 < Re_{cf} < 113.

Meanwhile, bed geometry can be a strong factor affecting fluidization behaviour as shown by Werther (1968). The author found that hydrodynamics of fluidization depends strongly on the bed diameter, particularly for the bed diameter smaller than 20 cm typically used in laboratory scale experiments and fluidization research. Similar effect is also observed by many authors (Frantz, 1966; Glicksman & McAndrews, 1985; Hilal et al., 2001; Delebarre, 2002; Mabrouk et al., 2005; Liu et al., 2008). Besides that, three research works by Wee et al. (2008, 2009) and Gorin et al. (2008) showed that the effective bed diameter, D_e plays an important role in affecting the fluidization quality, Q among the other competing factors in a compartmented reactor.

2.2.2 MULTICOMPONENT/BINARY SYSTEM

It is important to first identify the similarities and differences between U_{mf} determination for a single component of uniform sized and multicomponent/binary system of different particle sizes and/or densities.

The commonly used method in determining U_{mf} is by measuring the bed pressure drop as a function of decreasing superficial gas velocity, U. At U_{mf}, the bed weight is fully supported by the gas flow where the bed pressure drop, ΔP_b becomes constant, or ideally, is equal to the bed weight per cross sectional area. From the plot of ΔP_b versus U, U_{mf} is determined from the intersection point of the extrapolated fixed bed line and that of the constant bed pressure drop line in fluidized region.

The method that is derived from the single component system of uniform size requires bed fluidization to begin only at a definitive U_{mf} value. At superficial velocities below U_{mf}, all the particles remain at fixed bed condition, but at superficial velocities equal or greater than U_{mf}, a stepwise transition occurs and the whole bed is at a fluidized state.

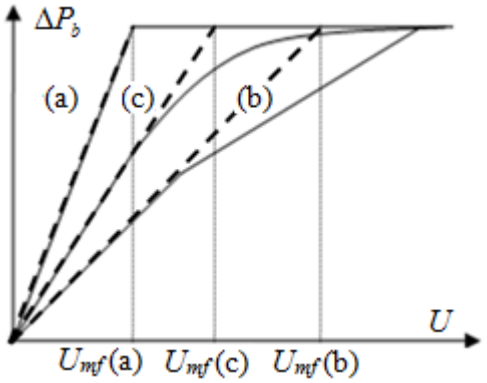

Figure 2-1: Bed pressure drop profiles adapted from Chiba et al. (1979).

S. Chiba et al. (1979) idealized three possibilities of ΔP_b versus U profiles using the binary system of near-spherical particles and their corresponding U_{mf} definitions in Figure 2-1.

For the binary system where both the components have only a small difference in particle size and of equal density, bed fluidization begins only when the superficial velocity is at U_{mf} (a). From the bed pressure drop profile (a), the minimum fluidization velocity is determined from the intersection point of the fixed bed line with the horizontal line representing a constant bed pressure drop in fluidized state. It also corresponds to the state where the bed is fully fluidized and has achieved constant ΔP_b, similar to that of the single component system.

However, when one component is significantly larger and denser than the other component in a binary system, partial fluidization may occur. The smaller size and lighter component attains fluidization first, but the larger size and denser component remains as a fixed bed and will only begin to fluidize at higher velocity. The bed pressure drop profile (c) consists of two fixed bed lines where the upper end point of

these lines is the respective component's minimum fluidization velocity. The apparent minimum fluidization velocity, U_{mf}(b) lies between these two end points.

In most cases where the differences in the particle properties are intermediate of the two binary systems presented above, a curvilinear bed pressure drop profile (c) is obtained. Bed fluidization occurs in a gradual manner and eventually achieves constant ΔP_b. The apparent minimum fluidization velocity, U_{mf} (c) is determined from the intersection point of the tangent line on the curvilinear bed pressure drop profile (c) with the horizontal line representing constant bed pressure drop in fluidized state.

The multicomponent system with wide particle size distribution and/or densities have been reported to exhibit similar bed pressure drop profile (c) (Delebarre et al., 1994; Gauthier et al., 1999; Lin, 2002).

It is often reported that the characteristic fluidization velocities are subjected to the procedures employed in determining them. They may vary depending on the initial state of fixed bed, whether it is carried out by increasing or decreasing the superficial velocity, or using a different rate in decreasing the superficial gas velocity (Delebarre et al., 1994).

The commonly used methods developed by Chiba et al. (1979) i.e. fast and slow defluidization procedures in determining the minimum fluidization velocity, U_{mf} and complete fluidization velocity, U_{cf} for binary system are preferred. Both methods are still based on the ΔP_b versus U profiles, differing only in terms of the rate of defluidization.

On U_{mf} determination using fast defluidization procedures, the mixture is initially fluidized vigorously to ensure constant ΔP_b is established, forming the fluidized bed line. Thereafter, the bed is defluidized rapidly, at bed pressure drop values below fluidized state. This is used to form the fixed bed line. U_{mf} is then determined from the intersection point between the fixed bed and fluidized bed lines. The underlying reason in fast defluidization procedure is to maximize the bed mixing when

determining U_{mf}. This is to establish "a wholly mixed bed" condition analogically to being a "monodisperse bed".

In the slow defluidization procedures to determine U_{cf}, the superficial gas velocity is gradually reduced from fully fluidized bed to fixed bed condition. U_{cf} is determined at the point where ΔP_b first deviated from the constant bed pressure drop line in fluidized region.

The fast and slow defluidization procedures have been adopted by many authors to determine the U_{mf} and U_{cf} values and develop the respective correlations (Rowe et al., 1976; Vaid & Gupta, 1978; Noda et al., 1986; Chyang et al., 1989; Mourad et al., 1994; Gauthier et al., 1999; Rao & Ram. Bheemarasetti, 2001).

Sand-Biomass Binary System

In general, biomass cannot be fluidized easily due to its peculiar shape, size and density. Fluidization test results from Abdullah et al. (2003) confirmed that biomass materials particularly from Geldart's A and D classification (Geldart, 1973) did not fluidize well. A second fluidizable material is often required to facilitate proper fluidization. The most commonly utilized fluidizing solid is sand, although other solid materials such as alumina oxide and dolomite were used.

Using two columns of 14 and 30 cm ID, Aznar et al. (1992a, 1992b) observed that the characteristic fluidization velocities (U_{mf} and U_{cf}) at first increased with the addition of biomass, but beyond a certain biomass loading, the mixture was no longer fluidizable. Similar behaviour was reported by Bilbao et al. (1987), although the maximum biomass loading (straw up to 15 wt%) in a smaller column of 8 cm ID was lower than that reported by Aznar et al. (1992a). These phenomenon actually distinguish the sand-biomass system from the other binary system where the mixtures remain fluidizable in any range of the component's fraction.

Meanwhile, when the biomass is below a certain amount in the mixture, depending on the biomass and sand properties, the U_{mf} and U_{cf} are determined principally by the sand size (Aznar et al., 1992b). Moreover, U_{cf}/U_{mf} ratio is found to decrease with the increase of the sand size.

Various authors have also found that U_{mf} and/or U_{cf} increase with the addition of biomass in sand regardless of the biomass properties (Mourad et al., 1994; Rao & Ram. Bheemarasetti, 2001[a]; Sun et al. 2005[a]). The U_{mf} and/or U_{cf} also increase with the increase of the sand size in the binary mixtures. This is because the addition of biomass and/or the increase of the sand size lead to the increase in the effective particle properties for the biomass-sand system (Zhong et al., 2008).

According to Noda et al. (1986), the bed aspect ratio (height to diameter ratio) does not have any effect on the characteristic fluidization velocities when it is greater than 0.5. Aznar et al. (1992a) reported a higher bed aspect ratio of 1÷2. They also observed that the characteristic fluidization velocities are 10÷20% higher in the column of larger ID for the sand-biomass binary system.

To summarize, minimum fluidization velocity, U_{mf} is considered as the key property in describing the fluidization behavior of single and binary system. For the binary system, a bed that is fully fluidized occurs at the complete fluidization velocity, U_{cf}. Both U_{mf} and U_{cf} are affected by the particle and fluid properties, as well as by the bed geometry. These characteristic fluidization velocities can be determined experimentally using the fast and slow defluidization procedures.

Characteristic Fluidization Velocity Correlations for Binary System

The existence of U_{mf} and U_{cf} in the binary mixtures has led to the development of their respective correlations. Generally, these correlations are based on two distinct features, either requiring the determination of component's U_{mf} or using effective mixture properties (density and size) as parameters. The latter is more likely applicable to biomass as they cannot be solely fluidized. Besides that, from the standpoint of engineering design, it is desirable that the mixture characteristic fluidization velocities should be estimated from their physical properties instead of measuring the component's characteristic fluidization velocities (Chyang et al., 1989).

The U_{mf} and U_{cf} correlations discussed below will be tested for the present binary system. These correlations are selected based on their similarity in terms of the

[a] The U_{mf} is determined using slow defluidization.

methodologies employed for determining U_{mf} and U_{cf}, particle properties or component from a variety of biomass material, and the size of their fluidized bed columns. Some of these correlations are listed by Li et al. (2005) but without discussion.

Minimum Fluidization Velocity Correlations

Goosens et al. (1971) modified Equation (2-5), the Wen and Yu correlation (1966) to predict U_{mf} for binary system by defining the effective mixture density, ρ_m and diameter, d_m as

$$\frac{1}{\rho_m} = \frac{w_F}{\rho_F} + \frac{w_P}{\rho_P} \tag{2-9}$$

$$\frac{1}{d_m} = \rho_m \left(\frac{w_F}{\rho_F d_F} + \frac{w_p}{\rho_P d_P} \right) \tag{2-10}$$

based on weighted average mixtures properties where subscript "*F*" and "*P*" represent the fluid and packed particle respectively. The two parameters, ρ_m and d_m are utilized in Equation (2-5) instead of ρ_p and d_p. Their correlation was reported to be applicable only for laminar flow region with Re_{mf} less than 5 (Chyang et al., 1989).

It is noted that the dimensionless parameters, namely Re_{mf} and Ar in all subsequent correlations are based on the effective mixture properties as defined in Goosens et al. (1971) unless otherwise specified.

Using large column with different ID up to 43.4 cm and inert particles from Geldart B and D classifications, Thonglimp et al. (1984) proposed a U_{mf} correlation similar to that of Goosens et al. (1971) but with different constant values of C_1 and C_2

$$\mathrm{Re}_{mf} = \left(19.9^2 + 0.03196 \cdot Ar\right)^{0.5} - 19.9 \tag{2-11}$$

Equation (2-11) is applicable for $0.1 < \mathrm{Re}_{mf} < 180$.

Meanwhile, Mourad et al. (1994) studied fluidization of sand-corn kernels with size and density ratio of 25 and 0.45 respectively, fluidized using air in a rectangular reactor of 0.04 m^2 cross sectional area. The biomass fraction was varied from 2.43 to 42.9 weight percent in constant sand weight. They proposed the U_{mf} correlation as

$$\mathrm{Re}_{mf} = 5.52 \cdot 10^{-4} \cdot Ar^{1.044} \tag{2-12}$$

valid for $1.67 < \mathrm{Re}_{mf} < 6.01$.

Complete Fluidization Velocity Correlations

Noda et al. (1986) proposed U_{cf} correlation adapted from the Wen and Yu correlation and Goosens et al. (1971). They estimate C_1 and C_2 in Equation (2-5) according to the bed mixing condition and component particle properties.

For general case where the bed is completely mixed after both components are fluidized, they suggested

$$C_1 = 19.30(\gamma)^{0.492} \tag{2-13}$$

where γ is defined as $\left(\frac{d_P}{d_F}\frac{\rho_F}{\rho_P}\right)$.

For specific case where the bed is partially mixed after both components are fluidized, they suggested

$$C_1 = 88.99(\gamma)^{-1.664} \tag{2-14}$$

and it is only applicable for the condition of $\frac{d_P}{d_F}$ greater than 3 and $\frac{\rho_F}{\rho_P}$ is close to unity.

The constant value, C_2 for both cases are defined as

$$C_2 = \frac{1}{36.2}(\gamma)^{0.196} \tag{2-15}$$

Noda's et al. (1986) correlation was developed based on the binary mixture including biomass-sand system with wide particle size and density ratio of 1.43÷27.5 and 0.34÷1.03 respectively.

Mourad et al. (1994) also developed a U_{cf} correlation for sand and corn kernel as

$$\mathrm{Re}_C = 1.06 \cdot 10^{-3} \cdot Ar_M^{1.04} \tag{2-16}$$

The mixture effective properties in Equation (2-16) are estimated from Equations (2-9) and (2-10) as the input parameters for the Reynolds (Re_C) and Archimedes (Ar_M) numbers. It is noted Re_C is the Reynolds number with U_{cf} as characteristic velocity. Equation (2-16) was tested for $6.01 < \mathrm{Re}_C < 12.20$.

Rao and Ram Bheemarasetti (2001) developed the U_{cf} correlation[b] for sand-biomass system in a 5 cm ID fluidized bed column using rice husk, sawdust and groundnut shell powder up to 15 weight percent in sand.

Their correlation is adapted from Ergun (1952) by taking only the contribution from the viscous effect in Equation (2-1) as

$$U_{cf} = \frac{d_M^2 (\rho_M - \rho_g) g}{1650 \mu} \tag{2-17}$$

Accordingly, their correlation is only valid for the condition of Reynolds number less than 20.

The mixture effective density in Equation (2-1) is computed using

$$\rho_M = \frac{w_F \rho_F + w_P \rho_P}{w_F + w_P} \tag{2-18}$$

while the mixture effective diameter is calculated using

$$d_M = k d_F \left[\left(\frac{\rho_F}{\rho_P} \right) \left(\frac{d_P}{d_F} \right) \right]^{w_P / w_F} \tag{2-19}$$

[b] The authors defined it as U_{mf}, although the methodology used was for U_{cf} determination.

where k varies according to the sand size as follow

$$k = \left(20 d_F + 0.36\right)^{0.5} \tag{2-20}$$

In summary, the U_{mf} and U_{cf} correlations for binary mixtures are generally adapted from Equations (2-4) and (2-5) by incorporating effective mixture properties. These correlations were developed using similar methodologies (fast and slow defluidization procedures), bed materials and column dimension. They will be tested with the present sand-biomass (palm shell) binary system.

2.3 MIXING QUALITY

A bed is said to be in good fluidization quality, Q when all the particles are fully supported by the gas. Unfortunately, for binary mixtures, good fluidization quality does not necessarily mean good mixing quality since the local composition may still differ significantly from point-to-point in the bed. In fact, fluidization of two dissimilar components tends to form two distinctive layers, one being much higher concentration than the other. This non-uniformity can actually cause severe problems in fluidized bed reactors such as weak/hot spot, ash agglomeration and product variations. This section of review will discuss the criteria to determine which component in a binary mixture tends to be of higher concentration on the top/bottom layer in a fluidized bed, the definition of mixing quality/index and the various factors affecting mixing quality particularly in the sand-biomass system.

2.3.1 CRITERIA FOR DETERMINATION OF JETSAM AND FLOTSAM

Rowe and Nienow (1976) who pioneered the extensive studies on the binary mixing proposed two terminologies, namely *jetsam* and *flotsam* to describe the components in the binary mixture that tend to sink or float respectively in a fluidized bed. They found that for the multi-component fluidized bed system differing in both particle density and size, the larger and denser component tends to be the *jetsam* while the smaller and lighter component tends to be the *flotsam* forming the two segregated parts.

Chiba et al. (1980) established the general criteria to determine which component is *jetsam* depending on the particle size, particle density and bulk density in Table 2-1. This provides a convenient tool to identify the *jetsam* and *flotsam* component in binary mixture.

Table 2-1: General criteria for *jetsam* determination in binary mixture (Adopted from Chiba et al., 1980).

General Criteria		
1. When $d_P/d_F \leq 10$,		
1a.	$\rho_P = \rho_F$	Bigger component is *jetsam*
1b.	$\rho_P \neq \rho_F$	Heavier component is *jetsam*
2. When $d_P >> d_F$ and bed material comprises nearly 100% of smaller component		
2a.	$\rho_P > (\rho_F)_{\text{bulk}}$	Bigger component is *jetsam*
2b.	$\rho_P < (\rho_F)_{\text{bulk}}$	smaller component is *jetsam*
3. When $d_P >> d_F$ and bed material comprises nearly 100% of larger component		
3a.	$\rho_P > (\rho_F)$	Bigger component is *jetsam*
3b.	$\rho_P < (\rho_F)$	Either component can be *jetsam*

2.3.2 MIXING INDEX

Nienow et al. (1978) quantified the overall mixing quality in terms of mixing index, M as a ratio of *jetsam* weight fraction (x_j) in the upper part of the bed to the *jetsam* loading in weight fraction (X_j),

$$\mathrm{M} = x_j / X_j \tag{2-21}$$

The mixing index can also be defined as the ratio of *flotsam* weight fraction in the bottom part of the bed to the *flotsam* loading in weight fraction (Wu & Baeyens, 1998). Accordingly, sampling data were collected only in the upper or lower layer of the fluidized bed.

M index varies from 0 for completely segregated to 1 for completely mixed.

On the other hand, Lacey (1954) suggested that statistics can be used to quantify the degree of mixing. The author developed the M index based on uniform particles differing only in colours. For a mixture of different size or density, he suggested the formula from Buslik (1950). However, a generalized equation for non-spherical particles of both different size and density has not been found.

2.3.3 PARAMETERS AFFECTING MIXING QUALITY IN BINARY SYSTEM

Mixing quality in the binary system depends on the operating superficial velocity, particle properties, their relative proportion and bed aspect ratio (Nienow et al., 1978; Wu & Baeyens, 1998; Formisani et al., 2001; Sahoo & Roy, 2007).

Nienow et al. (1978) conducted the studies using two fluidized bed columns with ID of 14.1 and 22.2 cm. The materials used were metal compounds, sand, glass, sugar, polystyrene and sodium perborate with particle density, size and sphericity ranging from 1050 to 8860 kg/m^3, 70 to 928 μm and 0.5 to 1.0 respectively. They reported that the mixing quality improves with the increase of *jetsam* proportion and bed aspect ratio but with decreasing particle size and density ratio.

Wu and Baeyens (1998) performed the binary mixing experiments using sand with different particle size ratio ranging from 0.222 to 9.714 in a 30 cm ID vessel. They also found that excess gas velocity ($U - U_{mf}$) required to achieve good mixing quality ($M \geq 0.9$) increases with the increase in particles size ratio. For equidensity binary system, the mixing index was found to be independent of the component's weight percent (Formisani et al., 2001; Wu & Baeyens, 1998), contrary to those reported by Sahoo and Roy (2007). The latter performed the experiments using dolomites with particle size ranging from 0.725 to 1.70 mm in a 15 cm ID column.

Binary mixing improved with increasing bed aspect ratio but was only significant at low H/D ratio (Wu & Baeyens, 1998; Formisani et al., 2001). The segregation tendency in shallow bed is related to the effect of local gas velocity peaks at the

distributor (Formisani et al., 2001). In this paper, the author observed that bed homogeneity was established when the superficial gas velocity is equal to complete fluidization velocity, U_{cf}, for fixed density binary system. However, for equisized binary system, uniform bed mixing was achieved at superficial velocity beyond U_{cf} (Formisani et al., 2008a). The tests were performed using glass ballotini, steel shot and ceramic in a 10 cm ID column. They found that the mixing quality improved with lower particle density ratio. Likewise, Delebarre et al. (1994) conducted fluidization study on multi-dispersed solids in sizes and densities reported that segregation was low at U_{cf} and was more pronouncedly affected by the density. They utilized a cylindrical and a square fluidized bed of 0.015 m^2 and 0.16 m^2 cross sectional area respectively. The bed material consisted of 8 different components with the mean particle size and density ranging from 293 to 553 μm and 770 to 1780 kg/m^3 correspondingly.

Sand-biomass binary system

Comparatively to the conventional binary system, there is only limited literature on the mixing quality for the biomass-sand mixtures. Wirsum et al. (2001) studied binary mixing of spherical particles made from wood and plastic (*flotsam*) in sand (*jetsam*) fluidized in a square column of 0.45 m. The *flotsam* particle size and density was varied from 20 to 40 mm and from 440 to 1420 kg/m^3 respectively. The *jetsam* was sand of two particle sizes, namely 410 and 910 μm that correspond to Geldart B and D particles. They observed that smaller and denser *flotsam* in general lead to better mixing quality. Besides that, smaller *jetsam* particle and higher excess gas velocity also improved the mixing quality. Similar results were obtained by Sun (2005) for sand-rice husk binary mixtures in a 0.11 m^2 rectangular fluidized bed. It is important to note that the larger sand particle used in both of the experiments belonged to Geldart D particles. Geldart D sands spout easily whereas Geldart B sands do not (Kunni & Levenspiel, 1991).

In sand (*jetsam*) and straw (*flotsam*) binary mixture, Bilbao et al. (1988) also reported that the solid mixing quality improved with higher superficial velocity, *jetsam* fraction and smaller *jetsam* or *flotsam* particle sizes. The straw and sand sizes were varied from 0.5 to 1.27 mm and 158 to 346 μm respectively fluidized in a 8 cm ID cylindrical column. But the effect of particle properties on solid mixing were

studied at fixed superficial velocities, despite of the characteristic fluidization velocity for each mixture was different (Bilbao et al., 1987).

Zhang et al. (2008) investigated the mixing behavior of the sand-cotton stalk binary mixtures in the setup described earlier in Zhong et al. (2008). The sand and biomass average particle sizes were 450 μm and 4.5 mm respectively, while the biomass density was 385 kg/m^3. They found that increasing the biomass weight percent in the sand may increase or decrease mixing quality depending on the operating superficial velocity.

To some extent, the effect of bed properties, composition and operating parameters on the mixing quality are similar in both the conventional and the sand-biomass binary system. When the component differs in both size and density, depending on the dominating effect, the segregation actions may be strengthened or counterbalanced (Formisani et al., 2008b).

2.4 COMPARTMENTED FLUIDIZED BED GASIFIER (CFBG)

2.4.1 ON FLUIDIZED BED BIOMASS GASIFICATION TECHNOLOGY

Biomass is an organic material derived from living or recently living plant or animal matter. In the context of biomass as a source of renewable energy, this often means agricultural residues such as oil palm shell and fibre, wood waste and rice husk (Kelly-Yong et al., 2007; Shuit et al., 2009).

Biomass gasification is a set of complex thermo-chemical reactions that converts biomass feedstock to combustible gases using air/oxygen, steam or combinations of these oxidizing agents. The gasification products consist of primarily hydrogen and carbon monoxide, with lesser amount of carbon dioxide, methane and trace amount of other volatiles and contaminants. In general, biomass gasification is endothermic. Hence, a portion of the biomass is always combusted with air/oxygen to satisfy the gasification heat requirement (Knoef, 2005).

In the conventional fluidized bed biomass gasifier, a single vessel is utilized for both the combustion and gasification reaction. This simple and economical design allows intense mixing between the two reaction zones, thus maximizing the heat and mass transfer rate. Air is the most widely used oxidant, avoiding the requirement for oxygen production but the flue gas (mainly nitrogen from the air) will inevitably contaminate the gasification products and reduce its heating value to producer gas quality suitable only for boiler and engine operation (Ciferno & Marano, 2002).

On the other hand, dual/twin fluidized bed (DFB) biomass gasifier is a more complex design that divides the combustion and gasification reaction zones in two vessels, namely combustor and gasifier so that the gas from the gasifier is separated from the combustor's flue gas. Early design of DFB incorporated downcomer and riser to circulate solid heat carrier between the two vessels but the use of long interconnecting lines lead to solid breakage and loss of energy (Bhattacharya et al., 1997). According to Corella et al. (2007), most of the DFB-based biomass gasification plants were shutdown as they were not economically viable, despite the capability to produce nitrogen-free and medium calorific value fuel gas (above 11 MJ/Nm^3) suitable for gas turbine power generation (Quaak et al., 1999).

In order to make biomass economically viable for power generation, it is necessary to utilize technologies which offer higher efficiency and lower capital cost at a modest scale. A single vessel compartmented into several fluidized beds has good potential to exhibit the positive features from both the conventional and DFB gasifier. Fox et al. (1989) reviewed different types of low cost and compact reactors including compartmented fluidized bed gasifier (CFBG) proposed by Rudolph et al. (1985) for coal and biomass gasification. CFBG is a single vessel partitioned into two discrete compartments as combustor and gasifier. While the gas streams are strictly separated, solid heat carrier is internally circulated between the two densely fluidized beds without mechanical moving parts (Yan, 1995). The advantages and possible industrial applications of this novel design were discussed in He et al. (1993), Sathiyamoorthy and Rudolph (1990), and the implementation of this technology for coal gasification was demonstrated by Yan (1995). He showed that

coal gasification using the CFBG was a sound concept and the bottlenecks were in the feeding location and equipment constraint.

2.4.2 SOLID CIRCULATION RATE (SCR)

The ability to circulate solids is one of the principal advantages of fluidized bed operations and a major reason for its successful commercialization and widespread use. An important aspect of the circulation system is the ability to control the solid circulation rate (SCR). This factor is significant in any system that requires two simultaneously and mutually dependent operations e.g. biomass gasification and the combustion of its residual chars (Salam & Gibbs, 1987).

In CFBG, the heat and mass transfer rate between the two compartments, i.e. combustor and gasifier are attained by means of solid circulation. The heat demand in the gasifier is fulfilled by the hot solid transferred from the combustor while the combustor is able to supply this heat via the combustion of the gasified solid fuel obtained from the gasifier. Hence, solid circulation rate (SCR) is one of the essential parameters for steady gasification and combustion to be realized in their respective compartments of CFBG.

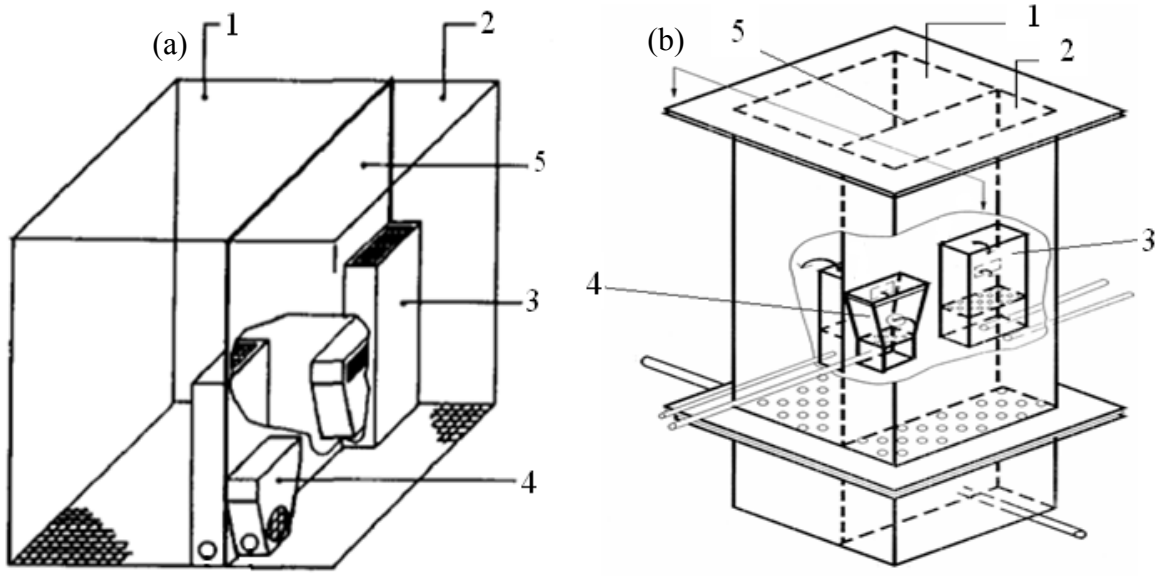

Figure 2-2: Compartmented reactor designs; (a) He (1993) and (b) Bhattacharya et al. (1999); (1: Compartment I; 2: Compartment II; 3: Riser; 4: V-valve: 5: Partition wall).

Figure 2-2 shows the predecessor design of CFBG. Solid circulation is realized in CFBG using two sets of V-valve and riser that could offer the possibilities to meet the requirement as follow:

- the adjacent fluidized beds could operate independently.
- the solid circulation rate between fluidized beds should be large and flexible.
- the gas seals are maintained between the adjacent fluidized beds.

In CFBG, the solid is circulated through the V-valve and riser. Using different aeration rates to the main bed/compartment, V-valve and riser, a pressure gradient is established across the V-valve inlet providing the driving force for the solids to flow from the upstream compartment to the other compartment. Through a second pair of V-valve and riser, solids can be circulated back to the first compartment (Bhattacharya et al., 1999).

Table 2-2 lists the solid circulation rate (SCR) studies performed in the compartmented reactor design for the past 20 years. These pioneer works (Bhattacharya et al., 1999; Yan, 1995; He, 1993; Sathiyamoorthy & Rudolph, 1990) are limited to laboratory scale experimental setup of rectangular reactor geometry and none of their empirical correlations are tested in industrial like scale reactor. They studied various types of inert especially sands; on one occasion, a sand-coal mixture was tested (Yan & Rudolph, 1996).

Three different methods have been employed in determining the solid circulation rate (SCR) in CFBG. In one of the methods, SCR was found by direct collection of solid from the riser discharged at a steady state condition (Sathiyamoorthy and Rudolph, 1990; He, 1993). The authors considered the establishment of a steady state when constant bed height was visually observed. In another method, Bhattacharya et al. (1999) determined SCR by measuring the temperature differences between the two compartments. In-bed heater was used to preheat the solid in one of the compartment and then solid was circulated until a steady state temperature was achieved in both compartments. The solid circulation rate was computed based on the heat balance assuming that: (i) no heat lost, (ii) heat was exchanged by means of circulating solid only and (iii) no changes in gas/solid physical properties.

Table 2-2: List of work details carried out on CFBG by various authors.

Descriptions	Bhattacharya et al. 1999	Yan[c] 1995	He[c] 1993	Sathiyamoorthy and Rudolph[c] 1990
Reactor cross section (mm^2)	240 × 240		300 × 300	
Gasifier cross section (mm^2)	80 × 240		100 × 300	
Combustor cross section (mm^2)	160 × 240		200 × 300	
V-valve orifice diameter (mm)	20		20	
V-valve bottom cross section (mm^2)	-		20 × 30	
V-valve-to-Riser inlet cross section (mm^2)	30 × 25		30 × 30	
Riser outlet cross section (mm^2)	-		30 × 30	
Riser height (mm)	-		250	
V-valve location (mm)	130 (above distributor)		On distributor	
Riser location (mm)	240 (above distributor)		On distributor	
Fluidizing medium	Air		Air	
Mean particle diameter (μm)	250, 325, 429	304	282	386, 119, 117
Mean particle density (kg/m^3)	2550	2620	2510	2445, 4500, 4300
Static bed height, H_b (mm)	255÷305	150÷200	100÷200	196
Main bed aeration, Q_b (U/U_{mf})	1÷4	1.3÷2.1	1÷4	1÷3
V-valve aeration, Q_v (U/U_{mf})	5÷60	7.88÷15.76	0÷15	3÷100
Riser aeration, Q_r (U/U_{mf})	0÷65	6.75÷13.50	2÷30	5÷25

[c] The authors in these papers utilized identical compartmented reactor design.

However, direct collection of hot solid from the riser discharge during combustion/gasification is difficult to be realized (Yan, 1995). In addition, the validity of the assumptions made by Bhattacharya et al. (1999) was questionable since Yan (1995) estimated that heat lost of up to 34% and He (1993) reported 7% gas/air leakage that could contribute to the extra heat in the gasification compartment.

Hence, the method proposed by Yan and Rudolph (1996) to measure SCR based on the differential bed pressure drop that was successfully tested in ambient/normal temperature and at higher temperature during combustion and gasification is preferred. Their method is easy to apply, requiring only shutting off the aeration to a set of V-valve and riser for a short period of time and monitoring the change in differential bed pressure drop. It does not require visual observation of bed height at steady state but can be inferred from the differential bed pressure drop. Moreover, the method is also independent of the operating temperature. Further development on this method to a more generalized equation and the implementation of curve fitting to determine the initial rate of change in bed pressure drop are presented in Chapter 5.

2.4.3 PARAMETERS AFFECTING SOLID CIRCULATION RATE (SCR)

Despite using 3 different methods to determine SCR, the authors who conducted the experiments using identical reactor design (as illustrated in Figure 2-2(a)) reported that solid circulation rate (SCR) increased with bed height and aerations to the main bed, riser and V-valve respectively. In addition, any increase in the aerations leads to an increase in the gas leakage from the main bed to the V-valve orifice, resulting in the increase in the SCR (He et al., 1993, 1997).

In a different compartmented reactor design, Figure 2-2(b), Bhattacharya et al. (1999) reported similar solid circulation rate (SCR) trend with the increased in the bed height and V-valve aeration. But they observed that the increase in the main bed aeration may increase or decrease the SCR depending on the net contribution of the main bed porosity and the gas leakage. Besides that, they reported that the effect of riser aeration on the SCR depends on the net contribution of the entrainment rate and, pressure and frictional pressure drop in the riser.

Sathiyamoorthy and Rudolph (1990) proposed an empirical correlation for the solid circulation rate (SCR) based on the different gas flow rates (i.e. main bed, V-valve and riser aeration), bed and gas properties, with a constant depending on the V-valve inlet diameter. Later, He and Rudolph (1997) developed a fully predictive model that allowed the solid circulation rate to be estimated from the knowledge of particle properties, system specification and operating conditions. Meanwhile, Yan and Rudolph (1996) utilized factorial design of experiment to obtain a statistical SCR model by linear regression as a function of operating variables. However, all these correlations were derived from specific reactor design.

The implementation of the factorial design proposed by Yan and Rudolph (1996) provides a simple, efficient and effective way to determine the most important effects and to identify the interacting operating variables affecting the solid circulation rate. In Chapter 5, the approach is developed further based on the combination of half normal plot and steepest ascent method that allows the determination of the optimum solid circulation rate for different sand sizes.

2.4.4 PALM SHELL AS FEEDSTOCK FOR GASIFICATION

Oil palm is one of the major economic crops in many countries such as Malaysia, Indonesia and Columbia (Kelly Yong et al., 2007). The palm oil industries generate substantial amount of biomass residuals namely palm shell, empty fruit bunch, fibre, fronds and trunks. In 2005, palm oil industry in Malaysia generates approximately 53.62 million tonnes of oil palm biomass (Shuit et al., 2009).

Generally, fronds, trunks and empty fruit bunch are not preferred as fuels due to their high moisture content (> 65 wt%) since biomass could not sustained burning at moisture content exceeding 20 wt% (Patumsawad et al., 2002). Fronds and empty fruit bunch are used for soil conservation. Frond is also a source of food for ruminants (e.g. cattle and goats). Oil palm trunks obtained during the replantation of oil palm trees are suitable as materials for making saw-wood and plywood (Sumathi et al., 2008).

Currently, palm oil mills utilize mainly palm shell and fibre as boiler fuels to generate steam, heat and power (Kawser & Nash, 2000; Yusoff, 2006). Little effort was made in the past to improve the efficiency of the oil palm biomass conversion to bioenergy, as the feedstock was substantially treated as waste that was incinerated to be disposed of (Sulaiman et al., 2011).

However, the present approach of burning oil palm biomass has serious emission problem. According to Ramli and Rozaine (1997), more than 80% of the boilers emit particles exceeding the permissible limit set by department of environment (0.4 g/Nm^3). Yusof and Rozainee (1993) reported that the dust emission of such boilers can reach up to 11.6 g/Nm^3.

Malaysia Palm Oil Board (MPOB) has carried out the research and development of fluidized bed gasification system for steam and power generation with the aim to replace the conventional boilers in palm oil mills (Azali et al., 2005). The air gasification system was able to generate producer gas from oil palm shell and fibre.

In the feasibility study conducted by Kelly Yong et al. (2007), they reported that steam gasification of oil palm biomass as a viable technology for the production hydrogen as a clean transportation fuel or as gaseous fuel for power generation. In addition, a recent bench scale experimental study on steam gasification of oil palm biomass (palm shell, fibre and empty fruit bunch) showed the potential of producing medium calorific value fuel gas (Li et al., 2009). The experiment was performed using an electrically heated fixed bed reactor.

Based on 11 types of biomass residuals available in Malaysia including oil palm biomass (frond, palm shell, fibre and empty fruit bunch), palm shell has been identified as the most preferred fuel for gasification (Abdullah & Yusup, 2010). The favourable compositions in palm shell i.e. high volatiles and calorific value, relatively low moisture and ash justified the utilization of the biomass as gasification feedstock.

2.5 SUMMARY

Extensive studies were published on the effect of gas and solid properties on the characteristic fluidization velocities for both single and binary system as evidently shown in the various reported U_{mf} and U_{cf} expressions. However, the effect of bed geometrical parameters (i.e. bed diameter and/or height) on characteristic fluidization velocities is also observed by many researchers; unfortunately, most fluidization research is concentrated on laboratory scale setup.

Biomass has distinct fluidization characteristics compared to those observed in the conventional system. In general, biomass cannot be fluidized solely due to its peculiar shape, size and density; a second fluidizable material, e.g. sand is often required to facilitate fluidization.

In the sand-biomass system, when the biomass is below a certain loading, the U_{mf} and U_{cf} are determined principally by the sand. On the other hand, there is a limitation on the amount of biomass in the sand where further addition of biomass will result in poor fluidization. Besides that, the hydrodynamics of sand-biomass system may depend strongly on the specific biomass used in the experiments.

Meanwhile, good fluidization quality does not necessarily means good mixing quality where the local compositions differ significantly from the overall average. The overall mixing quality represented in terms of M index depends primarily on particle properties, composition, bed geometry and operating superficial velocity. The pioneering researchers in binary mixing studies described the component that tends to sink or float in a fluidized bed as *jetsam* and *flotsam* respectively. Whether biomass is a *flotsam* or *jetsam* in sand will depend on its particle density and the bulk density of the bed. Most research work on the binary mixing, including those of biomass-sand system only focused on the bulk or overall mixing quality.

Different fluidized bed biomass gasification technologies have been reviewed; compartmented fluidized bed gasifier (CFBG) with the ability to transport solid internally and wide range of solid circulation rate (SCR) was tested with promising

results, but limited to laboratory scale. Only the conventional fuel, coal was tested as the feedstock in the gasifier.

Oil palm shell has been identified as the potential feedstock for biomass gasification due to its abundant availability and favourable chemical properties.

By using sand as a second fluidizing material, and adopting the concept of compartmented reactor for biomass gasification in pilot plant scale, the specific objectives of the present work are:

- To investigate the effect of bed diameter, sand size, palm shell size and weight percent on U_{mf} and U_{cf} of sand-palm shell binary mixtures.
- To determine the critical loading of palm shell in the binary mixture.
- To evaluate the applicability of the reviewed U_{mf} and U_{cf} correlations to the binary mixtures.
- To study palm shell vertical and lateral distribution by determining the local mixing quality (m) in different bed layer and operating superficial velocity.
- To investigate the effect of palm shell size and weight percent, effective bed diameter and height as well as operating superficial velocity on the overall mixing quality (M) of the binary mixtures.
- To investigate the effect of bed height and aerations to main bed, V-valve and riser on solid circulation rate (SCR).
- To determine the optimum solid circulation rate (SCR) for various sand sizes.
- Finally, to prove the concept of CFBG as a prospective technology for palm shell gasification to produce medium calorific value fuel gas by designing and operating the pilot plant based on the findings and operating range of the main process parameters determined from the studies above.

CHAPTER 3

MINIMUM AND COMPLETE FLUIDIZATION VELOCITIES DETERMINATION

3.1 INTRODUCTION

Minimum fluidization velocity, U_{mf} is one of the most basic parameters to design and operate any fluidized bed. For a multi-component/binary system differing in particle size and/or density, it is important as well to determine another important characteristic fluidization velocity, namely complete fluidization velocity, U_{cf} that represents a condition of a fully fluidized bed. Accordingly, the two commonly used methods in determining the U_{mf} and U_{cf}, i.e. via fast and slow defluidization are adopted (refer to Chapter 2) for pure sand and sand-palm shell binary mixtures. These allow comparative studies to be carried out on the various published correlations. Besides that, the effect of particle properties and bed geometry on the U_{mf} and U_{cf} are also included. In addition, this chapter introduces critical loading as a parameter to characterize the state when the characteristic fluidization velocities for the binary mixtures remain nearly unchanged from its pure sand values.

3.2 EXPERIMENTAL SETUP

A schematic diagram of the experimental setup is illustrated in Figure 3-1. The cold flow model of a pilot plant scale has a 0.66 m ID and is divided into two compartments i.e. a combustor and a gasifier by a vertical wall in 65:35 (based on 100%) cross-sectional area ratio (Figure 3-2). The total height of the reactor is 1.8 m, while the plenum height is 0.20 m. Perforated plate distributor is selected due to its simplicity and low cost.

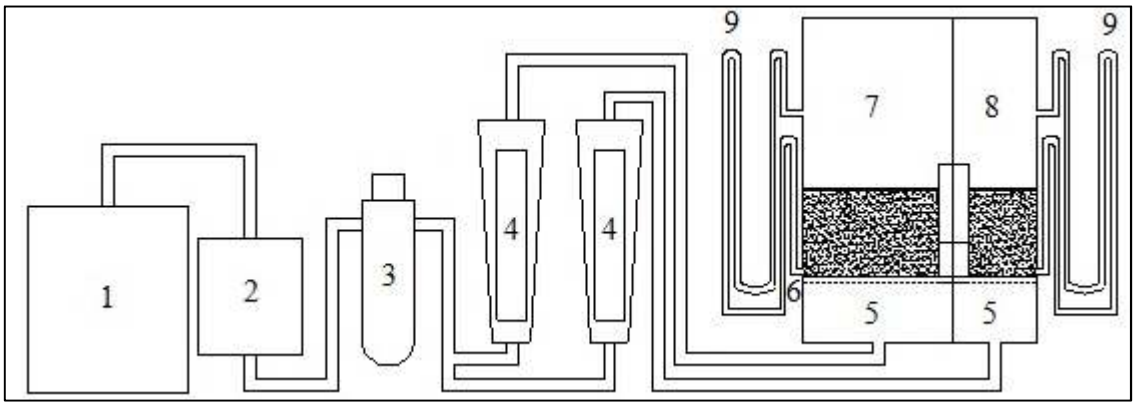

Figure 3-1: Schematic diagram of the experimental setup (1: air compressor; 2: air dryer; 3: pressure regulator; 4: air rotameters; 5: plenum; 6: perforated distributor; 7: combustor; 8: gasifier and 9: water manometers).

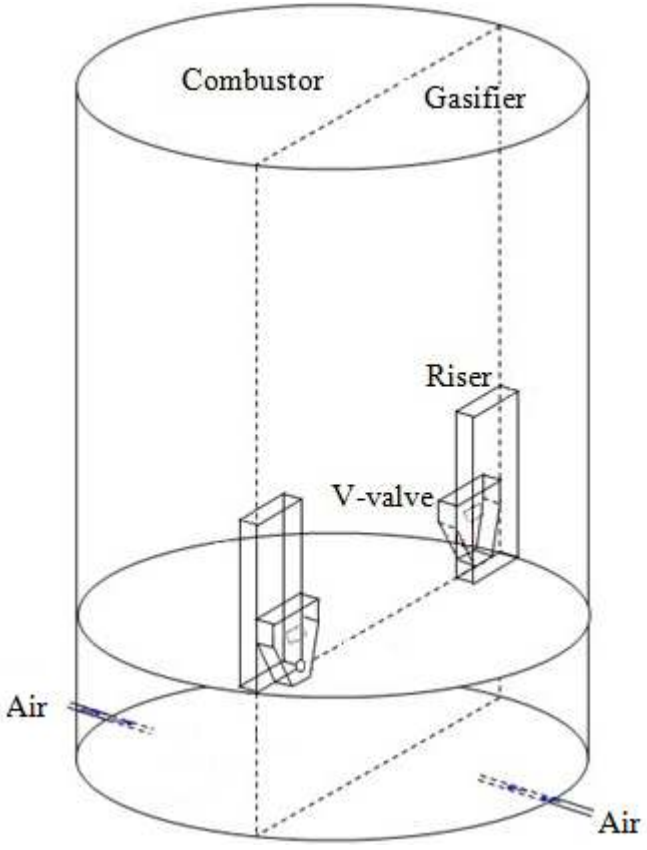

Figure 3-2: Isometric view of CFBG

Both of the compartments were fluidized using air (air was not supplied to V-valve and riser). The maximum air supply was 3,500 l/min. Rotameters were used to regulate the air flowrates to maintain bubbling mode of fluidization. The accuracy of the flowrate measurement is of ±5%. The bed pressure drops (ΔP_b) were measured with the accuracy of ±0.1 cmWg using water manometers.

The effective bed diameter, D_e is estimated based on Equation (3-1),

$$D_e = 4 \times \frac{mean\ cross\,sectional\ area\ of\ \ flow\ channels\ through\ bed}{mean\ wetted\ \ perimeter\ of\ \ flow\ channels} \qquad (3\text{-}1)$$

were found to be 0.413 m and 0.257 m for the gasifier and combustor respectively. The presence of the V-valve and riser pairs in the compartments has been addressed when considering the effective bed diameter.

In considering the typical bed aspect ratio of 1÷2, the experiments were carried out in both of the compartments at 0.4 m static bed height[d]. The total bed material used was 77 kg and 101 kg for the gasifier and combustor respectively. The as-received palm shell size distribution is shown in Figure 3-3. It can be clearly seen that the biomass consists mostly of larger particles with the mean sieve sizes of 3.56 mm and 7.13 mm.

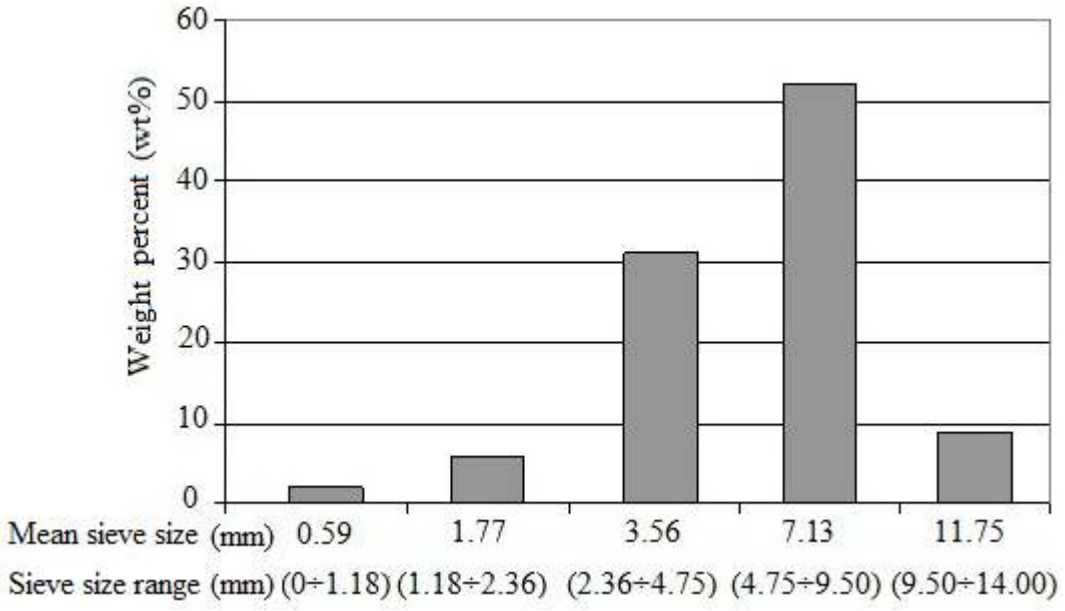

Figure 3-3: Palm shell size distribution.

The biomass residuals were obtained from a palm oil mill in Malaysia and underwent natural drying prior to utilization. The final moisture content was found to be 8÷10 wt%. The characteristic properties of the palm shell and sand are given in Table 3-1.

[d] The experiments to determine the U_{mf} and U_{cf} were performed in static bed height of 0.3÷0.5 m in both of the compartments confirmed the same results.

Palm shell of four different mean sieve sizes were used in this study, excluding the smallest palm shell mean sieve size that mostly consists of loose fibres. Palm shell weight fraction was varied at 2, 5, 10 and 15 wt%, following the experience from the other authors (Bilbao et al., 1987; Rao & Ram Bheemarasetti, 2001). Besides that, sand of four different mean particle sizes were selected as the inert materials.

Table 3-1: Palm shell and sand characteristic.

	Palm shell	Sand
Particle size (mm)	1.77	0.196
	3.56	0.272
	7.13	0.341
	11.75	0.395
Density (kg/m^3)	1500	2700
Moisture (%)	8÷10%	-
Weight percent (wt%)	2, 5, 10, 15%	-

Table 3-2 shows the sand particle size distribution. The mean particle size, d_p for the sand is computed based on Equation (3-2),

$$d_p = 1/\Sigma\left(x_i/d_{pi}\right) \tag{3-2}$$

Table 3-2: Sand size distribution.

Sieve range (μm)	Mean sieve size d_{pi} (μm)	Mean particle size, d_p (μm)			
		196	272	341	395
		Weight fraction of each sieve interval, x_i (wt%)			
425 - 600	512.5	0.23	0.10	7.46	51.05
300 - 425	362.5	0.85	53.73	80.84	40.27
212 - 300	256.0	59.24	31.74	9.60	6.66
150 - 212	181.0	32.36	12.41	1.29	1.32
0 - 150	75.0	7.32	2.02	0.81	0.71

Overall, the biomass is larger but lighter than the inert sand used, the particle size and density ratio for the palm shell-sand are about 4.5÷60 and 0.55 respectively.

3.3 SINGLE (INERT) COMPONENT

The experiments were first conducted using pure sand to determine the fluidization behavior, particularly the bed pressure drop profile in the CFBG using common bed material. Besides that, the characteristic velocities obtained in this condition provide the operating parameters for the CFBG when the presence of other bed material (e.g. biomass, char etc) is very small or negligible.

The typical bed pressure drop profile is shown in Figure 3-4, obtained from the sand mean particle size of 395 μm in the gasifier. It demonstrates that:

(1) the bed pressure drop reaches identical steady state value at fluidized condition in both fast and slow defluidization methods.

(2) the existence of the U_{mf} and U_{cf} .

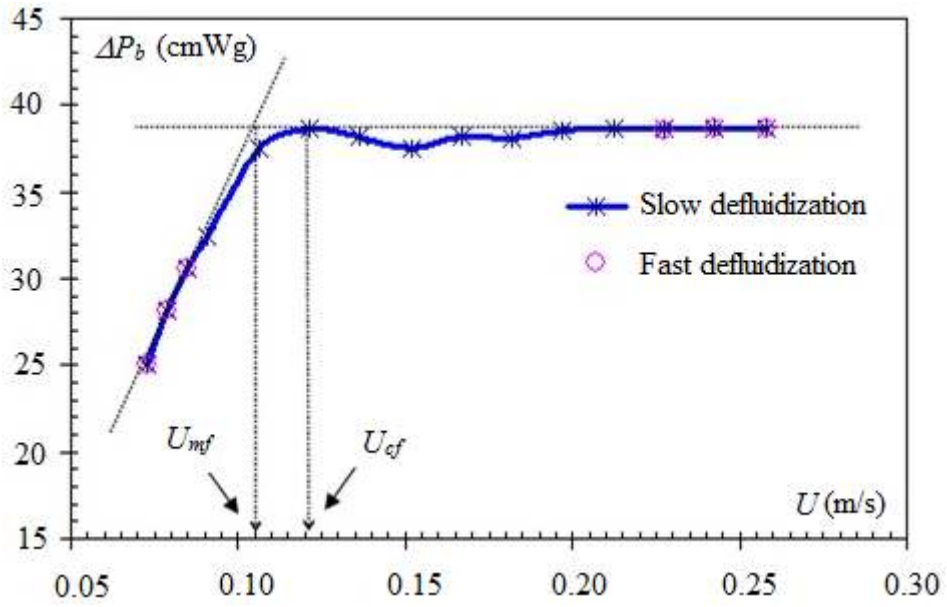

Figure 3-4: Typical sand bed pressure drop profile for U_{mf} and U_{cf} in the gasifier.

Similar bed pressure drop profile is obtained in the combustor and for all other sand mean particle sizes in both compartments. Hence, it is confirmed that the bed pressure drop profile obtained from the CFBG is very similar to those from the cylindrical column of laboratory scale (Kunni & Levenspiel, 1991). Besides that, the methodologies used to determine the U_{mf} and U_{cf} values can be implemented for the present system in spite of the geometrical features of CFBG.

The U_{mf} and U_{cf} values in both the compartments for the sand of 4 mean particle sizes are presented in Table 3-3. Both the U_{mf} and U_{cf} values increase with the increase in the sand mean particle size. Besides that, it is observed that the U_{cf} is always greater than the U_{mf}.

Table 3-3: Sand characteristic fluidization velocities

Sand	Gasifier, D_e = 0.257m		Combustor, D_e = 0.413 m	
d_p (μm)	U_{mf}(m/s)	U_{cf}(m/s)	U_{mf} (m/s)	U_{cf}(m/s)
196	0.032	0.042	0.021	0.030
272	0.077	0.087	0.053	0.064
341	0.102	0.117	0.073	0.085
395	0.105	0.121	0.083	0.100

Similar trends were reported by Aznar et al. (1992a) obtained from sand using fluidized bed with ID of 0.14 and 0.30 m.

However, Figure 3-5 shows that U_{cf}/U_{mf} ratio is approximately 1.15 for the gasifier and combustor, except for the sand mean particle size of 196 μm. This shows that U_{cf}/U_{mf} ratio is nearly independent of the sand mean particle size.

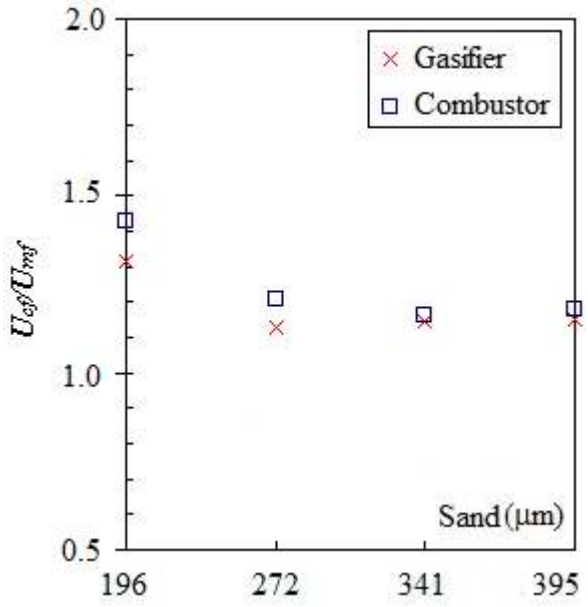

Figure 3-5: U_{cf}/U_{mf} ratio for various sand mean particle sizes.

Table 3-3 shows that the characteristic fluidization velocities for the gasifier (of smaller effective bed diameter) are always larger than those of the combustor.

Specific study on the effect of bed diameter on U_{mf} by Frantz (1966) and Hilal et al. (2001) demonstrated similar trends in cylindrical columns where the characteristic fluidization velocity increases with the decrease in the bed diameter.

It is observed that the effect of effective bed diameter on the U_{mf} and U_{cf} decreases with the increase in the sand mean particle size. As shown in Table 3-4, the gasifier-to-combustor U_{mf} and U_{cf} ratios decrease when the sand mean particle size increases from 196 to 395 μm.

Table 3-4: Sand characteristic fluidization velocities ratio of gasifier-to-combustor

Sand d_p (μm)	$\frac{U_{mf,gasifier}}{U_{mf,combustor}}$	$\frac{U_{cf,gasifier}}{U_{cf,combustor}}$
196	1.52	1.40
272	1.45	1.36
341	1.40	1.38
395	1.27	1.21

With the determination of U_{mf} and U_{cf}, it is desirable to check if the existing correlations are able to predict satisfactorily for the sand in a compartmented reactor design. Three U_{mf} correlations, namely Equation (2-5) from Wen and Yu (1966), Equation (2-6) from Bourgeois and Grenier (1968) and Equation (2-7) from Lucas et al. (1986) are selected. Besides that, U_{cf} correlation i.e. Equation (2-8) from Gauthier et al. (1999) is also included. These correlations were reviewed in Chapter 2.

Generally, it can be seen in Figure 3-6 that all the three U_{mf} correlations can only give good U_{mf} prediction for the gasifier, but not for the combustor. This is probably due to the fact that these correlations were developed from smaller ID columns. Equation (2-8) does not predict U_{cf} satisfactorily. Overall, the selected correlations either overestimate or underestimate the U_{mf} and U_{cf} values with errors more than 50%.

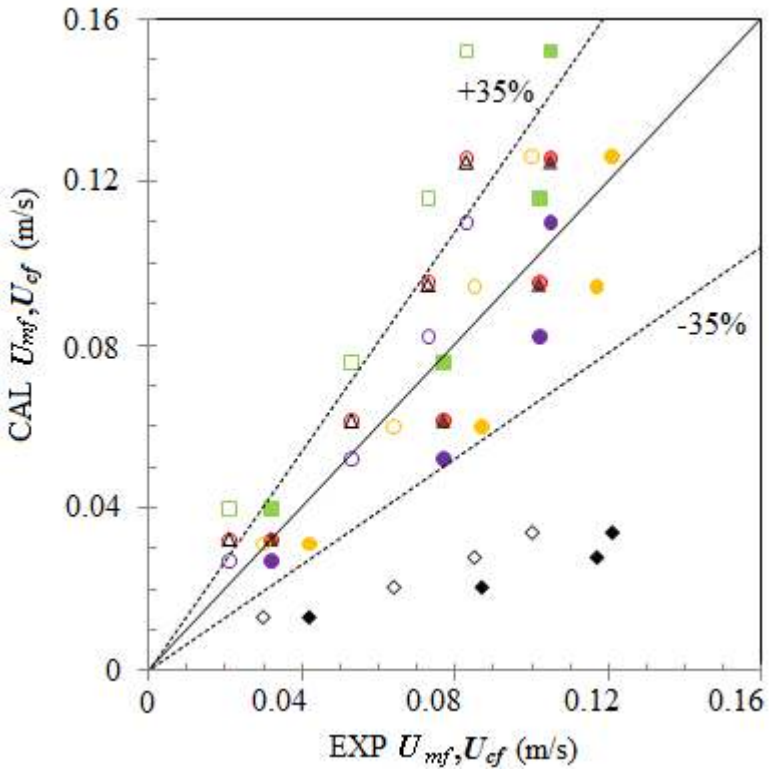

Figure 3-6: Comparison of the experimental (EXP) and the calculated (CAL) U_{mf} and U_{cf} with different correlations; Open and close symbols represent data for the combustor and gasifier respectively; On U_{mf}: ○● Equation (2-5), □■ Equation (2-6), △▲ Equation (2-7), ○● Present U_{mf} correlation, Equation (3-3); On U_{cf}: ◇◆ Equation (2-8); ○● Present U_{cf} correlation, Equation (3-4).

The present fluidized bed is established in the fully laminar condition since Re_{mf} is less than 5. Accordingly, the kinetic term in the Ergun's equation (1952) can be neglected while the constant in its viscous term is recommended to be 180 (Pattipati & Wen, 1981; Carman, 1937). Approximating the sphericity-voidage factor, $\frac{1-\varepsilon_{mf}}{\phi_s^2 \varepsilon_{mf}^3}$ for the viscous term as 11 (Wen & Yu, 1966), the proposed U_{mf} correlation is

$$Ar = 1980\,\mathrm{Re}_{mf} \tag{3-3}$$

As shown in Figure 3-6, Equation (3-3) is able to predict U_{mf} for both of the compartments within 35% accuracy. Based on the constant U_{cf}/U_{mf} ratio of 1.15 shown in Figure 3-5, the proposed U_{cf} correlation is

$$Ar = 2277\,\mathrm{Re}_{cf} \tag{3-4}$$

Similarly, Equation (3-4) is able to predict the U_{cf} satisfactorily for both of the compartments. These correlations will be useful to predict the U_{mf} and U_{cf} values when the inert particle properties dominate the characteristic fluidization velocities.

As a summary, despite of the specific geometrical feature of the CFBG, the fluidization characteristics for the single component system in the cold flow model is similar to that reported for cylindrical column of laboratory scale where: (i) the $U_{cf} > U_{mf}$, (ii) both the characteristic fluidization velocities increase with the increase in the sand mean particle size, and (iii) the characteristic fluidization velocities for the gasifier (of a smaller effective bed diameter) are larger than those observed in the combustor.

The existing correlations are modified to Equations (3-3) and (3-4) for the estimation of the characteristic fluidization velocities for the sand in the CFBG.

Based on these studies, the differences in the U_{mf} and U_{cf} between the two compartments can be minimized when utilizing larger sand mean particle size as a bed material, hence avoiding any physical modification on the vessel.

3.4 BINARY MIXTURES

3.4.1 BED PRESSURE DROP PROFILE

Palm shell is considered as Geldart D particle, a classification for spouting bed material. However, mixing palm shell with a second fluidizable material (sand) can facilitate proper fluidization, as observed by Fauziah et al. (2008). It has been confirmed in experiment that as-received palm shell cannot be fluidized solely. In the present study, palm shell of various mean particle sizes and weight percent have been added to the sand whose fluidization characteristics have been previously determined.

Figure 3-7 shows the typical sand-palm shell bed pressure drop profile obtained from the palm shell of 7.13 mm at 5 wt% in sand of 196 μm in the combustor. It can be seen that the binary mixture demonstrates similar profile as obtained in the single

component (sand) system, thus, permitting the identification of characteristic fluidization velocities using the same methods.

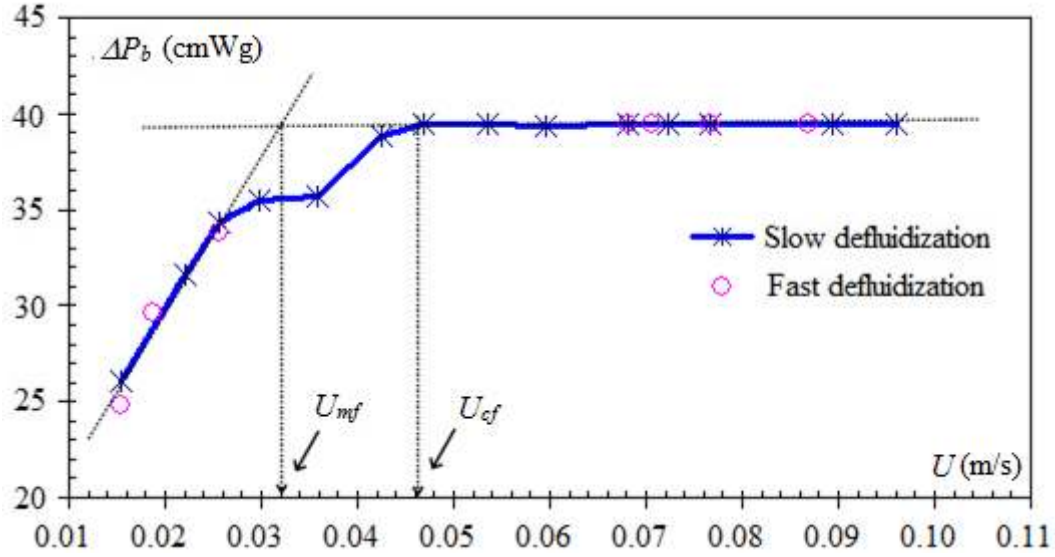

Figure 3-7: Typical sand-palm shell bed pressure drop profile for U_{mf} and U_{cf} in the combustor.

However, unlike the single component system, depending on the palm shell mean sieve size and weight percent in the sand, the binary mixtures may exhibit severe segregating condition that leads to channelling.

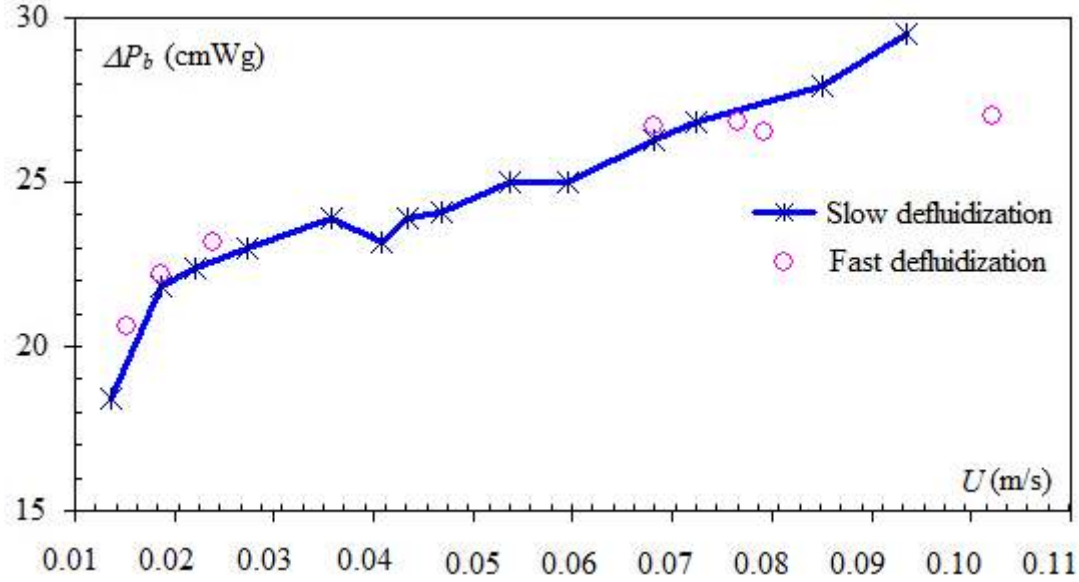

Figure 3-8: Typical sand-palm shell channelling bed pressure drop profile in the combustor.

As shown in Figure 3-8, during fast defluidization, the bed pressure drop at fluidized state shows a significantly lower stable value (<70%) compared to those obtained from experiments where proper fluidization is attained (refer to Figure 3-7). During slow defluidization, the steady state bed pressure drop cannot be established at fluidized state as well. In fact, the bed pressure drop profile is showing an upward trend. Such behavior is analogous to that observed in a single component system that exhibits channelling. Besides that, visual observation also confirmed the presence of stationary portion of palm shell "chunks" in the vigorously fluidized bed. The bed pressure drop profile shown is obtained from the palm shell of 7.13 mm at 15 wt% in sand of 196 μm in the combustor.

This behaviour is often observed for biomass-sand fluidization (Bilbao et al., 1987; Aznar et al., 1992a, 1992b).

It is worthy to mention here that in this particular experiment, the operating superficial velocity (U) was increased up to 0.221 m/s, corresponding to about 10 times of the pure sand U_{mf}, producing a turbulent bed. Even in this test condition, the mixtures fluidization was unsatisfactory.

Accordingly, the characteristic fluidization velocities for the binary mixtures are reported only when their bed pressure profiles exhibit steady state values at fluidized condition for both of the defluidization methods (refer to Figure 3-7).

3.4.2 EFFECT OF EFFECTIVE BED DIAMETER

Table 3.5 shows the effect of effective bed diameter on the U_{mf} and U_{cf} for the sand-palm shell binary mixture. It is observed that the characteristic fluidization velocities are always larger for the gasifier than that of the combustor. These results are consistent with the trends obtained for the single component (sand) system discussed earlier.

Table 3.5: Effect of effective bed diameter on the U_{mf} and U_{cf} for the binary mixtures.

Sand	Palm shell		Gasifier, D_e = 0.257 m		Combustor, D_e = 0.413 m	
Size (μm)	Size (mm)	Composition (wt%)	U_{mf} (m/s)	U_{cf} (m/s)	U_{mf} (m/s)	U_{cf} (m/s)
196	1.77	2	-[e]	-[e]	0.021	0.030
272	3.55	5	0.078	0.091	0.054	0.060
341	7.13	10	0.117	0.165	0.079	0.102
395	11.75	15	0.145	0.273	0.083	0.083

Besides that, channelling occurred at a greater extent in the gasifier. It is found that fluidization in the gasifier was unsatisfactory for the binary mixtures with sand mean particle size of 196 μm. Channelling is observed as well in the combustor for the binary mixtures of the same sand mean particle size but only with the palm shell mean sieve size of 7.13 mm at 15 wt% and 11.75 mm at 10 and 15 wt%. Proper fluidization can be achieved in both compartments in other tested binary mixture.

3.4.3 EFFECTIVE MIXTURE PROPERTIES

The subsequent section describes the specific studies on the effect of palm shell weight percent, palm shell and sand sizes respectively on the U_{mf} and U_{cf}. In a binary system, the bed mixture properties take into account the contribution from each of the component's properties. The effective particle density (ρ_m) and diameter (d_m) for the binary mixture can be estimated based on the weighted average mixtures properties, namely Equations (2-9) and (2-10) as reported by the various authors (Goosens et al., 1971; Noda et al., 1986; Mourad et al., 1994). The sand and palm shell are considered as fluid ("*F*") and packed ("*P*") particles respectively in these equations (refer to Chapter 2).

Effect of Palm Shell Size

Table 3-6 shows that the U_{mf} and U_{cf} exhibit the tendency to increase with the increase of palm shell mean sieve size from 1.77 to 11.75 mm in both compartments.

[e] Data are not available since channelling occurred in the gasifier.

Table 3-6 U_{mf} and U_{cf} of sand d_p = 272 μm and palm shell of 10 wt%.

Palm shell size (mm)	Effective mixture properties		Characteristic fluidization velocity			
			Combustor		Gasifier	
	d_m (mm)	ρ_m (kg/m^3)	U_{mf} (m/s)	U_{cf} (m/s)	U_{mf} (m/s)	U_{cf} (m/s)
1.77	317	2500	0.054	0.066	0.084	0.090
3.56	321		0.054	0.068	0.082	0.091
7.13	324		0.065	0.090	0.079	0.129
11.75	325		0.074	0.114	0.180	0.188

This is consistent with the findings in other sand-biomass binary system as reported by various authors (Aznar et al., 1992; Mourad et al., 1994; Rao & Ram. Bheemarasetti, 2001; Sun et al., 2005)

The increase of palm shell mean sieve size in the binary mixture increases the effective particle diameter but the effective particle density remains constant since there is no change in the bed composition. According to Zhong et al. (2008), an increase in the effective particle diameter leads to an increase in the characteristic fluidization velocities in a sand-biomass binary mixture.

Effect of Palm Shell Weight Percent

As shown in Table 3-7, the increase of palm shell weight percent from 2 to 15 wt% increases both the U_{mf} and U_{cf} values in both of the compartments.

Table 3-7: U_{mf} and U_{cf} of sand d_p = 341 μm and palm shell of 11.75 mm.

Compartment	Combustor				Gasifier			
Palm shell (wt%)	2	5	10	15	2	5	10	15
d_m (μm)	353	372	407	445	(Same as combustor)			
ρ_m (kg/m^3)	2657	2597	2500	2411	(Same as combustor)			
U_{mf} (m/s)	0.084	0.095	0.100	0.106	0.116	0.122	0.138	0.166
U_{cf} (m/s)	0.087	0.102	0.111	0.127	0.167	0.166	0.180	0.258

It can be seen that the increase in the palm shell weight percent increases the effective particle diameter but decreases the effective particle density. However, the

percentage of increase in the effective particle diameter is higher than the percentage of decrease in the effective particle density.

Effect of Sand Size

An increase of sand mean particle size in the binary mixtures leads to an increase in the effective particle diameter with no change in the effective particle density. Consequently, one might expect that the characteristic fluidization velocities would show the tendency to increase with the increase of the sand mean particle size as observed above. As shown in Table 3-8, there is a tendency for the U_{mf} and U_{cf} to increase with the increase in the sand mean particle size.

Table 3-8: U_{mf} and U_{cf} values of palm shell of 7.13 mm at 5 wt% in sand.

Sand	Effective mixture properties		Characteristic fluidization velocities			
			Combustor		Gasifier	
d_p (μm)	d_m (μm)	ρ_m (kg/m^3)	U_{mf} (m/s)	U_{cf} (m/s)	U_{mf} (m/s)	U_{cf} (m/s)
272	297		0.057	0.072	0.081	0.098
341	372	2596	0.072	0.087	0.115	0.132
395	430		0.083	0.097	0.112	0.136

However, there is also a tendency for the U_{mf} and U_{cf} to decrease with the increase in the sand mean particle size as shown in Table 3-9 for the palm shell of 11.75 mm at 10 wt% in the binary mixtures.

Table 3-9: U_{mf} and U_{cf} values of palm shell of 11.75 mm at 10 wt% in sand.

Sand	Effective mixture properties		Characteristic fluidization velocity			
			Combustor		Gasifier	
d_p (μm)	d_m (μm)	ρ_m (kg/m^3)	U_{mf} (m/s)	U_{cf} (m/s)	U_{mf} (m/s)	U_{cf} (m/s)
272	325		0.082	0.114	0.180	0.191
341	407	2500	0.099	0.111	0.138	0.180
395	471		0.082	0.097	0.124	0.167

The different tendencies for the U_{mf} and U_{cf} observed in Tables 3-8 and 3-9 may be due to the greater contribution of particle-particle interaction of the sand in the binary mixture in attaining fluidization. To elucidate this effect, the characteristic fluidization velocities from Tables 3-8 and 3-9 are represented in Tables 3-10 and 3-11 in terms of dimensionless velocity ratios, i.e. $\left(\frac{U_{mf}}{U_{mf,sand}}\right)$ and $\left(\frac{U_{cf}}{U_{cf,sand}}\right)$ where the denominators are the characteristic fluidization velocities of pure sand.

Table 3-10: Dimensionless velocity ratios for palm shell of 7.13 mm at 5 wt%.

Sand	Dimensionless velocity ratios			
	Combustor		Gasifier	
d_p (μm)	$\left(\frac{U_{mf}}{U_{mf,sand}}\right)$	$\left(\frac{U_{cf}}{U_{cf,sand}}\right)$	$\left(\frac{U_{mf}}{U_{mf,sand}}\right)$	$\left(\frac{U_{cf}}{U_{cf,sand}}\right)$
272	1.08	1.12	1.05	1.13
341	0.99	1.02	1.13	1.13
395	1	0.93	1.06	1.12

Table 3-11: Dimensionless velocity ratios for palm shell of 11.75 mm at 10 wt%.

Sand	Dimensionless velocity ratios			
	Combustor		Gasifier	
d_p (μm)	$\left(\frac{U_{mf}}{U_{mf,sand}}\right)$	$\left(\frac{U_{cf}}{U_{cf,sand}}\right)$	$\left(\frac{U_{mf}}{U_{mf,sand}}\right)$	$\left(\frac{U_{cf}}{U_{cf,sand}}\right)$
272	1.55	1.78	2.34	2.20
341	1.36	1.31	1.35	1.54
395	0.99	0.93	1.16	1.38

In fact, both Tables 3-10 and 3-11 show that the dimensionless velocity ratios tend to reduce with the increase of the sand mean particle size from 272 to 395 μm. These patterns are observed in all the experiments with more noticeable downward trend for the largest palm shell mean sieve size and/or weight percent.

Figures 3-9 and 3-10 show the dimensionless velocity ratios for the different sand mean particle sizes in the combustor for the palm shell mean sieve size of 7.13 and 11.75 mm respectively from 5 to 15 wt%. Data for mixtures consist of palm shell at 2 wt% are not included since their characteristic fluidization velocities generally do not vary appreciably from the pure sand values.

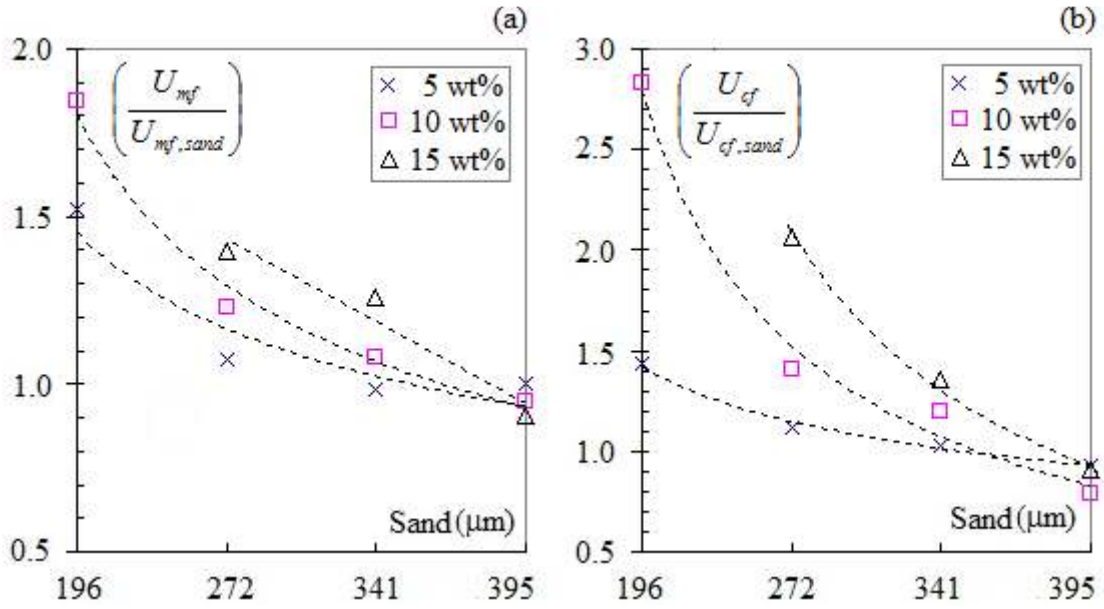

Figures 3-9(a) and 3-9(b): Dimensionless velocities ratios in the combustor for different sand mean particle sizes; palm shell of 7.13 mm at 5 to 15 wt%.

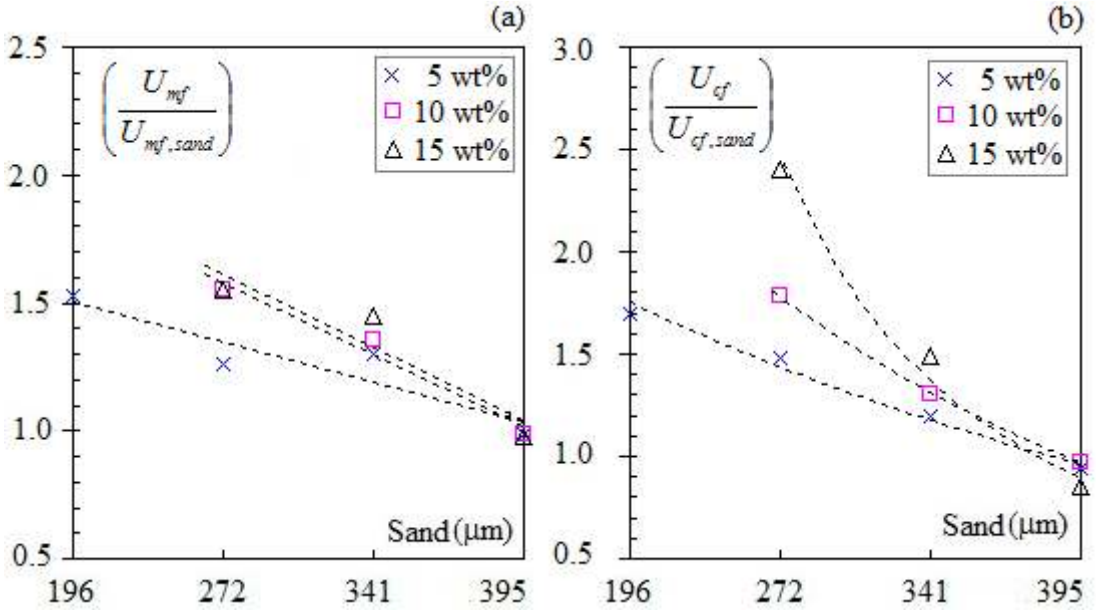

Figures 3-10(a) and 3-10(b): Dimensionless velocities ratios in the combustor for different sand mean particle sizes; palm shell of 11.75 mm at 5 to 15 wt%.

As observed in Figures 3-9 and 3-10, the $\left(\frac{U_{mf}}{U_{mf,sand}}\right)$ and $\left(\frac{U_{cf}}{U_{cf,sand}}\right)$ ratios not only reduce with the increase in the sand mean particle size, but also approach unity for the largest sand mean particle size in the combustor. The dimensionless velocity ratios also decrease with the decrease of palm shell weight percent. Similar trends are observed in the gasifier, although they are not as profound as those observed in the combustor.

Gauthier et al. (1999) suggested that the decreasing difference between U_{mf} and U_{cf} can be considered as the result of increasing particle-particle interaction (fine-to-large particle collision) in achieving fluidization. Figures 3-11(a) and 3-11(b) illustrate the U_{cf}/U_{mf} ratio for the combustor and gasifier respectively for the different sand mean particle sizes with the palm shell mean sieve size of 7.13 mm at 5 to 15 wt%.

For the combustor, Figure 3-11(a) indicates that the U_{cf}/U_{mf} ratios generally reduce and approach unity with the increase of the sand mean particle size for all the palm shell weight percent and thus, indicating a greater contribution of the particle-particle interaction.

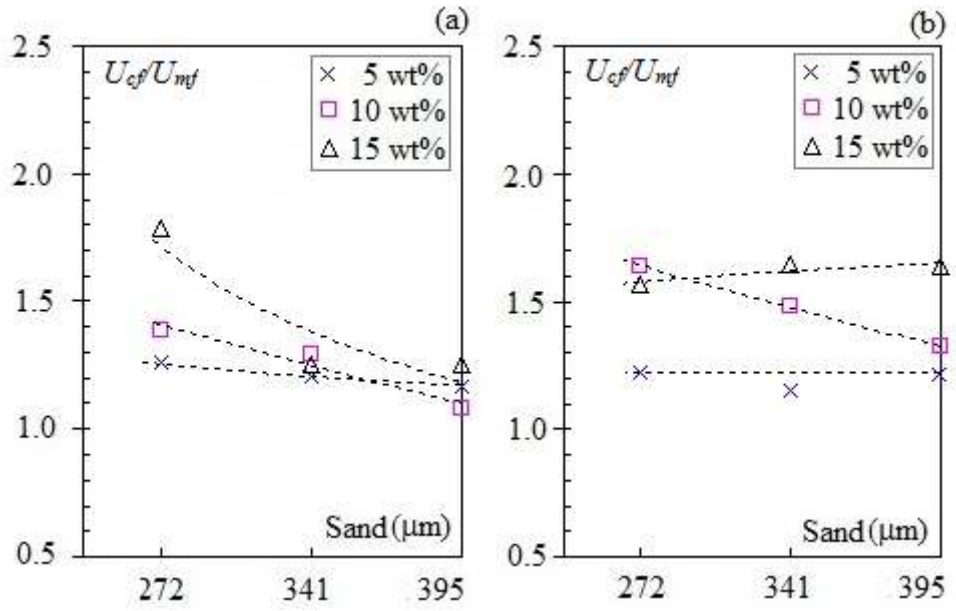

Figures 3-11: U_{cf}/U_{mf} ratio in the (a) combustor and (b) gasifier for different sand mean particle size; palm shell mean sieve size of 7.13 mm at 5 to 15 wt%.

Similar trends are reported by Aznar et al. (1992) for the different sand-biomass mixtures studied in cylindrical columns.

However, this is not the case for the gasifier. Figure 3-11(b) shows that the U_{cf}/U_{mf} ratio is unaffected by the increase of the sand mean particle size for the palm shell of 5 wt%. With palm shell of 10 wt%, the U_{cf}/U_{mf} ratio reduces with the increase in the sand mean particle size, a tendency similar to that obtained in the combustor. In contrast, at 15 wt% of palm shell, it is observed that the U_{cf}/U_{mf} ratio tends to increase, but relatively small, with the increase of the sand mean particle size. The different U_{cf}/U_{mf} trends in the combustor and gasifier may probably be due to the additional effect of the effective bed diameter.

For a binary system, the difference between U_{mf} and U_{cf} tends to diminish for a bed of well-mixed solid (Li et al., 2005). It can be seen that the sand mean particle size of 272 μm in the binary mixture generally has the highest U_{cf}/U_{mf} ratio. The subject on the mixing behavior of the sand-palm shell mixture will be discussed in Chapter 4.

In summary, for the binary mixture, it is found that the characteristic fluidization velocities for the gasifier are always larger than those observed in the combustor. These results are consistent with the trends obtained for the single component (sand) system discussed earlier.

The characteristic fluidization velocities exhibit the tendency to increase with the increase of the palm shell mean sieve size and weight percent in both the compartments.

When a larger sand mean particle size is used in the binary mixture, the analysis of the $\left(\frac{U_{mf}}{U_{mf,sand}}\right)$ and $\left(\frac{U_{cf}}{U_{cf,sand}}\right)$ ratio in both compartments shows that the characteristic fluidization velocities for the binary mixture approach its pure sand values. Besides that, the U_{cf}/U_{mf} ratios decrease and approaching unity with the increase in the sand mean particle size in the combustor. This is also observed in the gasifier but only for specific composition of the binary mixture.

3.4.4 MINIMUM AND COMPLETE FLUIDIZATION VELOCITY CORRELATIONS

The U_{mf} and U_{cf} values for the sand-palm shell mixtures are determined using common methods employed for the multi-components systems. These allow comparative studies to be carried out from the various published correlations reviewed in Chapter 2.

Three U_{mf} correlations are selected for comparison with the present experimental U_{mf} values, namely correlation from Goosens et al. (1971) developed from Equation (2-5)[f], Equation (2-11) from Thonglimp et al. (1984) and Equation (2-12) from Mourad et al. (1994).

Three U_{cf} correlations are also chosen, namely correlation from Noda et al. (1986) developed from Equation (2-5)[g] as well, Equation (2-16) from Mourad et al. (1994) and Equation (2-17) from Rao and Ram Bheemarasetti (2001).

In Figures 3-12 and 3-13, it can be seen that all the U_{mf} and U_{cf} correlations are generally able to describe the qualitative variation of the characteristic fluidization velocities for the sand-palm shell binary mixtures, i.e. the correlations are able to show the increasing or decreasing U_{mf} and U_{cf} trends consistent with the experimental data.

[f] The particle density and size described in Equation (2-5) are replaced with effective particle density and size estimated based on Equation (2-9) and Equation (2-10) respectively.

[g] The constants, C_1 and C_2 described in Equation (2-5) are replaced by Equation (2-13) and Equation (2-15) respectively. Besides that, the particle density and size described in Equation (2-5) are estimated based on Equation (2-9) and Equation (2-10) respectively.

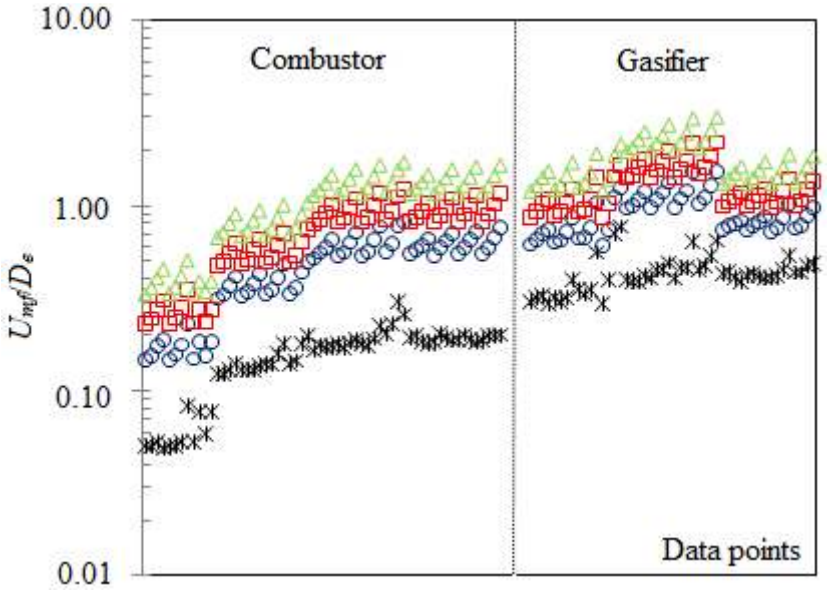

Figure 3-12: Comparison of present experimental data as U_{mf}/D_e in common logarithm scale with different correlations; ✳Present experimental data, □correlation by Goosens et al. (1971), △ Equation (2-11) and ○Equation (2-12).

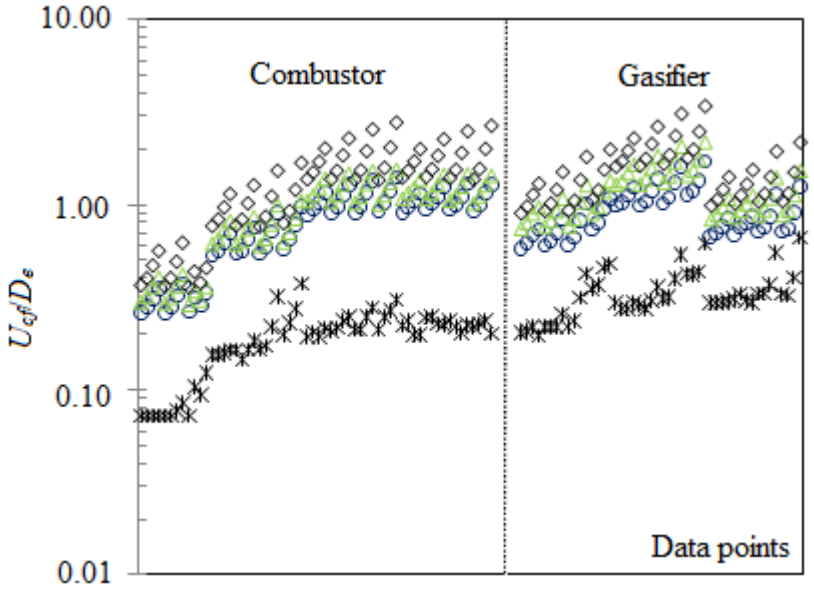

Figure 3-13: Comparison of present experimental data as U_{cf}/D_e in common logarithm scale with different correlations; ✳ Present experimental data, △ correlation by Noda et al. (1986), ○Equation (2-16) and ◇Equation (2-17).

However, quantitatively, the correlations are unsatisfactory as they mostly over-estimated these values. As shown in Figure 3-14, none of the selected binary U_{mf} correlations can predict satisfactory for all the sand-palm shell binary system. Similar observed in Figure 3-15, no U_{cf} correlations can give satisfactory prediction.

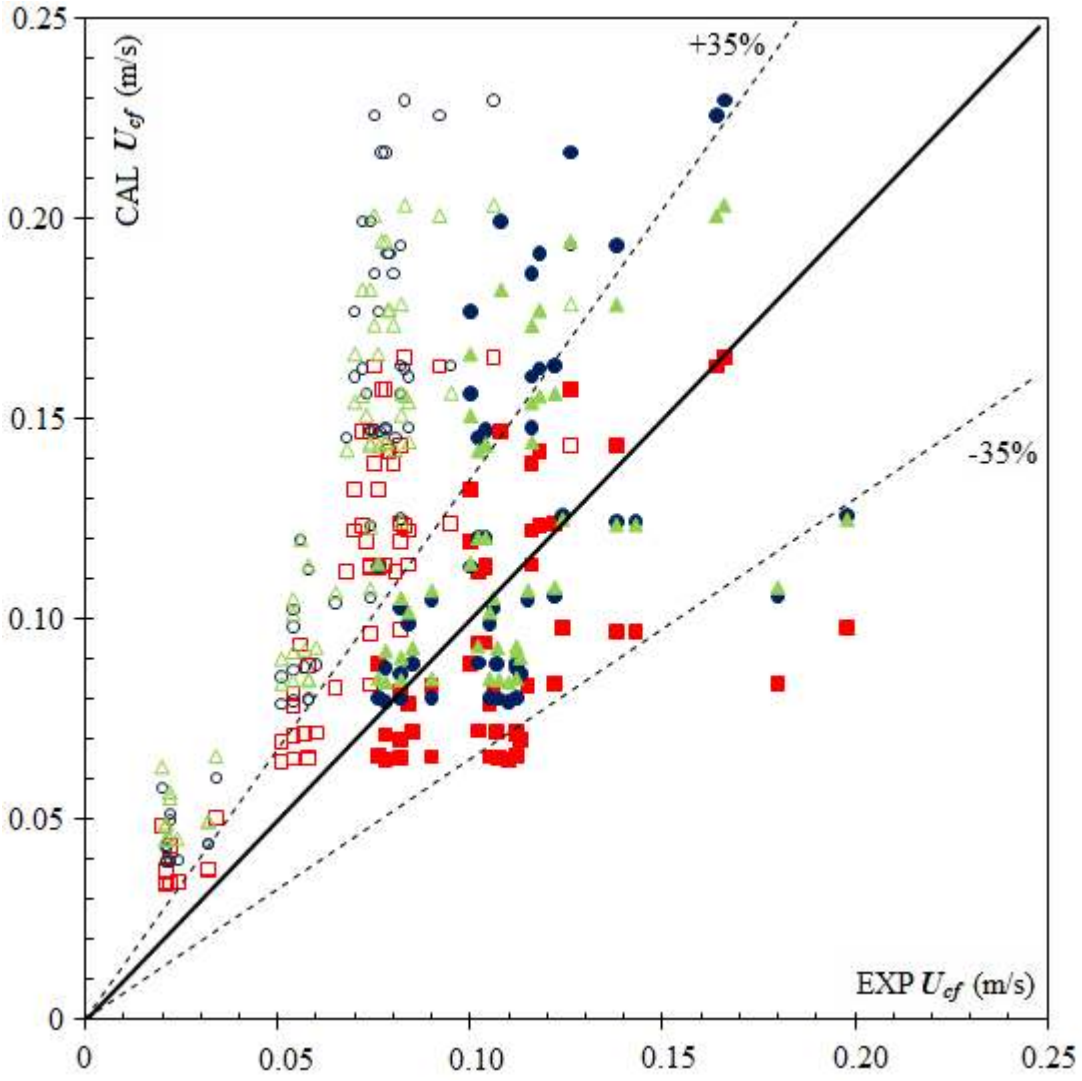

Figure 3-14: Comparison of the present experimental (EXP) data and calculated (CAL) U_{mf} with different correlations; Open and close symbols represent data for the combustor and gasifier respectively; □ ■ correlation by Goosens et al. (1971), △ ▲ Equation (2-11) and ○ ● Equation (2-12).

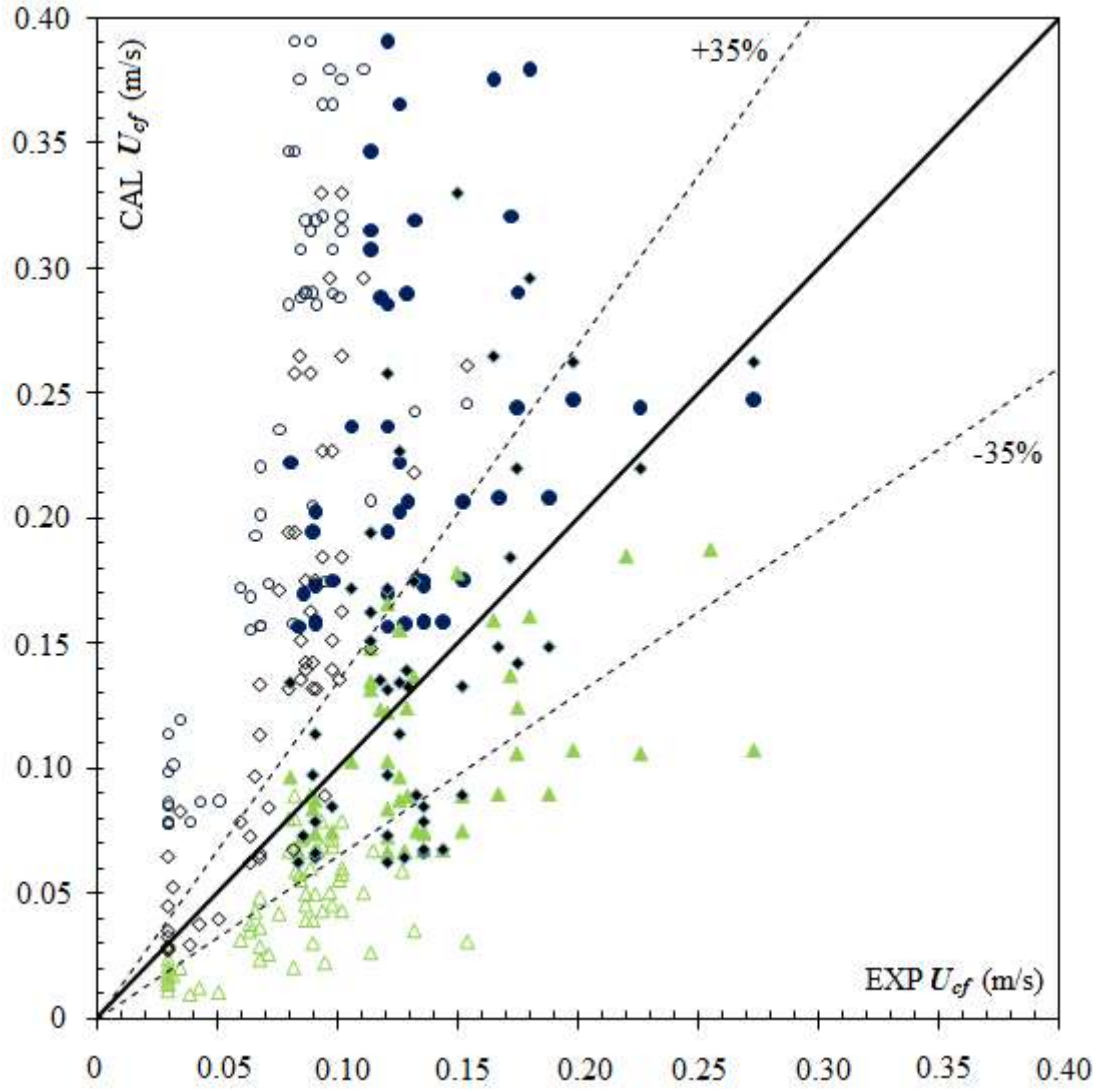

Figure 3-15: Comparison of present experimental data (EXP) and calculated (CAL) U_{cf} with different correlations; Open and close symbols represent data for the combustor and gasifier respectively; △▲ correlation by Noda et al. (1986), ○● Equation (2-16) and ◇◆ Equation (2-17).

Although for a specific palm shell size and sand, experimental U_{mf} or U_{cf} can be fitted into a semi-empirical equation, no correct equation that can correlate all the data has been found. Aznar et al. (1992), Cui and Grace (2007) concluded that none of the existing correlations are able to give reliable predictions for sand-biomass mixtures.

3.4.5 CRITICAL LOADING

It is recognized that there are some instances where the characteristic fluidization velocities for the binary mixture remain nearly unchanged from the pure sand values.

Aznar et al. (1992a, 1992b) reported similar findings for mixtures of agricultural and forest residues with a second fluidized solid.

The regime of constant U_{mf} and U_{cf} values can be observed in both of the compartments, and can be established depending on the sand mean particle size, palm shell mean sieve size and weight percent. Two typical experimental U_{mf} and U_{cf} plots for various palm shell mean sieve sizes and weight percent are used to illustrate the existence of this regime in the combustor and gasifier respectively.

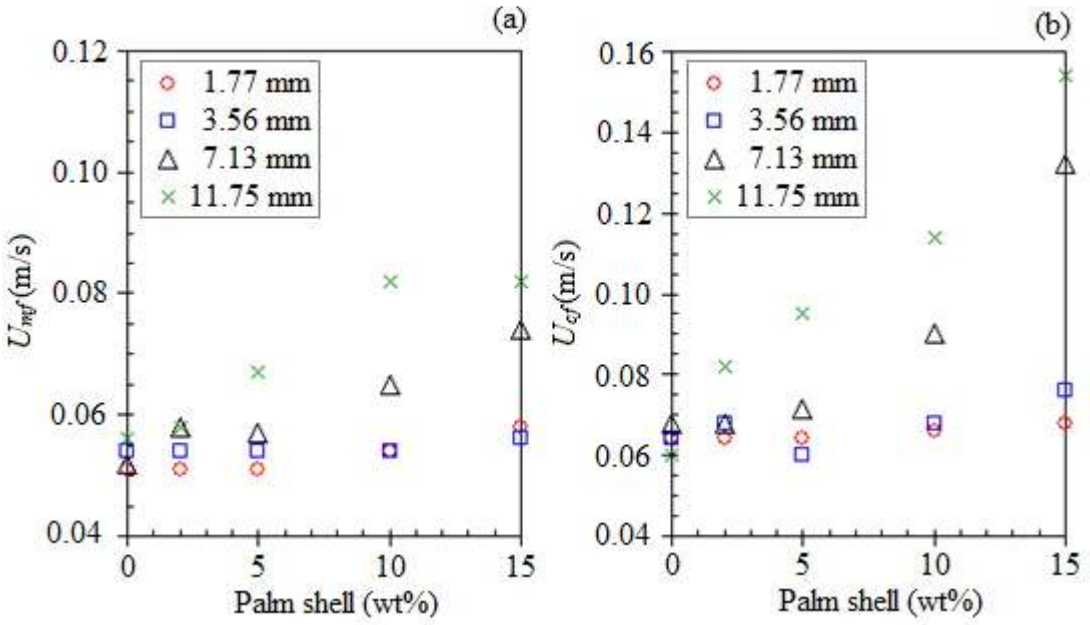

Figures 3-16: (a) U_{mf} and (b) U_{cf} in the combustor; sand d_p = 272 μm and palm shell of various mean sieve sizes and weight percent.

Figures 3-16(a) and 3-16(b) show the U_{mf} and U_{cf} values in the combustor for the different palm shell mean sieve sizes and weight percent in the sand of 272 μm. It can be seen that for the palm shell mean sieve size of 1.77 mm, both the U_{mf} and U_{cf} values remain unchanged from the pure sand values. Similarly, for the palm shell mean sieve size of 3.56 mm, the U_{mf} values remain unaffected from 2 to 15 wt% of

palm shell while the U_{cf} value increases only at 15 wt%. For the palm shell mean sieve size of 7.13 mm, both the characteristic fluidization velocities increase at ≥ 10 wt%. For the largest palm shell mean sieve size of 11.75 mm, the U_{mf} increases with palm shell at 5 wt% onwards while U_{cf} increases when the palm shell is of ≥ 2 wt%.

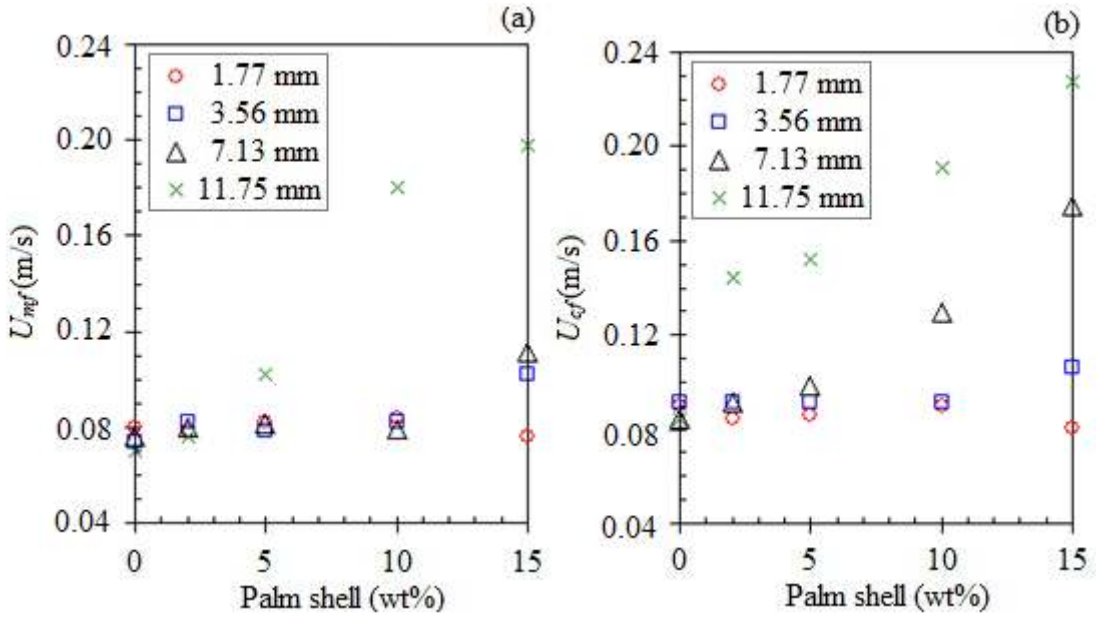

Figures 3-17: (a) U_{mf} and (b) U_{cf} in the gasifier; sand d_p = 272 μm and palm shell of various mean sieve sizes and weight percent.

Figures 3-17(a) and (b) illustrate another U_{mf} and U_{cf} plots respectively for the gasifier for the binary mixture with the sand mean particle size of 272 μm. As shown in these figures, the U_{mf} and U_{cf} values generally remain unaffected with the addition of palm shell mean sieve size of 1.77 and 3.56 mm in the sand, except at the highest palm shell weight percent of 15 wt%. For the palm shell mean sieve size of 7.13 mm, the U_{mf} increases only at the highest palm shell weight percent of 15 wt%, while the U_{cf} shows an upward trend for the palm shell of ≥ 10 wt%. For the largest palm shell mean sieve size, the U_{mf} shows significant increase when the palm shell weight percent is increased to ≥ 5 wt%, while the U_{cf} increase at ≥ 2 wt% of palm shell.

It is desirable to establish the regime of constant U_{mf} and U_{cf} values since the characteristic fluidization velocities for the binary mixtures can be determined using bed material properties made up from entirely pure sand values (not requiring the estimation of the effective mixture properties).

Accordingly, the concept of "critical loading" is introduced as the maximum palm shell content (mean sieve size and weight percent) that can be present in the sand where the U_{mf} and U_{cf} for the binary mixtures are nearly the same as its pure sand values. The characteristic fluidization velocities of the pure sand and binary mixture are considered identical when their variations are within ±15%.

Table 3-12 and 3-13 show the palm shell critical loading in the combustor and gasifier respectively. Generally, the critical loading increases with the decrease of palm shell mean sieve size or with the increase of sand mean particle size. For the palm shell mean sieve size of 1.77 mm, up to 15 wt% of palm shell can be present in the mixture with any sand mean particle sizes. On the other hand, the largest sand mean particle size (i.e. 395 μm) has the highest critical loading.

Table 3-12: Palm shell critical loading in weight percent (wt%) in the combustor for U_{mf} and U_{cf} (the first value refers to U_{mf} and the second value refers to U_{cf}).

Sand	Palm shell mean sieve size (mm)			
d_p (μm)	1.77	3.56	7.13	11.75
196	15/15	10/5	2/2	2/-[h]
272	15/15	15/10	5/5	2/-[h]
341	15/15	15/10	10/5	2/2
395	15/15	15/15	15/15	15/10

Table 3-13: Palm shell critical loading in weight percent (wt%) in the gasifier for U_{mf} and U_{cf} (the first value refers to U_{mf} and the second value refers to U_{cf}).

Sand	Palm shell mean sieve size (mm)			
d_p (μm)	1.77	3.56	7.13	11.75
272	15/15	10/10	10/5	2/-[h]
341	15/15	10/10	10/5	2/-[h]
395	15/15	15/15	10/10	5/5

[h] No critical loading is found.

3.5 SUMMARY

The baseline study using common inert material showed that the fluidization behaviour for the single component (sand) system in the compartmented reactor was similar to those observed in a cylindrical column with $U_{cf} > U_{mf}$, U_{mf} and U_{cf} increasing with the increase of sand mean particle size, and the characteristic fluidization velocities for the gasifier (of a smaller effective bed diameter) were larger than those of the combustor.

The differences in the characteristic fluidization velocities between the compartments can be minimized by utilizing the larger sand mean particle size as a bed material, hence avoiding physical modification on the CFBG.

The existing correlations were modified to predict satisfactorily the U_{mf} and U_{cf} for the sand in both the compartments.

The methodologies (the fast and slow defluidization) for the single component have been implemented for the sand-palm shell binary mixtures in the compartmented reactor. The bed pressure drop profiles provide useful insight on the fluidization behaviour (whether it is fully or partially fluidized bed) and are used to determine the U_{mf} and U_{cf} for the binary mixtures.

In the gasifier, the U_{mf} and U_{cf} for the binary mixtures are found to be larger than that of the combustor. This is consistent with the findings for the single component (sand) system.

It is found that the characteristic fluidization velocities for the binary mixture have the tendency to increase with the increase in the palm shell mean sieve size and weight percent.

When the larger sand mean particle size is used in the binary mixture, the analysis on the $\left(\frac{U_{mf}}{U_{mf,sand}}\right)$ and $\left(\frac{U_{cf}}{U_{cf,sand}}\right)$ ratios revealed the trends of reducing the ratios and approaching unity in both the compartments.

The concept of the "critical loading" is introduced for the binary mixture to characterise the maximum palm shell content (size and weight percent) in the sand where the characteristic fluidization velocities for the binary mixtures values are determined principally by the pure sand values. The critical loading is found to increase with the increase in the sand mean particle size and with the decrease in the palm shell mean sieve size.

Within the regime of the critical loading, the proposed U_{mf} and U_{cf} correlations, namely Equation (3-3) and (3-4) respectively for the sand can be applied for the binary mixtures in both the compartments.

It is important to note that, within the critical loading, a single operating superficial velocity (U) can be set for the respective compartment based on the pure sand value and this is independent on the variation of the palm shell size and weight percent in the mixtures (especially during combustion or gasification process). Ultimately, the state of fluidization (e.g. bubbling or vigorously fluidized) and the mixing quality in each compartment, that depend on the relative magnitude of the operating superficial velocity and characteristic fluidization velocities (e.g. U/U_{mf}) can be identified and maintained.

CHAPTER 4

MIXING QUALITY

4.1 INTRODUCTION

The attainment of the constant bed pressure drop values as described earlier is imperative for determining the characteristic fluidization velocities. Although this implies that the fluidized bed is fully supported by the fluidizing gas, it does not necessary mean that a good mixing quality is established, since the local composition may differ significantly from point-to-point in the bed. This non-uniformity affects the fluidized bed by contributing to undesirable operational problems such as weak/hot spot, ash agglomeration and product variations.

A binary system (e.g. sand-palm shell mixture) exhibits segregation tendency because of the difference in their particle properties, namely size and/or density. This is due to the variation of their respective drag forces when subjected to flowing gas, and the interaction forces between the particles. The degree of segregation/mixing depends on the operation and the geometrical parameters of the fluidized bed. Hence, it is the purpose of this chapter to study the mixing profiles of sand-palm shell binary mixture in different bed sections of the combustor and the gasifier, and also to determine the operational superficial velocity that produces good overall mixing quality and its dependency on particle properties and bed geometrical parameters.

4.2 DEFINITION OF MIXING QUALITY

Due to the complex CFBG geometry, it seems to be reasonable to estimate the local mixing quality in terms of the local mixing index (m) in different locations throughout the compartments (the combustor and the gasifier).

Analogous to Equation (2-21), the local mixing index (m) is defined as

$$m = x/X \tag{4-1}$$

where x is the local palm shell mass concentration (weight percent in the sample), and X is the palm shell loaded in weight percent. m = 1 represents perfect mixing, while segregation may lead to two conditions, either "dilution" (m < 1) or accumulation (m > 1).

The overall mixing quality (M) is determined as

$$M = 1 - \left(\frac{1}{n}\right)\sum_{i=1}^{n}\left|\left(\frac{x_i - X}{X}\right)\right| \tag{4-2}$$

where "n" is the number of sampling locations throughout the bed.

M = 1 and M < 1 correspond to perfect mixing and segregation respectively. For convenience, the condition of purely segregation when M < 0 is taken as zero.

It is assumed that a portion or the whole fluidized bed to be of good mixing quality when m = 1.00 ± 0.15 or M = 0.85÷1.00 respectively.

4.3 METHODOLOGY

The sand-palm shell mixing studies are performed using the experimental setup as described in the preceding chapter. The bed materials used are the sand mean particle size of 272 μm and palm shell of 3 mean sieve sizes namely 1.77, 3.56 and 7.13 mm comprising of 2, 5, 10 and 15 wt%. The sand mean particle size is selected based on the overall highest U_{cf}/U_{mf} ratio as discussed in Chapter 3. Depending on the compartment, the operating superficial velocity (U) is varied from 0.069 to 0.159

m/s; these values also corresponded to different magnitude of U/U_{mf} or U/U_{cf} ratio where the characteristic fluidization velocities have been previously determined. All the experiments are conducted at constant total bed weight of 77 kg, except for the study on the effect of the bed height on the mixing quality.

Prior to the experiments, the sand is filled into the respective compartments to a desired weight/height. The compartments are tapped until the sand is compacted. Palm shells are then uniformly loaded on the top of the sand bed forming two segregated layers. This approach is selected to track palm shell migration and it also represents top-bed feeding.

Starting from the fixed bed state, the experiments are initially performed by increasing the superficial velocity in the specified range. Once the maximum superficial velocity is achieved, the experiments are then continued by decreasing the superficial velocity. These procedures allow samples to be taken in two directions i.e. at increasing and decreasing superficial velocities. It exemplifies the typical mode of operation in a bubbling fluidized bed combustor/gasifier where the operating superficial velocity is initially increased to promote fuel mixing during the plant startup (Basu, 2006); as the fluidized bed reaches a higher bed temperature e.g. 800÷900°C, the operating superficial velocity is reduced to about 1/3 of the requirement at the ambient condition (Yan, 1995).

Sampling method

The conventional "freezing" method as described by Rowe and Nienow (1976) for determining local solid concentration in fluidized bed is very time consuming and may not be suitable for particle size ratio greater than 6.45 (present mixture is of about 5÷53) where spontaneous percolation occurs (Scott & Bridgewater (1975)).

A preferred approach is to use an end-sampling "thief" probe, which has the following advantages: (i) fast response (ii) able to collect sample while the bed is fluidized (iii) able to collect sample at different locations in the bed, and (iv) able to collect several samples under various operating conditions.

The end-sampling "thief" probe is imbedded vertically into the fluidized bed at a set

location. A sampling container (commonly known as the end-cup sampler), located at the end of the probe, is initially at closed position during the insertion into the fluidized bed. Once insertion is complete, its enclosure cap is opened allowing solids to flow into the end-cup sampler. It is then closed and the probe is withdrawn from the bed. The collected mixtures are sieved and weighed to determine the component weight fraction. Once measured, the mixtures are returned to the fluidized bed for the subsequent sampling exercise.

However, just as in any invasive techniques, this method has several inherent shortcomings. The insertion of the sampling probe may interfere with the flow pattern and/or the solid may flow unevenly into the opening of the end-cup sampler.

To minimize these shortcomings, the thief probe and the end-cup sampler sizes are kept to the minimum. Here, the thief probe is made of a thin rectangular plate of 25 mm wide and 2 mm thick. The cylindrical end-cup sampler is of 50 x 50 mm in diameter and length respectively, i.e. large enough for the solid to enter but small when compared to the compartment diameter. The enclosure cap of the end-cup sampler is manoeuvred by a 2 mm ID rod.

In addition, solid samples are collected from 3 different columns and in 3 different rows respectively constituting 9 sampling locations (n) as shown in Figure 4-1, in contrast to measuring the local solid concentration only in a fixed location (top/bottom section). By increasing the sampling locations systematically throughout the bed will give a better representative data.

Meanwhile, 3 repetitive data are collected from each cell, with the sampling interval of 5 minutes each, to allow for re-establishment of mixing state after the previous sampling. Shen et al. (2007) and Zhang (2008) observed that equilibrium mixing in fluidized bed is attained within 1 minute.

The sampling weight measurement has the accuracy of ±0.005%. A total of 1,809 data points are collected in all the experiments where about 90% is within ±15% of standard deviation. This shows that the data collected by this method is reproducible (the remaining data has the maximum standard deviation of 32%).

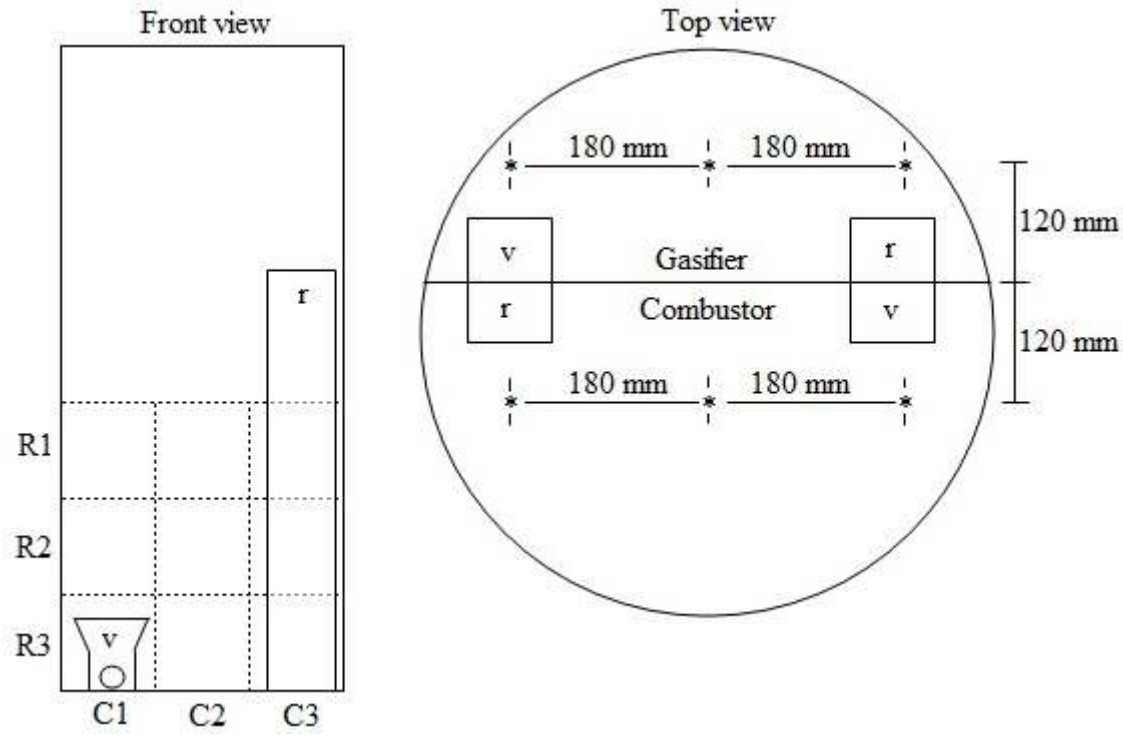

Figure 4-1: Sampling locations (R, C, v and r are referred as to row, column, V-valve and riser respectively; '*' represents the entry points of the sampling probe).

4.4 PALM SHELL, A FLOTSAM OR JETSAM?

For a binary system differing in both particle density and size, the larger and denser component tends to sink (as *jetsam*) while the smaller and lighter component tends to float (as *flotsam*) forming two segregated parts. Although the palm shell to sand particle size ratio is relatively large, the bulk density of the sand can be the determining factor on whether palm shell is a *flotsam* or *jetsam* (refer to Table 2-1).

A simple calculation using a typical value of incipient bed voidage for sand of 0.40 (Kunni & Levenspiel, 1991) corresponds to a bulk density of 1620 kg/m^3, which is greater than the palm shell particle density (1500 kg/m^3). The guideline in Table 2-1 suggests that palm shell is a *flotsam*. As shown later, this is consistent with the findings in the studies of palm shell vertical and lateral distribution at various operating superficial velocity.

4.5 PALM SHELL LOCAL MIXING QUALITY

4.5.1 VERTICAL AND LATERAL DISTRIBUTION IN THE COMBUSTOR

Palm Shell Vertical Distribution in the Combustor

Figures 4-2 to 4-4 show the typical palm shell vertical distribution at various superficial velocities in the combustor. Data on the mixing quality is presented graphically such that the deviation of the perfect mixing line (m = 1) indicates segregation. The data is based on the palm shell mean sieve size of 1.77 mm at 10 wt% in the sand of 272 µm. Hence, the maximum m index is 10 if the collected sample is purely palm shell. The palm shell content in this mixture is within the critical loading as it was found in the preceding chapter. The operating superficial velocity (U) ranges from 0.069 to 0.133 m/s that corresponds to 1.30÷2.50 U/U_{mf} (or 1.08÷2.08 U/U_{cf}).

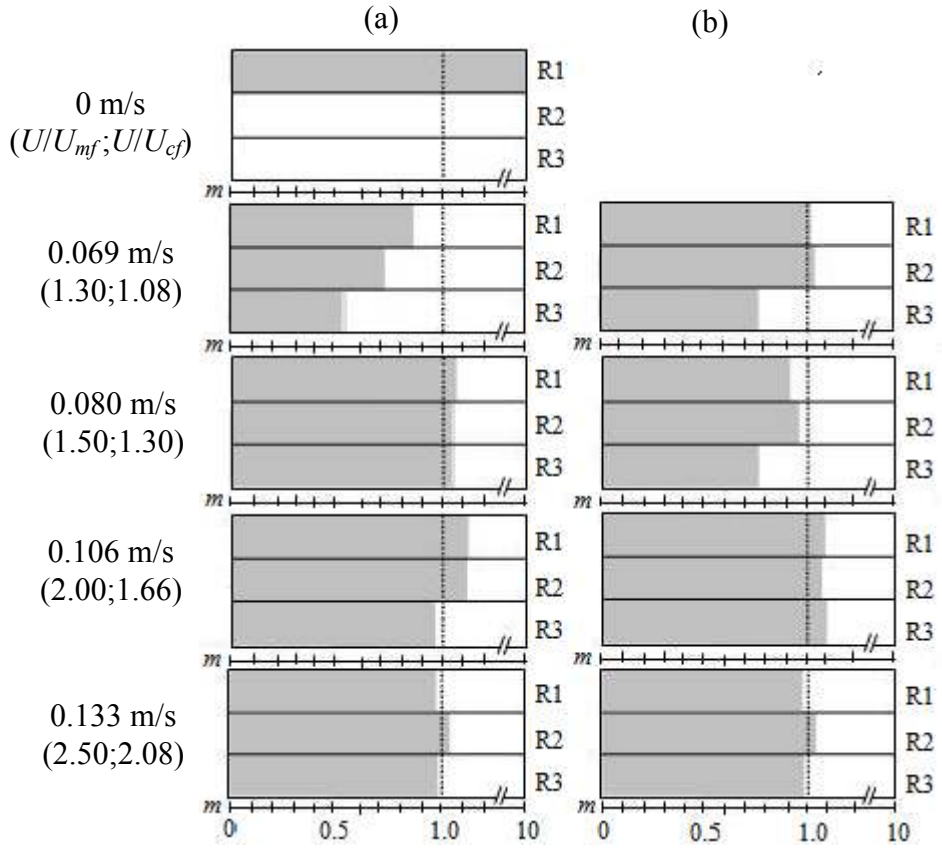

Figure 4-2: Palm shell vertical distribution in the combustor, column C1; (a) Increasing, and (b) decreasing superficial velocity.

Figure 4-2 shows the palm shell vertical distribution in column C1. In Figure 4-2(a), starting from a fixed bed condition (at $U = 0$), the palm shell is initially stacked uniformly on the bed surface. By increasing the superficial velocity to 1.3 U/U_{mf}, the palm shell sank to the lower region of the bed. The downward movement of the palm shell is due to the fluidized sand percolating through the palm shell voidage enabling the biomass to fall to the lower bed section. In addition, on the bed surface, bubble formation is visible although at a lesser degree, as compared to the bed center. As the superficial velocity increases further to 1.5 U/U_{mf} onwards, a good local mixing quality is established.

It is known that an increase in the operating superficial velocity increases the number and size of bubbles in the fluidized bed. This results in greater bubble motions and solid flow circulation leading to a good mixing quality (Lu et al. (2007)).

Starting from a mixed fluidized bed, column C1 is in good mixing quality when decreasing the superficial velocity from 2.5 U/U_{mf} to 2.0 U/U_{mf} as shown in Figure 4-2(b). Further reduction from 1.5 U/U_{mf} to 1.3 U/U_{mf} leads to m index of 0.75÷1.0 in the three different rows.

From the experiments, it can be seen in Figure 4-2(a) and 4-2(b) that the palm shell local concentration tends to be lower in the bed bottom as compared to the middle/upper bed layer. This means that the palm shell tends to be *flotsam* in the binary mixture. Similar trends are also observed in columns C2 and C3 in the combustor, as shown later in Figures 4–3 and 4–4 respectively.

Figure 4-3 shows the palm shell vertical distribution in the middle column, C2 at various superficial velocities using the same bed material. The local mixing profile similar to that in Figure 4-2 can be seen at increasing and decreasing the superficial velocities as depicted in Figures 4-3(a) and 4-3(b) respectively.

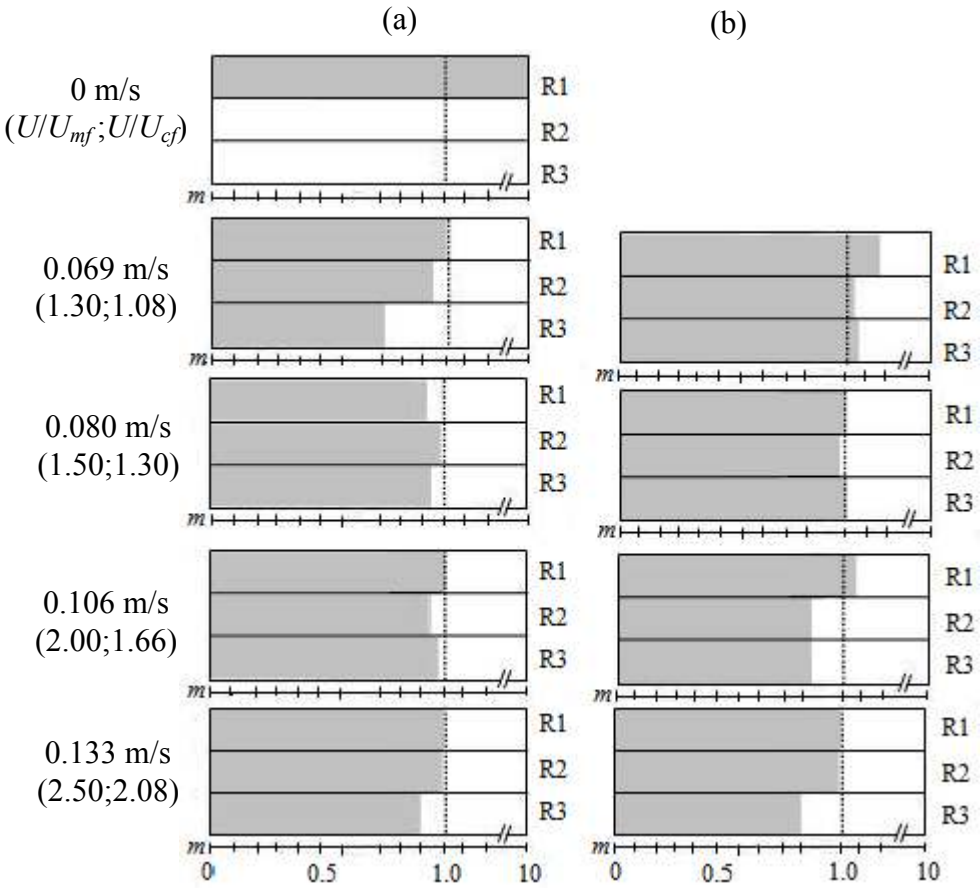

Figure 4-3: Palm shell vertical distribution in the combustor, column C2; (a) Increasing, and (b) decreasing superficial velocity.

The relatively better local mixing quality as compared to column C1 (and column C3, as shown later in Figure 4-4) is due to the absence of V-valve or/and riser in the middle column of the fluidized bed. Good local mixing quality is achieved at increasing and decreasing superficial velocities in the range of 1.5÷2.5 U/U_{mf}.

Figure 4-4 shows palm shell vertical distribution in the column C3. In Figure 4-4(a), at increasing superficial velocity from 1.3 to 1.5 U/U_{mf}, although the palm shell submerged to the bed bottom, the palm shell concentration is considerably above those observed in columns C1 and C2. The presence of the riser in column C3 has resulted in greater restriction of the palm shell movement, leading to the biomass accumulation. A good local mixing quality is obtained at 2.0 U/U_{mf}. At 2.5 U/U_{mf}, the m index is ranging from 0.8 to 1.0 across rows R3 to R1.

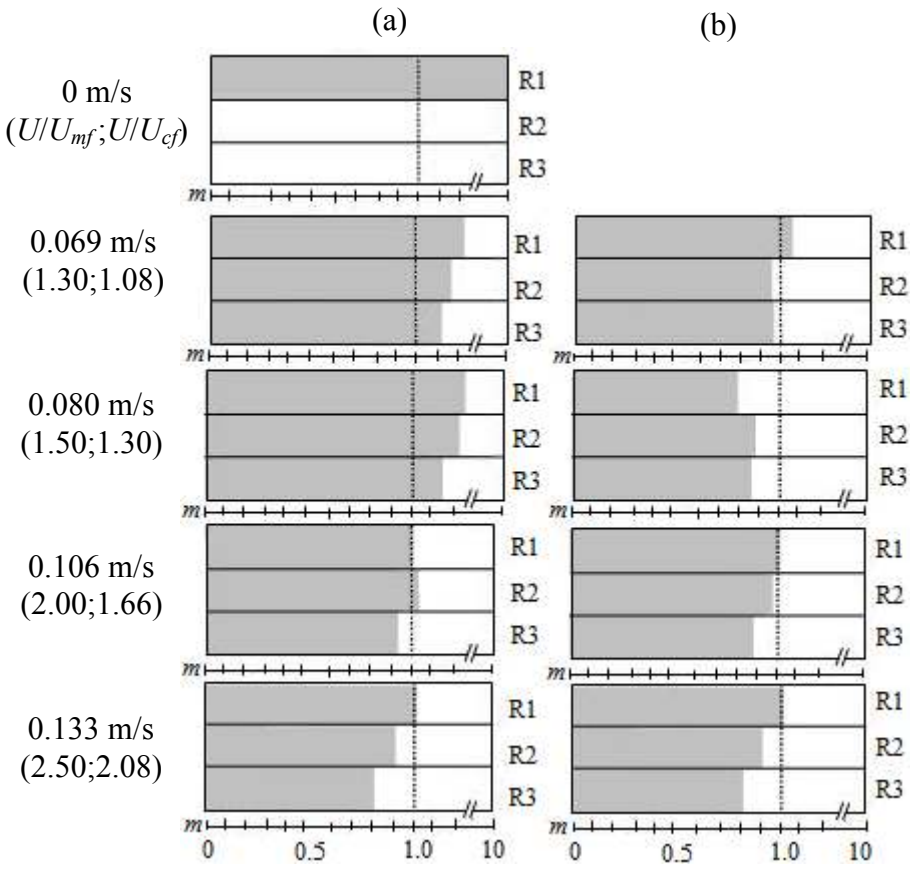

Figure 4-4: Palm shell vertical distribution in the combustor, column C3; (a) Increasing, and (b) decreasing superficial velocity.

When decreasing the superficial velocity, Figure 4-4(b) shows that the good local mixing quality is maintained at the specific superficial velocity, i.e. at 2.0 and 1.3 U/U_{mf}. At 2.5 and 1.5 U/U_{mf}, m index is in the range of 0.75 to 1.0 in three different rows. Meanwhile, the local mixing index generally decreases from the top to the bottom bed at increasing and decreasing superficial velocities.

Palm Shell Lateral Distribution in the Combustor

Binary mixing can occur in the vertical and lateral directions. Figures 4-5 to 4-7 show the typical palm shell lateral distribution in 3 different rows, R1 to R3 at various superficial velocities in the combustor. Data on mixing is presented graphically such that the deviation of the perfect mixing line (m = 1) indicates segregation. The data is also based on the palm shell mean sieve size of 1.77 mm at 10 wt% in the sand of 272 μm.

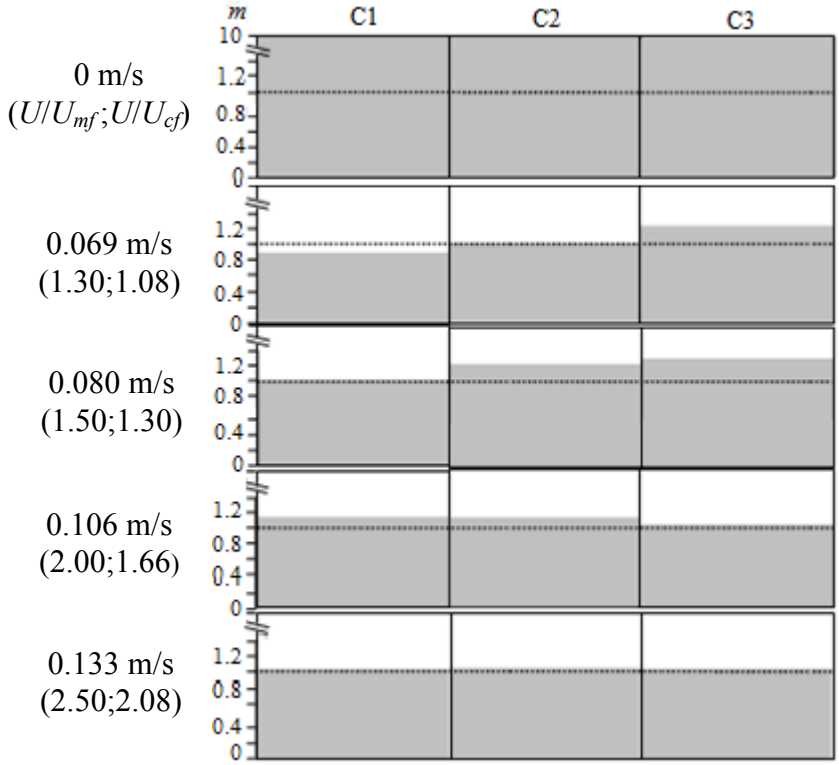

Figure 4-5(a): Palm shell lateral distribution in the combustor, row R1 at increasing superficial velocity.

In Figure 4-5(a), starting from a fixed bed condition, palm shell is initially loaded on the sand where m = 10 in row R1. At 1.3 U/U_{mf}, since palm shell is submerged below the bed surface when fluidized resulting the m index in the range of 0.86÷1.23 for columns C1 to C3. At 1.5 U/U_{mf}, m index is in the range of 1.00÷1.20 across the three columns.

Visually, it is observed that the lateral mixing of the palm shell in the row R1 is due to the bubble eruptions dispersing the biomass on the bed surface. However, the presence of the riser that is extended up to the bed surface leads to the palm shell build-up (in column C3). Correspondingly, at the low superficial velocity of 1.30 and 1.50 U/U_{mf}, the local mixing index increases laterally from columns C1 to C3. As shown later, this is also observed in rows R2 and R3. A good local mixing quality is established at 2.0 U/U_{mf} onwards.

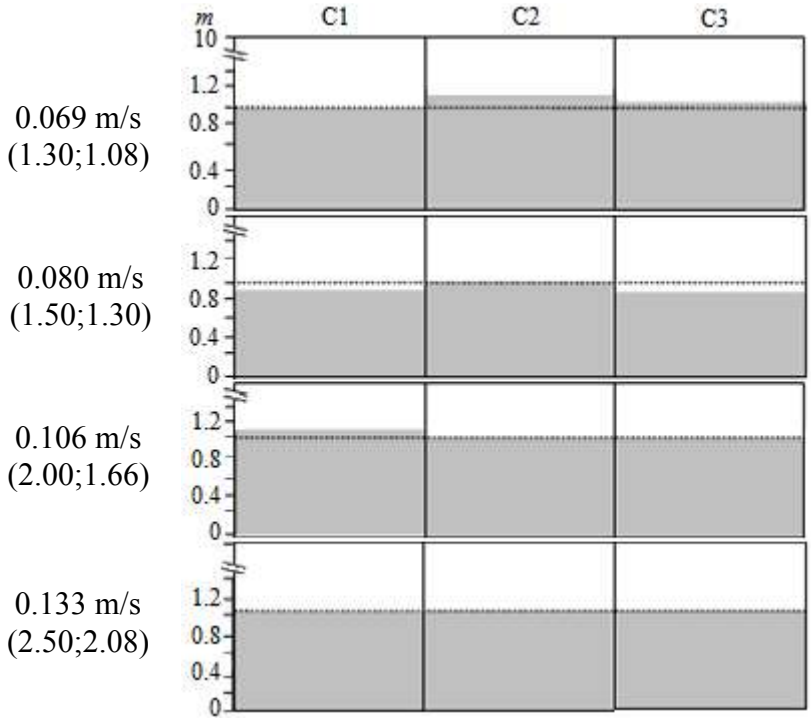

Figure 4-5(b): Palm shell lateral distribution in the combustor, row R1 at decreasing superficial velocity.

Once the bed is well mixed, as shown in Figure 4-5(b), the good local mixing quality in row R1 is maintained at the decreasing superficial velocity from 2.5 to 1.3 U/U_{mf}.

Figure 4-6(a) shows $m = 0$ in row R2 at the initial fixed bed condition. At 1.3 U/U_{mf}, the local mixing index increases in the range of 0.72÷1.10 in columns C1 to C3. Further increase of the superficial velocity to 1.5 U/U_{mf} changes the m index to the range of 1.00÷1.20 across the three columns. At 2.0 U/U_{mf} onwards, a good local mixing quality is achieved.

Figure 4-6(b) shows that at decreasing superficial velocity from 2.5 to 1.3 U/U_{mf}, minor local variation of palm shell concentration is observed where the mixing index decreases laterally from columns C1 to C3, but the bed remains to be in good local mixing quality ($m = 1.00 \pm 0.15$).

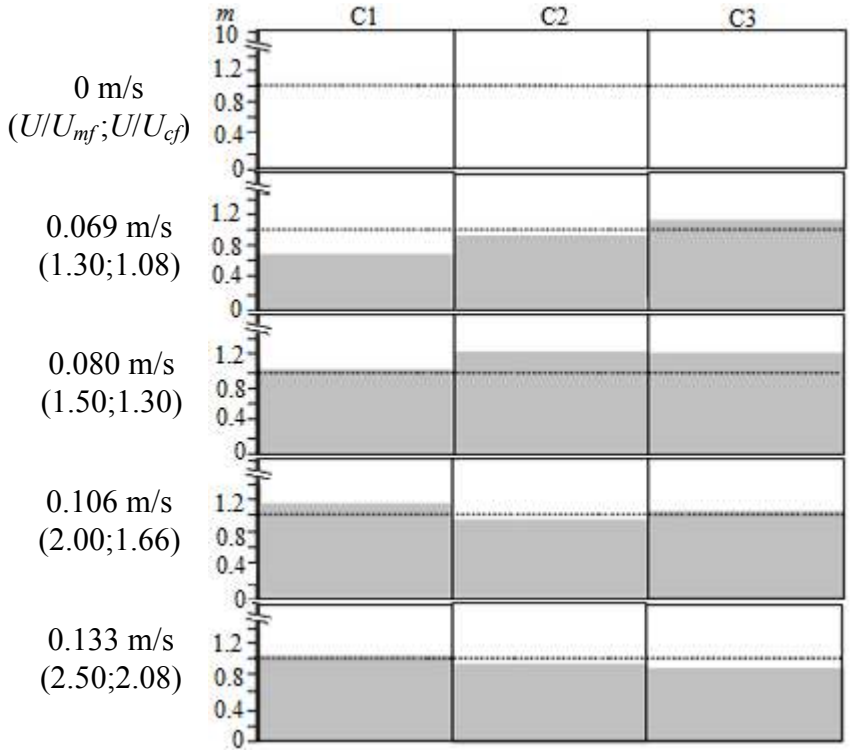

Figure 4-6(a): Palm shell lateral distribution in the combustor, row R2 at increasing superficial velocity.

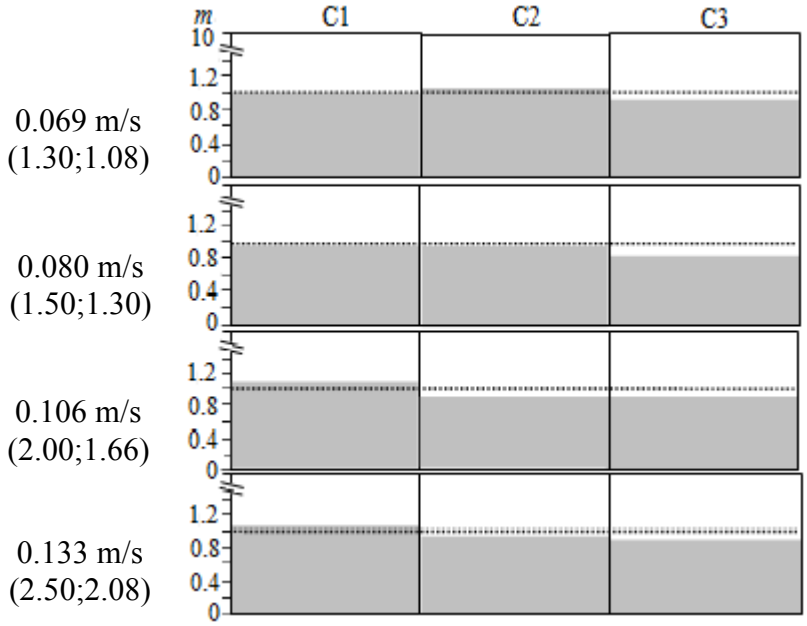

Figure 4-6(b): Palm shell lateral distribution in the combustor, row R2 at decreasing superficial velocity.

The presence of the riser (in column C3) as a bed internal has two opposite effects on the palm shell lateral distribution. The palm shell dispersion due to bursting bubbles leads to the accumulation of the biomass in the riser section as described earlier. On

the other hand, the smaller cell volume in column C3 corresponds to the higher local superficial velocity when compared to columns C1 and C2. Accordingly, large particles such as palm shell could be swept upwards more intensively due to greater bubble activity, since the increase in the superficial velocity also increases the average bubble size.

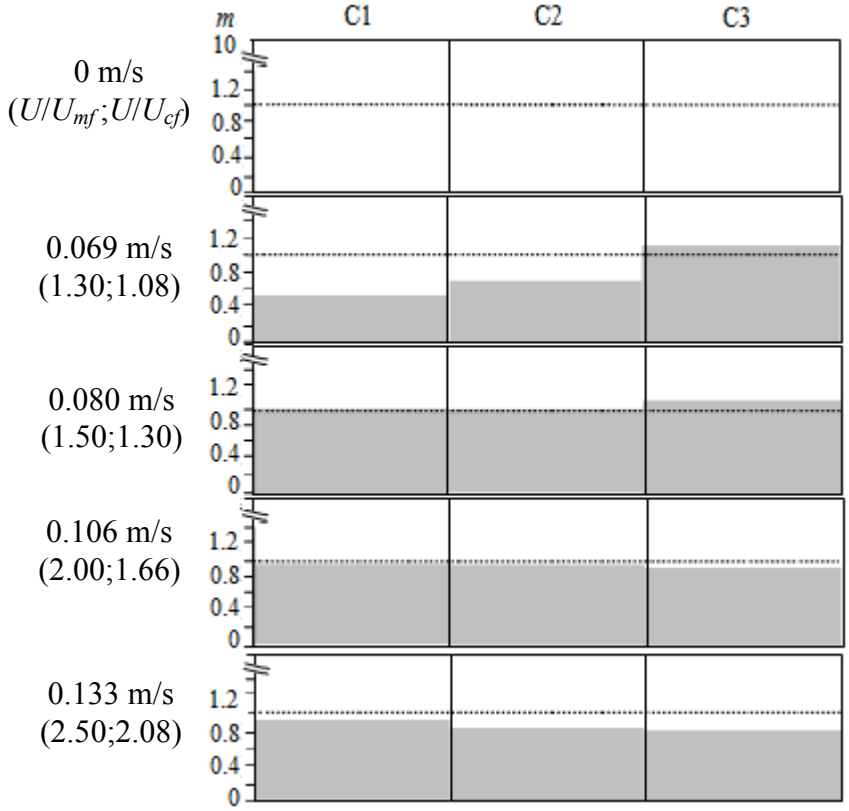

Figure 4-7(a): Palm shell lateral distribution in the combustor, row R3 at increasing superficial velocity.

Row R3 is the region nearest to the distributor. As indicated in Figure 4-7(a), starting from a fixed bed condition with m = 0, the local mixing index increases to the range of 0.50÷1.10 across columns C1 to C3 at 1.3 U/U_{mf}. A good local mixing quality is attainable at 1.5 and 2.0 U/U_{mf}. At 2.5 $U/U_{mf,}$ m = 0.80÷0.90 from columns C3 to C1. This is due to the fact that at the distributor, bubbles formation is intensified with higher excess gas velocity providing extra "upward push" to the palm shell.

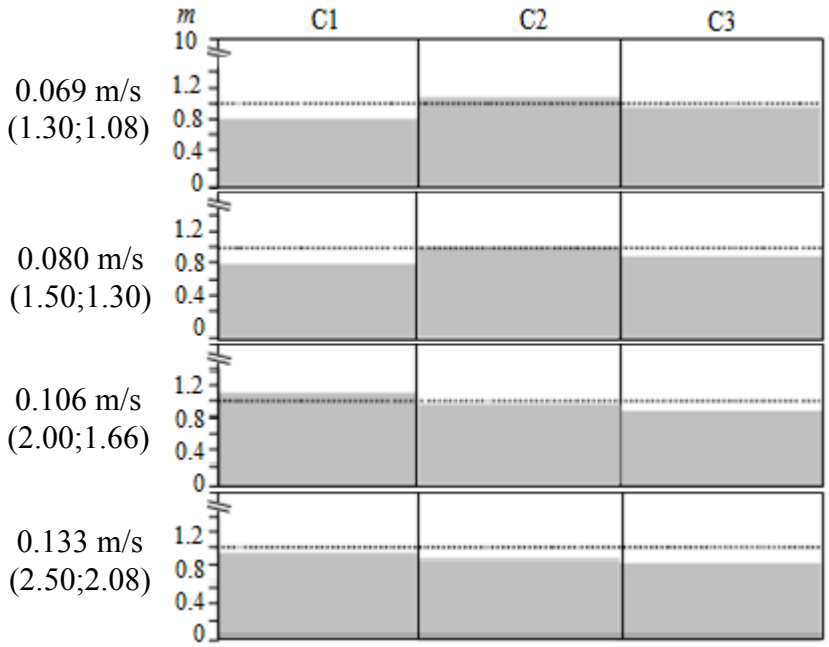

Figure 4-7(b): Palm shell lateral distribution in the combustor, row R3 at decreasing superficial velocity.

Once the bed is mixed, good local mixing quality is achieved only at 2.0 U/U_{mf} as shown in Figure 4-7(b). In the other operating superficial velocity, the local mixing index is in the range of 0.80÷1.10 in the three columns. Similar to that observed in row R2, the local mixing index decreases laterally from columns C1 to C3 at higher superficial velocity, i.e. at 2.0 and 2.5 U/U_{mf}.

4.5.2 VERTICAL AND LATERAL DISTRIBUTION IN THE GASIFIER

Palm Shell Vertical Distribution in the Gasifier

Figures 4-8 to 4-10 show the typical palm shell vertical distribution at various superficial velocities in the gasifier. Similar to the combustor, the binary mixture is also based on the palm shell mean sieve size of 3.56 mm and at 10 wt% in sand of 272 µm, which is within the critical loading. The operating superficial velocity (U) is in the range of 0.069÷0.159 m/s. This corresponds to the U/U_{mf} ratio of 0.90÷2.06 (or U/U_{cf} ratio of 0.79÷1.83).

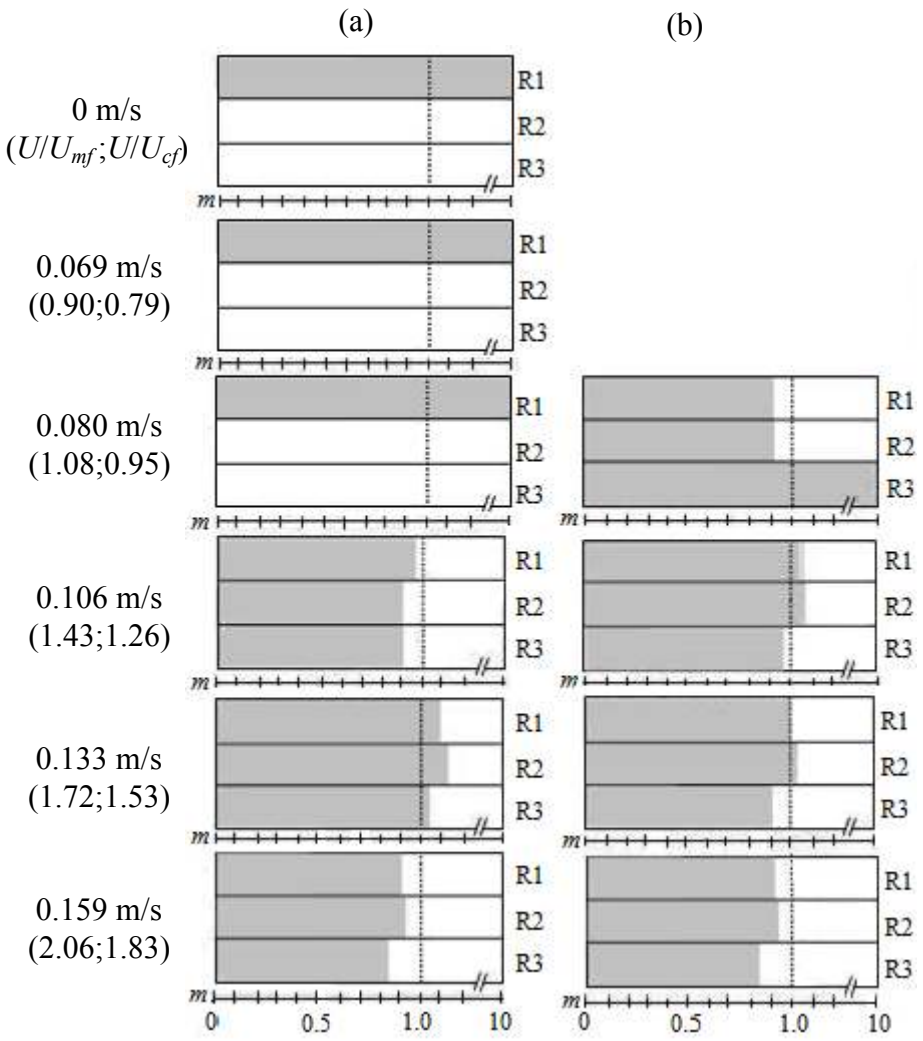

Figure 4-8: Palm shell vertical distribution in the gasifier, column C1; (a) Increasing, and (b) decreasing superficial velocity.

Figure 4-8 shows the palm shell vertical distribution in the first column, C1. In Figure 4-8(a), starting from U = 0 m/s to U = 0.080 m/s, no vertical movement of the palm shell is observed; the palm shell remains on the bed surface. By increasing the superficial velocity to 0.106 m/s, which corresponds to 1.43 U/U_{mf} (or 1.26 U/U_{cf}), the palm shell is distributed to the lower section of the bed. A good local mixing quality is achieved from 1.43 to 2.06 U/U_{mf}.

Starting from a well-mixed bed, Figure 4-8(b) shows that the good local mixing quality is maintained when decreasing the superficial velocity from 2.06 to 1.43 U/U_{mf}.

From both Figures 4-8(a) and 4-8(b), it can be seen that the palm shell local concentration is lower at the bed bottom within the superficial velocity of 1.43÷2.06 U/U_{mf}. This finding is consistent with the observations in the combustor since palm shell tends to become *flotsam*.

At 1.08 U/U_{mf}, a condition below the U_{cf}, palm shell "chunks" can be visually observed at the bed bottom where the V-valve is located. Spout is formed right above the palm shell "chunks" which breaks down into bubbles at the upper tiers. This explains why the palm shell vertical dispersion (in rows R1 and R2) can still occur under this condition. At 0.90 U/U_{mf}, the bed is stagnant, hence sampling is not performed.

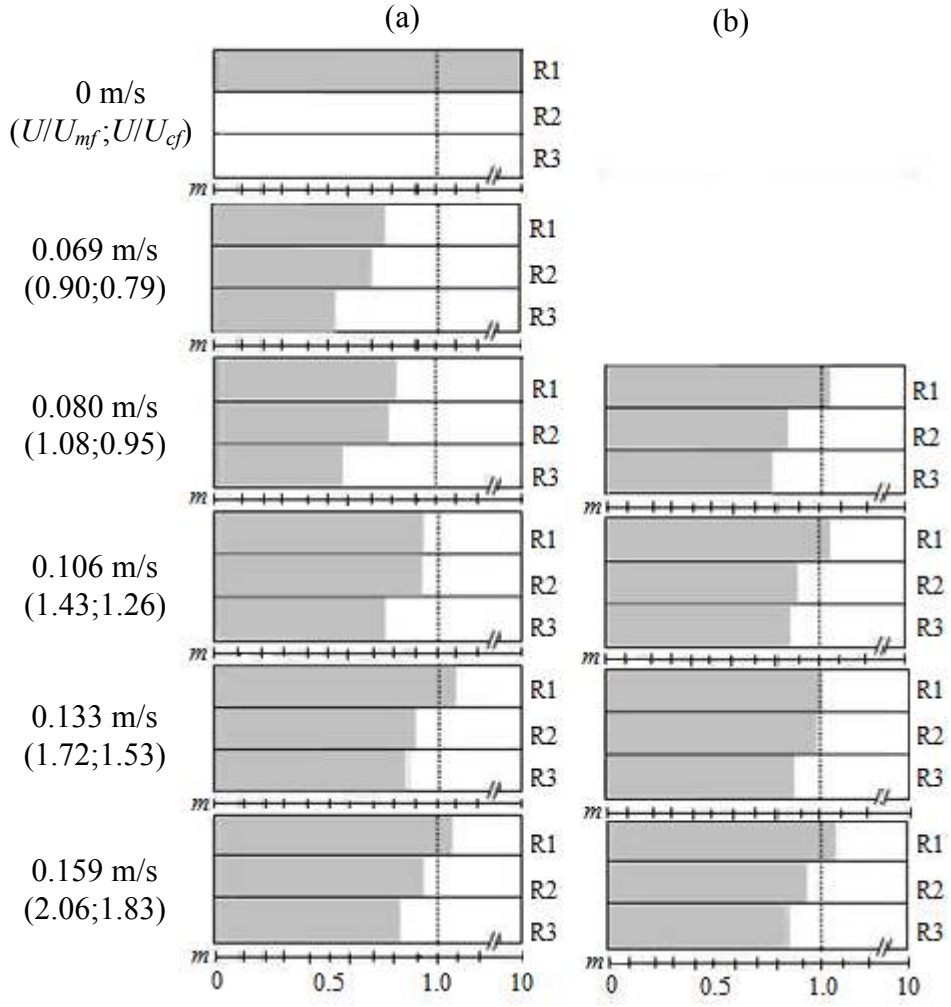

Figure 4-9: Palm shell vertical distribution in the gasifier, column C2; (a) Increasing, and (b) decreasing superficial velocity.

Figure 4-9 shows palm shell vertical distribution in the middle column, C2. At the point just before attaining the minimum fluidization velocity (i.e. at 0.90 U/U_{mf}) as shown in Figure 4-9(a), palm shell migration occurs due to gravity, where the biomass partially sinks to the bottom when the sand bed is expanded. This is in contrast to the findings in column C1 (and in column C3, as shown later in Figure 4-10) discussed above where the palm shell vertical movement was not observed until U_{mf} was achieved. This suggests that the bed section in column C2 is more expanded due to the absence of the V-valve and riser. Furthermore, when the superficial velocity is at 1.08 U/U_{mf}, it is visually observed that bubble eruptions on the bed surface occur only in column C2. It is noted that the palm shell that erupted from column C2 is due to the bursting bubbles which actually provided the additional biomass layer on the surface of columns C1 and C3.

At 1.43 U/U_{mf}, the local mixing index is in the range of 0.75÷0.90 from rows R3 to R1. A good local mixing quality is attained at 1.72 U/U_{mf}. At a higher superficial velocity of 2.06 U/U_{mf}, the *m* index is in the range of 0.80÷1.10 with the lowest value at the distributor (i.e. row R3).

When decreasing the superficial velocity from 1.72 to 1.43 U/U_{mf}, the good local mixing quality is maintained as shown in Figure 4-9(b). At 1.08 U/U_{mf}, the palm shell vertical dispersion can still occur where the local mixing index is of 0.78÷1.05 from rows R3 to R1. But, with further reduction of the superficial velocity to 0.90 U/U_{mf}, the bed becomes stagnant.

The local mixing index decreases downward from rows R1 to R3 when the superficial velocity is in the range of 1.08÷2.06 U/U_{mf}. This trend is observed in both increasing and decreasing superficial velocities, similar to that obtained in the combustor. Nonetheless, the local mixing index in column, C2 in general, and specifically at the distributor, is always lower than that observed in the combustor. This is probably due to the presence of a relatively higher excess gas velocity ($U-U_{mf}$) in the gasifier compared to the combustor, for the same operating superficial velocity ratio (U/U_{mf}). Consequently, more bubbles are formed and the larger bubble size could drag palm shell to the bed surface of the gasifier.

Figure 4-10 above depicts the palm shell vertical distribution in column C3. In Figure 4-10(a), m = 1.10÷1.30 for the superficial velocity ranging from 1.08 to 1.72 U/U_{mf}. A good local mixing quality is achieved at 2.06 U/U_{mf}.

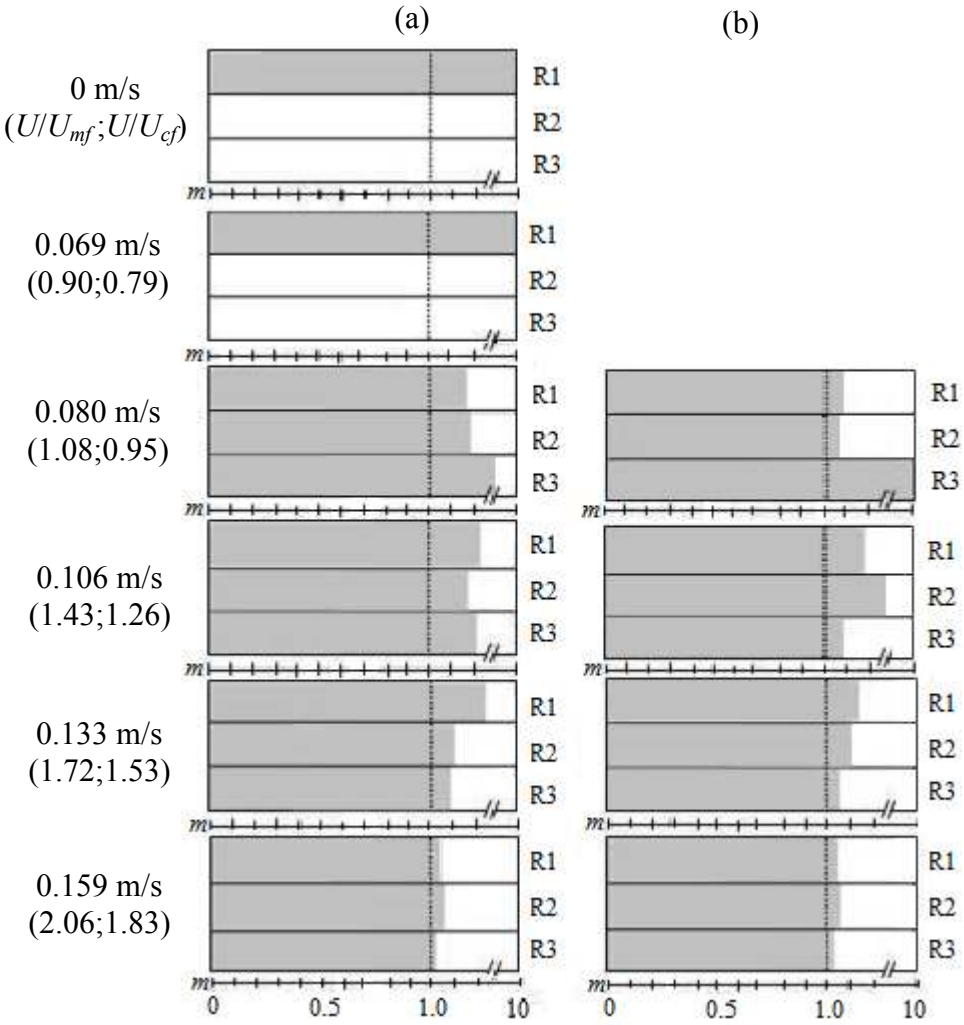

Figure 4-10: Palm shell vertical distribution in the gasifier, column C3; (a) Increasing, and (b) decreasing superficial velocity.

Once the bed is mixed, the good local mixing quality is maintained at the decreasing superficial velocity of 1.72÷2.06 U/U_{mf} as shown in Figure 4-10(b). When the superficial velocity is reduced further to 1.43 U/U_{mf}, the local mixing index becomes 1.10÷1.30 in the three rows. At 1.08 U/U_{mf}, similar to the findings in column C1 (refer to Figure 4-8), some portion of the palm shell is immobilized and turned into a passive distributor.

Palm Shell Lateral Distribution in the Gasifier

The palm shell lateral distribution in the gasifier is shown in Figures 4-11 to 4-13 in three different rows, R1 to R3 respectively. The data is also based on the palm shell mean sieve size of 1.77 mm at 10 wt% in sand particles of 272 µm.

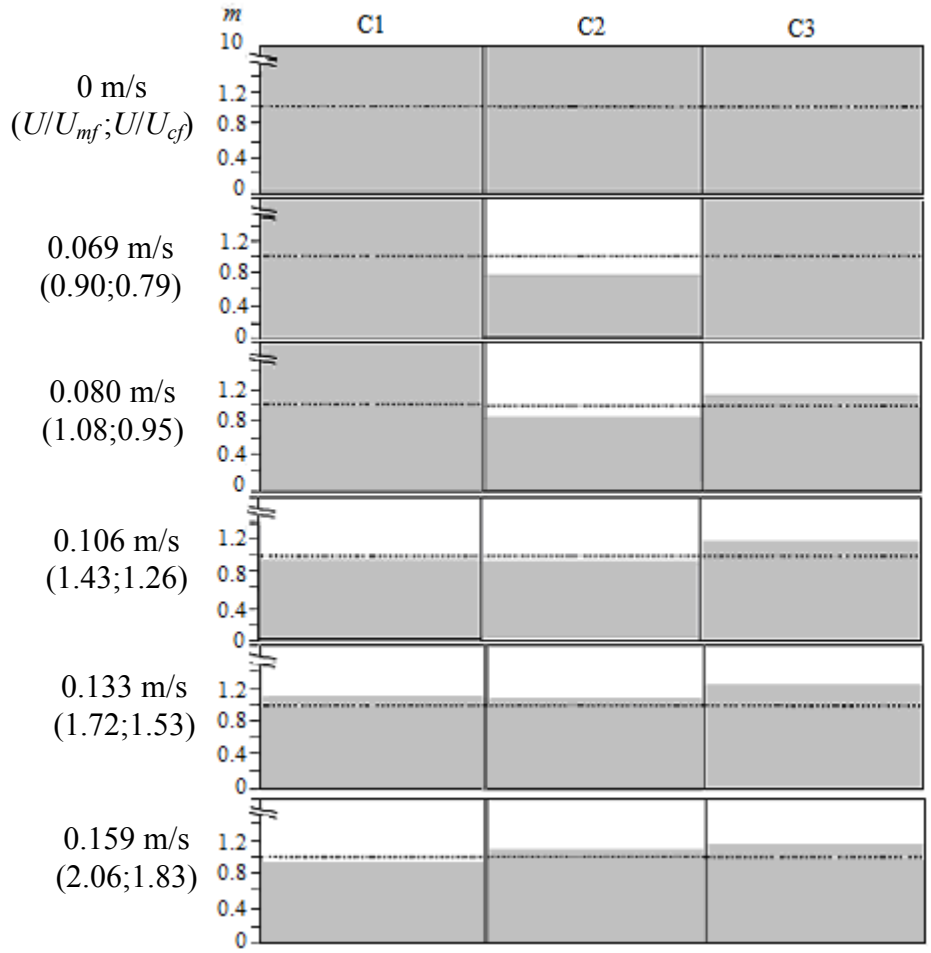

Figure 4-11(a): Palm shell lateral distribution in the gasifier, row R1 at increasing superficial velocity.

Figure 4-11 shows the palm shell lateral distribution in the first row, R1. At fixed bed condition, m = 10 as shown in Figure 4-11(a). At 0.90 U/U_{mf}, the change in the m index is due to the greater bed expansion in the middle column, C2 as described earlier. When the superficial velocity is at 1.08 U/U_{mf}, the bubble eruption observed in the middle column begins to disperse palm shell by ejecting them to the sides leading to its accumulation on the surface of columns C1 and C3. Due to the palm shell build-up in column C3 (where the cell volume is much smaller, being mainly occupied by the riser), the biomass begins to descend and disperse laterally. This

supports the fact that the local mixing index in column C3 is generally higher compared to columns C2 and C3 at higher superficial velocity. Similar trends are obtained for the palm shell lateral distribution in other rows as shown later in Figure 4-12 and 4-13. At superficial velocity of 1.43÷2.06 U/U_{mf}, m = 0.90÷1.20 across the three columns.

Similarly, starting from a mixed bed, the local mixing index is in the range of 0.90÷1.20 when reducing the superficial velocity from 2.06 to 1.08 U/U_{mf}, as depicted in Figure 4-11(b). Generally, the local mixing index increases laterally from columns C1 to C3 in both increasing and decreasing superficial velocities.

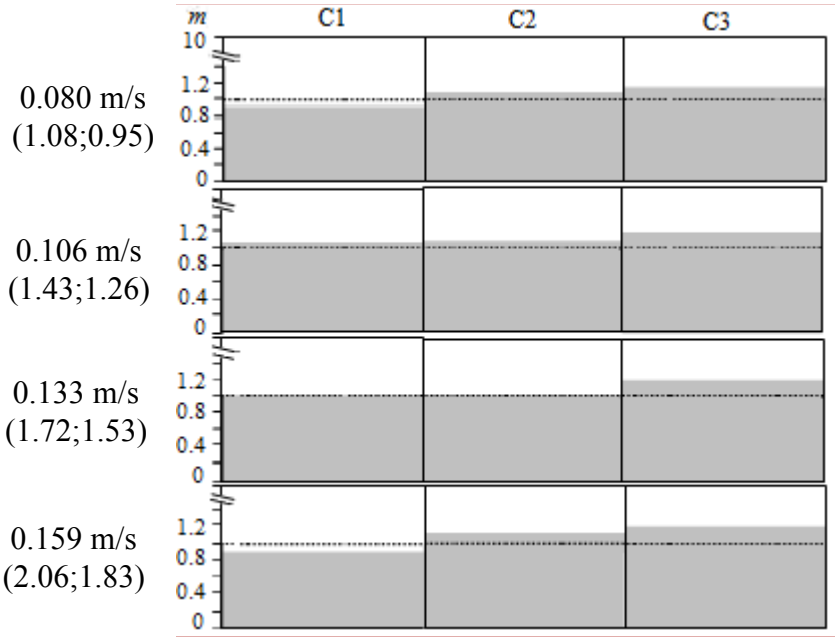

Figure 4-11(b): Palm shell lateral distribution in the gasifier, row R1 at decreasing superficial velocity.

Figure 4-12 shows the palm shell lateral distribution in the middle row, R2 of the gasifier. As shown in Figure 4-12(a), when the operating superficial velocity is below the complete fluidization velocity (or 0.90÷1.08 U/U_{mf}), the palm shell is observed only in specific columns C2 and/or C3. However, with further increase in superficial velocity from 1.43 U/U_{mf} onwards, the palm shell is dispersed in all the columns and the bed is in good local mixing quality.

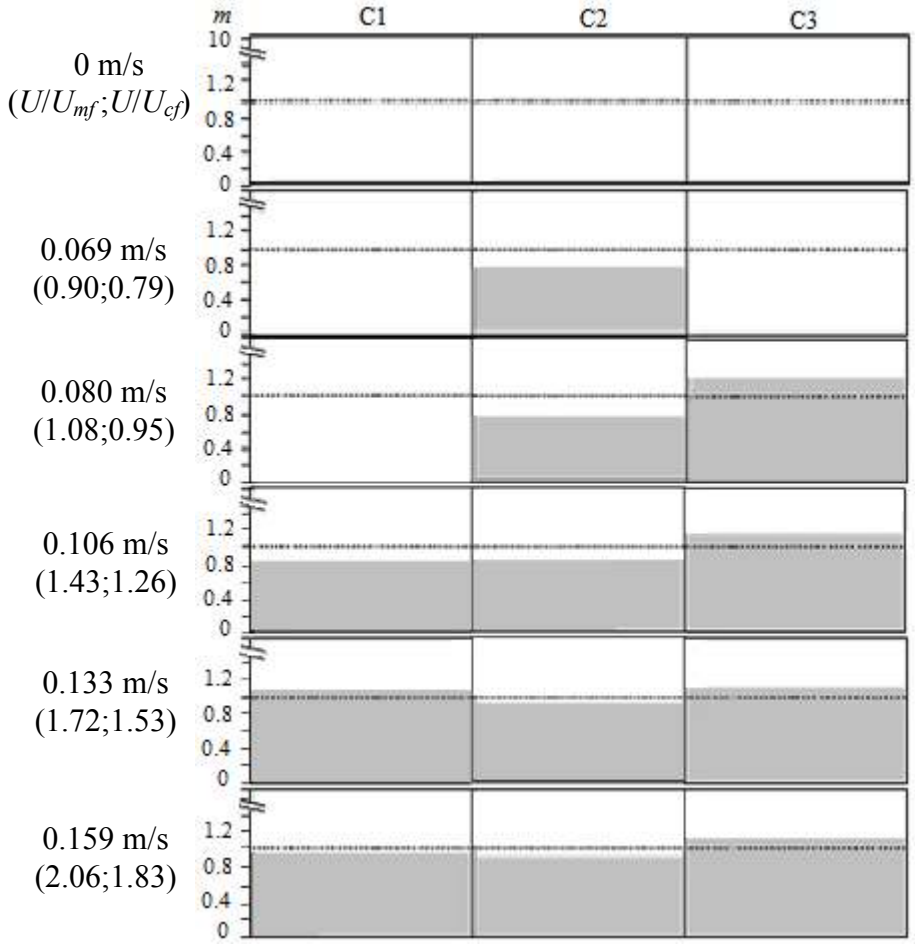

Figure 4-12(a): Palm shell lateral distribution in the gasifier, row R2 at increasing superficial velocity.

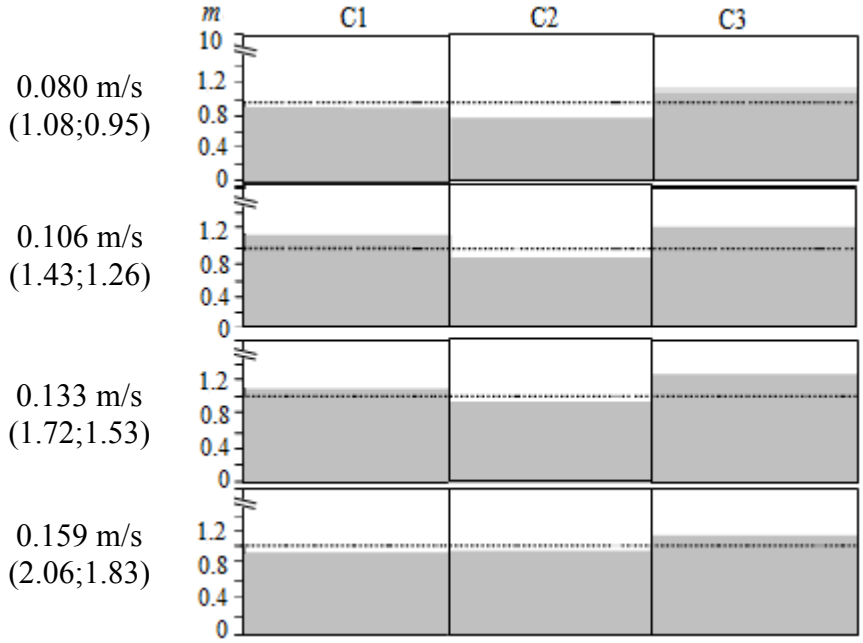

Figure 4-12(b): Palm shell lateral distribution in the gasifier, row R2 at decreasing superficial velocity.

Similarly, starting from the mixed bed, Figure 4-12(b) shows that the good local mixing quality is maintained at reducing superficial velocity from 2.06 to 1.08 U/U_{mf}. The local mixing index increases laterally from columns C1 to C3 in the gasifier in both increasing and decreasing superficial velocities, in contrast to that observed in the combustor. The flow restriction on the riser section (column C3) is more severe in the gasifier of smaller effective bed diameter than in the combustor resulting in greater accumulation of the palm shell.

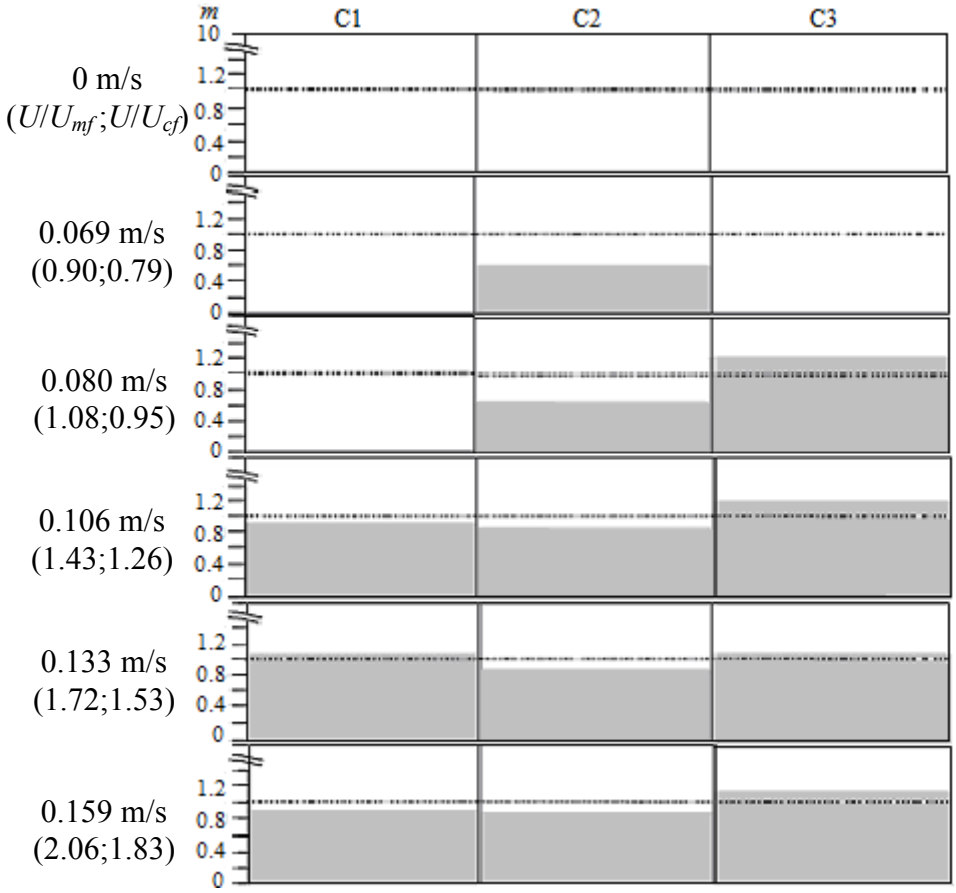

Figure 4-13(a): Palm shell lateral distribution in the gasifier, row R3 at increasing superficial velocity.

Figure 4-13 shows the palm shell lateral distribution in row R3. When the superficial velocity is below the complete fluidization velocity, the palm shell has not dispersed to all the columns as illustrated in Figure 4-13(a). At 1.43 U/U_{mf}, the local mixing index is in the range of 0.85÷1.20 across the three columns. From 1.72 U/U_{mf} onwards, good local mixing quality is established.

Starting from the mixed bed, the good mixing quality is maintained at the decreasing superficial velocity from 2.06 to 1.72 U/U_{mf} as observed in Figure 4-13(b). At 1.43 U/U_{mf}, m = 0.80÷1.00 from columns C3 to C1 but further reduction of the superficial velocity to below the complete fluidization velocity leads to stagnation of the palm shell in columns C1 and C3. Generally, the m index increases laterally from columns C1 to C3 when the superficial velocity ranges from 1.72 to 2.06 U/U_{mf}.

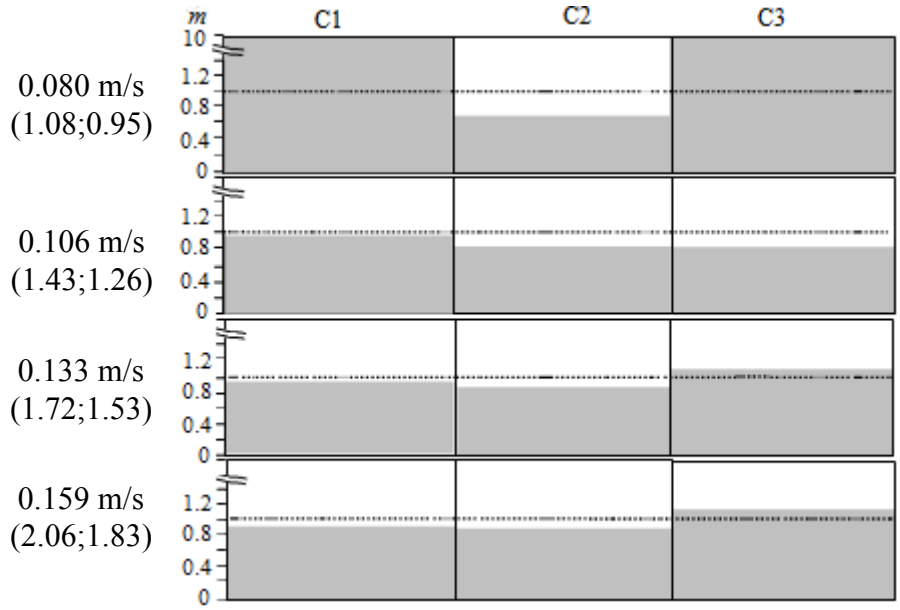

Figure 4-13(b): Palm shell lateral distribution in the gasifier, row R3 at decreasing superficial velocity.

To conclude, the palm shell vertical distribution is found to be similar in both the combustor and gasifier. The local palm shell concentration is lower at the bed bottom. This indicates that the palm shell tends to become *flotsam* in the binary mixture.

To the contrary, the palm shell lateral distribution is different for the two compartments. It is found that the local mixing index increases laterally (from V-valve to riser section) in the gasifier but shows decreasing trend in the combustor at higher superficial velocity. This is due to the geometrical effect associated with the presence of the bed internal, particularly the riser.

Nevertheless, good local mixing quality for the binary mixture can be found in both the combustor and gasifier at the superficial velocity of 1.50÷2.50 and 1.43÷2.06 U/U_{mf} respectively.

Collectively, the local mixing indices can be used to determine the overall mixing quality in the fluidized bed. In the next section, the overall mixing index, M that represents the bulk mixing quality of the binary mixture is discussed. The effects of the palm shell weight percent and mean sieve size as well as the bed geometrical parameters (i.e. bed height and effective bed diameter) on the overall mixing quality are also presented.

4.6 OVERALL MIXING QUALITY

4.6.1 EFFECT OF PALM SHELL WEIGHT PERCENT

Figure 4-14 shows the effect of palm shell weight percent on the overall mixing index, M. The palm shell content remains in the critical loading only up to 10 wt% in the sand as discussed in Chapter 3.

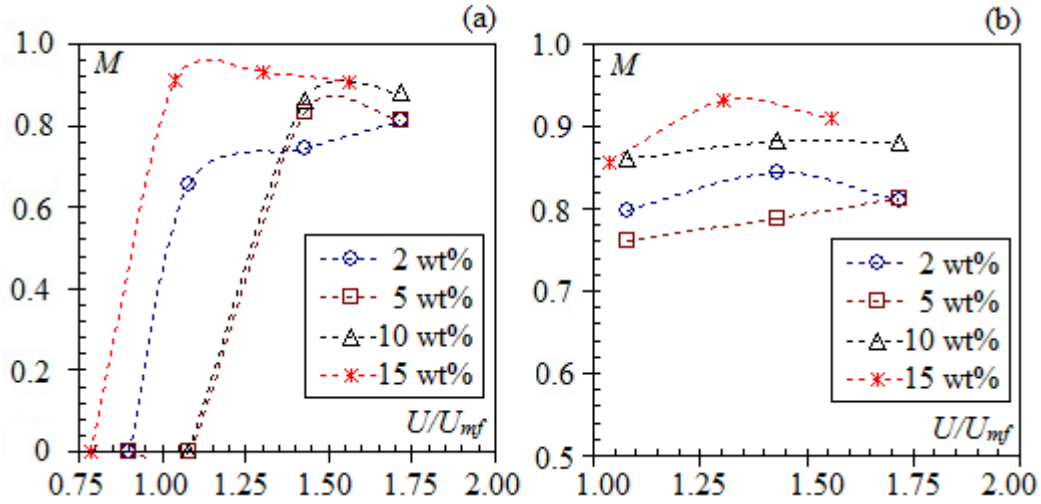

Figure 4-14: Overall mixing quality at different weight percent in the gasifier; (a) increasing, and (b) decreasing superficial velocity (palm shell mean sieve size of 3.56 mm in sand mean particle size of 272 μm).

Generally, the M index increases with the palm shell weight fraction at the higher superficial velocity (≥ 1.43 U/U_{mf}) as shown in Figure 4-14(a) and 4-14(b) respectively, except for the palm shell of 2 wt% in decreasing superficial velocity.

Figure 4-14(a) shows that a good overall mixing quality (M = 0.85÷1.00) is achieved for the palm shell of 10 and 15 wt% at the superficial velocity ≥ 1.43 U/U_{mf}. Once the bed is well mixed, the good overall mixing quality is maintained at the decreasing superficial velocity from 1.75 to 1.05 U/U_{mf} as observed in Figure 4-14(b). Besides that, the M index does not change appreciably with the superficial velocity.

This trend is consistent with the findings from Zhang et al. (2008) who studied binary mixing quality of cotton stalk, a *flotsam* at different weight percent in sand (*a jetsam*). Their results showed minor variation of mixing quality at higher superficial velocity. They also found that higher *flotsam* weight percent in the sand has higher stable value of mixing quality.

4.6.2 EFFECT OF PALM SHELL SIZE

The effect of palm shell mean sieve size on the binary mixing is not straightforward. Firstly, the addition of the palm shell to the sand may alter the characteristic fluidization velocities for the binary mixture. It has been reported earlier that the characteristic fluidization velocity for the binary mixture increases with the increase of the palm shell mean sieve size (refer to Chapter 3). Secondly, segregation tendency is proportional to the large-to-small particle size ratio (Cheremisinoff, 1993).

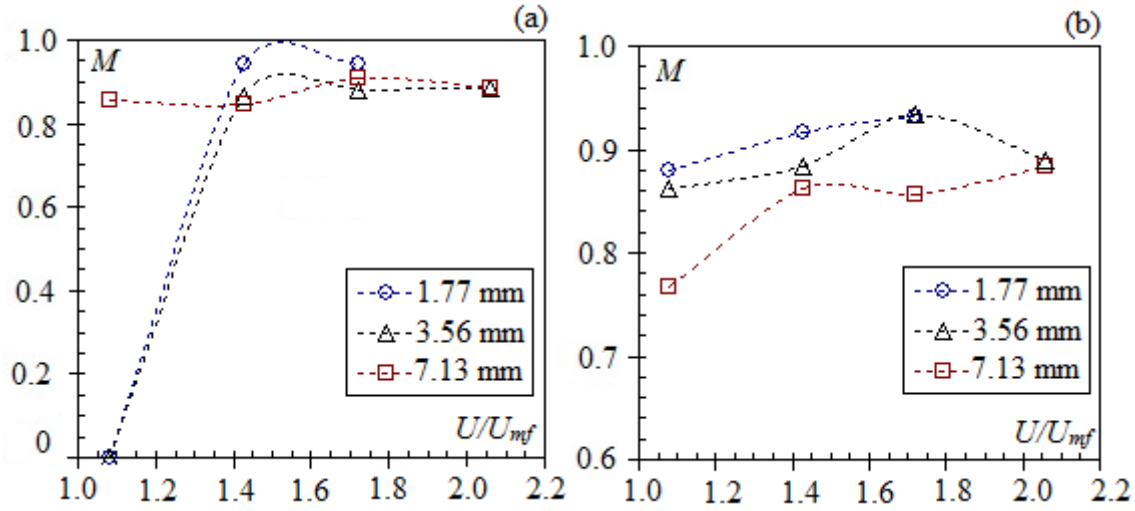

Figure 4-15: Overall mixing quality for different palm shell mean sieve sizes in the gasifier; (a) increasing, and (b) decreasing superficial velocity (palm shell of 10 wt% in sand of 272 μm).

Initially at 1.08 U/U_{mf}, Figure 4-15(a) shows that the palm shell mean sieve size of 7.13 mm has the highest M index. This is probably related to better percolation effect during the initial stage of fluidization. To the contrary, at 1.43 U/U_{mf} onwards, the smallest palm shell mean sieve size of 1.77 mm has the highest overall mixing index. Similarly, starting from a well-mixed bed and at decreasing superficial velocity, the smallest palm shell mean sieve size has the highest overall mixing index (Figure 4-15(b)). It can be seen in both figures that the overall mixing quality does not change appreciably at the higher superficial velocity (≥ 1.43 U/U_{mf}).

Hence, it can be said that the overall mixing quality generally improves with the reduction of the palm shell mean sieve size. Since the palm shell is within the critical loading (no change in the characteristic fluidization velocities), the variation of M index is attributed to the effect of particle size ratio.

Similar results were obtained by Wirsum et al. (2001) where smaller *flotsams* (wood or plastic) lead to better mixing quality in the binary system (with sand).

4.6.3 EFFECT OF BED HEIGHT

Figure 4-16 shows the overall mixing quality of palm shell at different bed heights in the gasifier. It is generally regarded that a higher bed height produces larger bubble diameter (Werther (1968)) thus, implying greater bubble action.

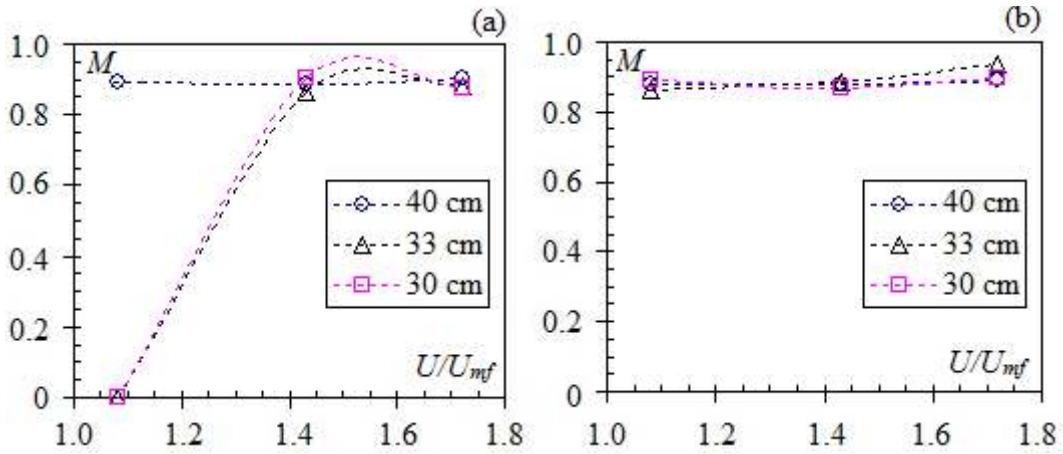

Figure 4-16: Overall mixing quality for different bed heights in the gasifier; (a) increasing, and (b) decreasing superficial velocity (palm shell mean sieve size of 3.56 mm at 10 wt% in sand of 272 μm).

Figure 4-16 shows that there is no noticeable effect of the bed height on the overall mixing quality, except at the initial state of fluidization as depicted in Figure 4-16(a). Visual observation on the bed surface shows that bubble size just before eruption is larger in the taller bed (i.e. at 40 cm). This allows the stacked palm shell to quickly disperse into the bed. A good overall mixing quality is attained in all the bed heights when increasing the superficial velocity to 1.43 U/U_{mf} onwards.

Once the bed is well mixed, the good overall mixing quality is maintained in all the bed heights at the decreasing superficial velocity from 1.70 to 1.08 U/U_{mf} (Figure 4-16 (b)).

4.6.4 EFFECT OF EFFECTIVE BED DIAMETER

Figure 4-17 shows the effect of the effective bed diameter (included the V-valve and riser in Equation 3-1) on the overall mixing quality by comparing the *M* index in the combustor and gasifier. Generally, the combustor of a larger effective bed diameter exhibits better overall mixing quality as compared to the gasifier.

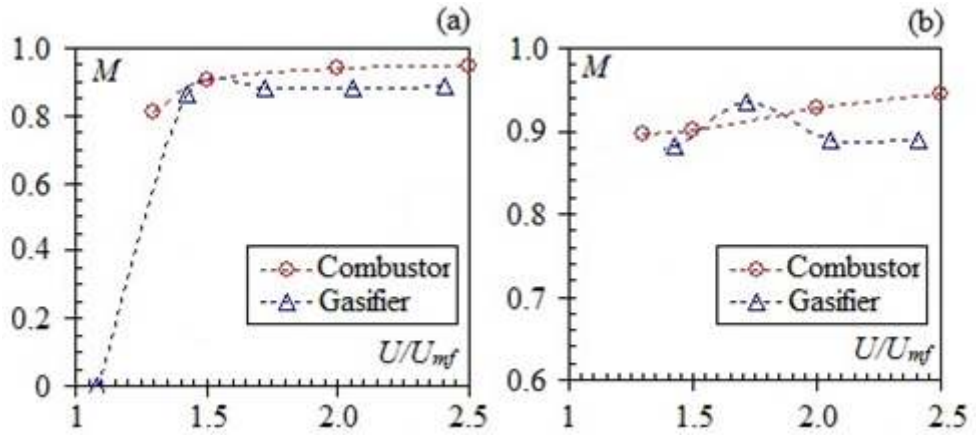

Figure 4-17: Overall mixing quality for different compartments; (a) increasing, and (b) decreasing superficial velocity (palm shell mean sieve size of 3.56 mm at 10 wt% in sand of 272 μm).

This is in agreement with the discrete particle simulation by Limtrakul et al. (2003) conducted for cylindrical columns with ID of 0.12 to 0.30 m. They reported a better solid mixing and higher solid circulation in the larger bed diameter. Their binary mixture was made up of equidensity particles of 2500 kg/m^3 with size of 4÷10 mm.

In Figure 4-17(a), both the combustor and gasifier are in good overall mixing quality by increasing the superficial velocity to 1.43 U/U_{mf} onwards. Once the bed is mixed, the binary mixture remains to be of good overall mixing quality at decreasing superficial velocity from 2.50 to 1.43 U/U_{mf} (Figure 4-17(b)).

4.7. SUMMARY

The tendency for the palm shell to become a *flotsam* in the binary mixture is observed in both the compartments.

It is found that the palm shell vertical distribution is similar for both the combustor and gasifier. When the bed is in completely fluidized state, the local mixing index at the bed bottom is generally lower than that of the other bed sections.

However, the palm shell lateral distribution is different for the combustor and gasifier due to the geometrical factor associated with the presence of the bed internal particularly the riser. The local mixing index increases laterally (from the V-valve to riser section) in the gasifier due to the accumulation of the palm shell at the riser section. However, the local mixing index exhibits a decreasing trend for the combustor due to the higher local superficial velocity at the riser section especially at higher superficial velocity.

In spite of the local variation of the palm shell concentration, a good overall mixing quality ($0.85 \leq M < 1.0$) can be established in both the combustor and gasifier at the superficial velocity of 1.50÷2.50 and 1.43÷2.06 U/U_{mf} respectively. It is also beneficial to operate within this range of superficial velocity since the effect of the initial bed arrangement (i.e. segregated or well mixed) and the mode of fluidization (i.e. increasing or decreasing superficial velocities) on the overall mixing quality is minimized.

It is found that the overall mixing quality (M) is enhanced for the smaller palm shell mean sieve size and larger palm shell weight percent.

The study also shows that the combustor of larger effective bed diameter exhibits a better overall mixing quality as compared to the gasifier.

On the other hand, the bed height does not significantly affect the overall mixing quality, although it contributes to the fastest dispersion of palm shell during the initial stage of fluidization.

CHAPTER 5

SOLID CIRCULATION RATE

5.1 INTRODUCTION

In CFBG pilot plant, heat and mass transfer rate between the compartments is attained by means of internal solid circulation. The heat demand in the gasifier is fulfilled by the hot solid transferred from the combustor. The combustor is able to supply this heat via the combustion of the gasified solid fuel obtained from the gasifier. Hence, solid circulation rate (SCR) is one of the leading parameters for the steady gasification and combustion to be realized in their respective compartments of CFBG.

In this chapter, the two compartments, in distinction from Chapter 3 and 4, are connected for the solid in the fluidized state to interchange internally via aeration to V-valve and riser pairs. The objective of this chapter is to study the effect of the 4 main operating variables, namely the bed height, main bed, V-valve and riser aerations on the solid circulation rate (SCR). It discusses factorial analysis in combination with half normal plot and steepest ascent method to determine the optimum SCR by simultaneously adjusting the selected operating variables.

The fluidized bed consists mostly of inert particles whose properties dominate the fluidization characteristic. This fact is also supported by the findings in Chapter 3 where the characteristic fluidization velocities for the sand-palm shell binary mixture remain close to the pure sand values within the critical loading. Hence, the SCR studies are conducted using sand.

5.2 EXPERIMENTAL SETUP

The experimental setup used earlier (refer to Figures 3-1 and 3-2) is equipped with four air rotameters for the aerations to the two pairs of V-valve and riser as shown in Figure 5-1.

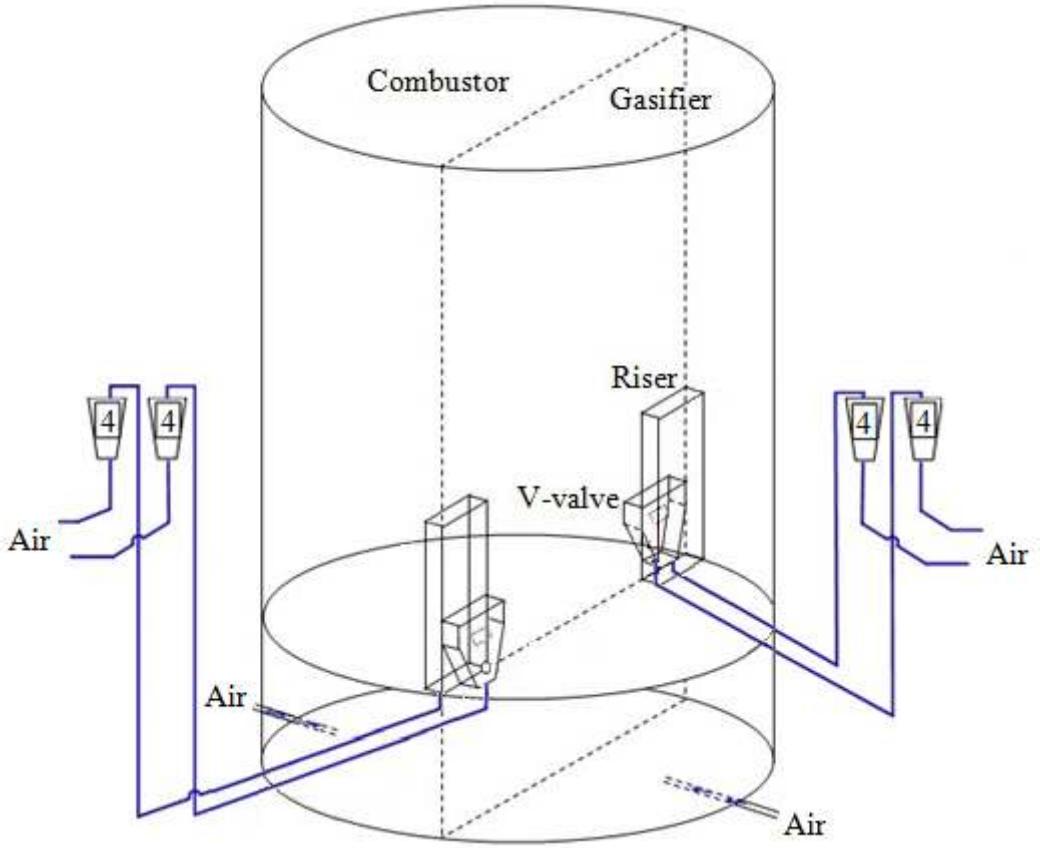

Figure 5-1: Isometric view of CFBG; the addition of air rotameters are denoted as '4'.

The geometrical details of the cold flow model are given in Table 5-1[i]. It is expected that four operating variables, namely static bed height (H_b), aeration to the bed (Q_b), V-valve (Q_v) and riser (Q_r), to mainly affect the solid circulation rate in the CFBG.

[i] The list of work details carried out by other researchers on compartmented reactor design is given Table 2-1.

Table 5-1: Geometrical details of the CFBG cold flow model.

Descriptions		
Reactor cross section	mm^2	108900π
Gasifier cross section	mm^2	38115π
Combustor cross section	mm^2	70785π
V-valve orifice diameter	mm	30
V-valve bottom cross section	mm^2	50 × 50
V-valve to riser inlet cross section	mm^2	50 × 100
Riser outlet cross section	mm^2	50 × 100
Riser height	mm	600
V-valve location	mm	On distributor
Riser location	mm	On distributor

As shown in Figure 5-2, the V-valve pumps the solid from a compartment (e.g. combustor) and transports it pneumatically through the riser, finally discharging the solid to the other compartment (e.g. gasifier). The other set of the V-valve and riser performed in the same manner to circulate the solids back to the first compartment (e.g. combustor).

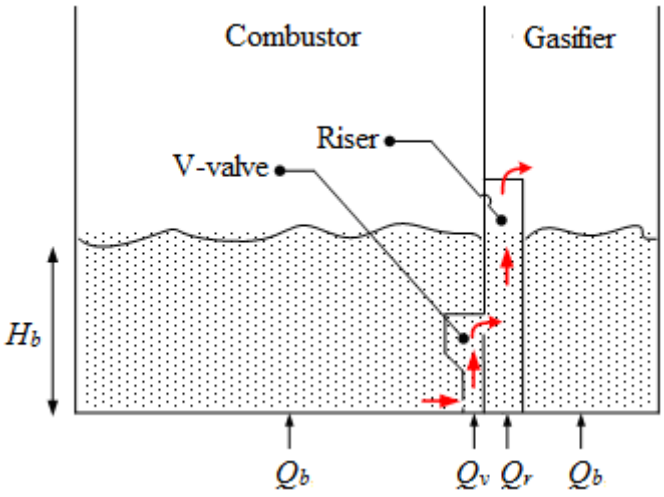

Figure 5-2: Schematic diagram of CFBG; red arrows showing the solid is transferred from the combustor to the gasifier.

The static bed height is varied in the range of 0.2÷0.4 m within the typical bed aspect ratio of 1÷2. The main bed aeration is controlled at 1.30÷1.70 U/U_{mf} to include the

operating superficial velocity for establishing good overall mixing quality as obtained in Chapter 4. The aerations to V-valve and riser are regulated at 5÷9 U/U_{mf} and 8÷12 U/U_{mf} respectively, following the experience from other researchers in the compartmented reactor design (Yan, 1995; He & Rudolph, 1997). Within the operating ranges to be studied, the air supply (up to 3500 l/min) is adequate for the experiments using the sand mean particle size of 196, 272 and 341 μm.

5.3 METHODOLOGY

Principle

The methodology for determining the solid circulation rate in a compartmented reactor, developed and verified in both cold and hot conditions by Yan and Rudolph (1996) is adapted in the present work.

Modification is made by introducing K value in Equation (5-1) on the pressure drop across the bed to a more generalized consideration of different geometrical parameters and/or particle properties effects. Besides that, the use of curve fitting is deployed to determine the initial rate of the pressure response curve.

In a bubbling fluidized bed, the bed pressure drop is given by

$$\Delta P_b = K\rho_s g H_b \left(1-\varepsilon_b\right) \tag{5-1}$$

where for compartmented reactor, experimental K values vary from 0.6 to 1.0 depending on the bed geometry and particle properties (Wee et al. 2008, 2009).

Given that $\rho_b = \rho_s\left(1-\varepsilon\right)$ and $\rho_b = \dfrac{m_s}{V_b}$, from Equation (5-1), it follows that

$$\Delta P_b = K\left(\frac{m_s g}{A_b}\right) \tag{5-2}$$

It is noted that the bed pressure drop functions in Equations (5-1) and (5-2) once established provide a convenient way to determine the bed mass or height in both cold and hot conditions.

Taking constant $k_1 = K\left(\frac{g}{A_b}\right)$, Equation (5-2) becomes

$$\Delta P_b = k_1(m_s) \tag{5-3}$$

where k_1 is the gradient of the curve of experimental bed pressure drop versus cumulative bed mass.

The differential form of the bed pressure drop defines the solid circulation rate

$$\frac{d(\Delta P_b)}{dt} = k_1\left(\frac{dm_s}{dt}\right) \tag{5-4}$$

where $\left(\frac{dm_s}{dt}\right)$ is the rate of solid transferred to or received from the other compartment.

When the solid circulation rate is at a steady state, there is no net change in ΔP_b while the solid is circulated between both compartments. By temporarily interrupting the solid transfers (i.e. shut off the V-valve and riser pair for one of the compartments), the differential bed pressure drop can be represented as

$$d(\Delta P_b) = -\Delta P_b\, dt \tag{5-5}$$

The negative sign represents the decrease of the differential bed pressure drop for the compartment that is transferring the solid. On the other hand, positive sign is used to characterize the pressure change in the compartment that is gaining the solid.

From Equation (5-5), the initial rate of the pressure response curve can be found by fitting the data in exponential function as

$$\Delta P_b = k_2 e^{-k_3 t} \tag{5-6}$$

This has been confirmed in all the experiments carried out in the present study where each set of the experimental data can produce a good linear fit ($R^2 \approx 1$) in

$$\ln(\Delta P_b) = -k_3 t + \ln k_2 \tag{5-7}$$

Then, differentiating the exponential function and setting $t \rightarrow 0$,

$$\left.\frac{d(\Delta P_b)}{dt}\right|_{t\rightarrow 0} = k_2 k_3 \tag{5-8}$$

where k_2 and k_3 are determined experimentally from the curve of natural logarithmic bed pressure drop versus time.

The initial value of solid circulation rate (SCR) just after the interruption is essentially the solid circulation rate at a steady state, or $SCR = \left.\left(\frac{dm_s}{dt}\right)\right|_{t\rightarrow 0}$.

Thus, by combining Equations (5-4) and (5-8), it follows that

$$SCR = \frac{k_2 k_3}{k_1} \tag{5-9}$$

Procedures

Solid circulation rate (SCR) is computed from the k values. To find k_1, k_2 and k_3 respectively, two different experimental plots are required, namely (i) bed pressure drop versus cumulative bed mass and (ii) pressure response curve. Both the experimental procedures are described here and can be implemented either on the combustor or gasifier to determine the solid circulation rate.

The plot of the bed pressure drop versus cumulative bed mass is obtained by measuring the bed pressure drop, ΔP_b when a known solid (sand) mass is added to the compartment in a fluidized state. The data is recorded until the bed inventory reaches the required bed height. Figure 5-3 shows the gradients, indicated as k_1 for the combustor and gasifier are 0.41 and 0.68 cmWg/kg respectively.

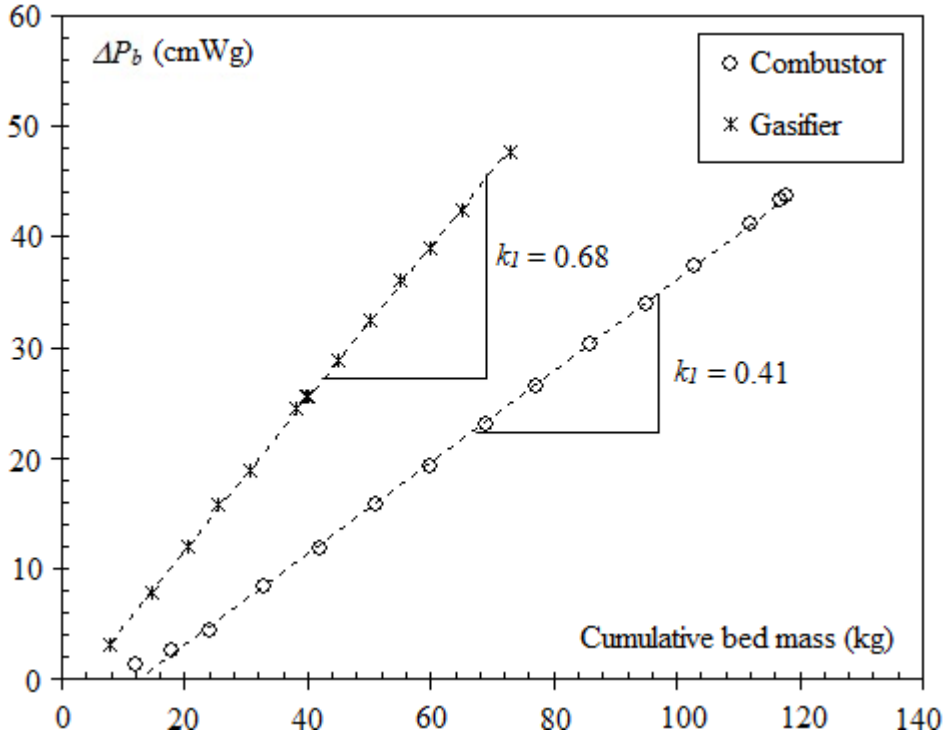

Figure 5-3: Typical bed pressure drop versus cumulative bed mass for sand of 341 μm.

On the other hand, the steps to obtain the pressure response curve are as follows:

(i) the solid of a known mass is filled to the same bed height in both of the compartments.

(ii) aerations to the bed, V-valve and riser pairs in both compartments are configured to the required settings as stated in Table 5-1.

(i) solid circulation between the compartments is allowed to occur until a steady state is achieved[j].

(ii) solid circulation is then interrupted by shutting the aerations to a pair of the V-valve and riser only[k].

(iii) Once sufficient data is collected for the pressure response curve, aerations to the closed V-valve and riser are resumed to the required settings as in (ii) to restore the steady state solid circulation rate and bed pressure drop.

(iv) A new set of configurations is introduced and steps (i) to (v) are repeated.

[j] At steady state, there is no net change in bed pressure drop (or expanded bed height) in both the compartments.

[k] The compartment without the V-valve and riser aerations will exhibit an upward trend on its pressure response curve since it is gaining solid. In contrast, the other compartment will show a downward trend since it is losing solid.

The typical pressure response curve presented in natural logarithmic ΔP_b versus time function is shown in Figure 5-4. In this example, the product of k_2 and k_3 is equal to 0.197 cmWg/s. It can be seen that the pressure response curve has a good linear fit in the exponential form. This is found on all the experiments where $R^2 \approx 1$.

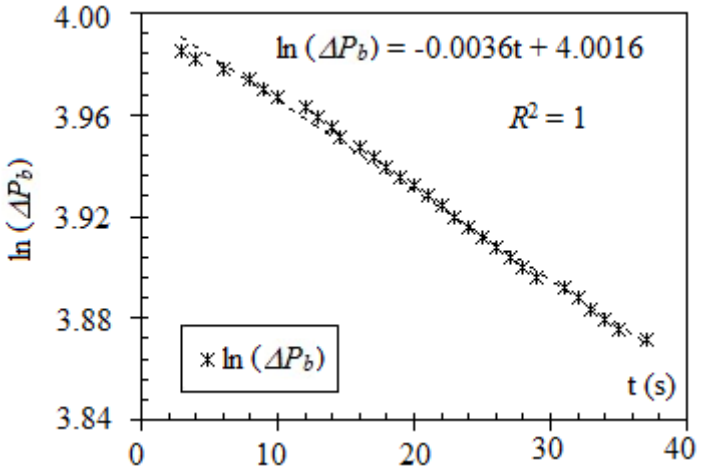

Figure 5-4: Typical pressure response curve in the gasifier; H_b = 0.4 m, Q_b = 1.7 U/U_{mf}, Q_v = 5 U/U_{mf} and Q_r = 8 U/U_{mf}.

5.4 PARAMETRIC STUDIES ON THE SOLID CIRCULATION RATE

In the following section, each set of data used in the figures corresponds to the condition where one of the four operating variables, namely bed height (H_b), aeration ratio to bed (Q_b), V-valve (Q_v) and riser (Q_r) is varied over the range specified in Section 5-2. This allows the study of the individual effect on the solid circulation rate (SCR). The larger sand mean particle size of 341 μm is selected as the bed material to minimize the differences in the characteristic fluidization velocity between the two compartments (Chapter 3).

Effect of Bed Height

The effect of bed height on the solid circulation rate (SCR) is shown in Figure 5-5. It can be observed that the SCR increases with the increase in the bed height. This can be expected since an increase in the bed height increases the bed pressure drop, which is the main driving force for the solid circulation in the compartmented reactor.

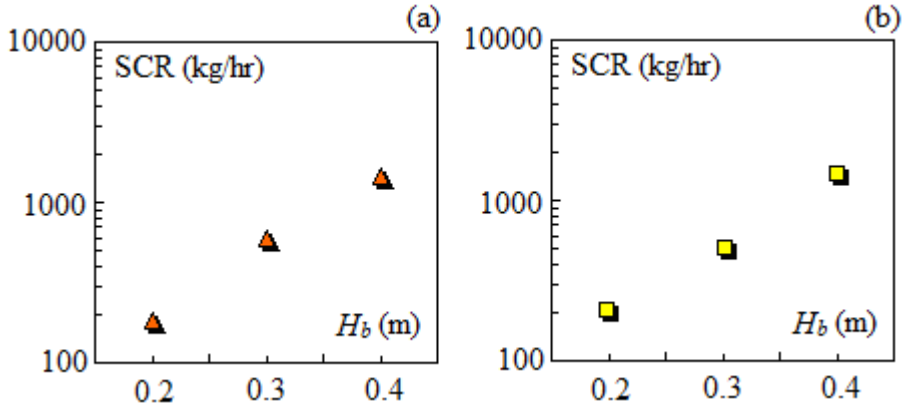

Figure 5-5: Solid circulation rate (SCR) versus bed height; (a) Q_b = 1.3 U/U_{mf}, Q_v = 5 U/U_{mf}, Q_r = 12 U/U_{mf}, and (b) Q_b = 1.3 U/U_{mf}, Q_v = 9 U/U_{mf}, Q_r = 8 U/U_{mf}.

These trends are similar to those observed by all the researchers in a compartmented reactor design (He, 1993; Yan, 1995; Bhattacharya et al., 1999).

Effect of Main Bed Aeration

When the bed is fluidized, the bed pressure drop remains virtually unchanged with further increase in the main bed aeration. Consequently, one can expect the SCR remains constant when the compartmented bed is fluidized within this range of superficial velocity. This is confirmed in Figure 5-6 where the SCR is almost unchanged with the variation in the main bed aeration from 1.3 to 1.7 U/U_{mf}.

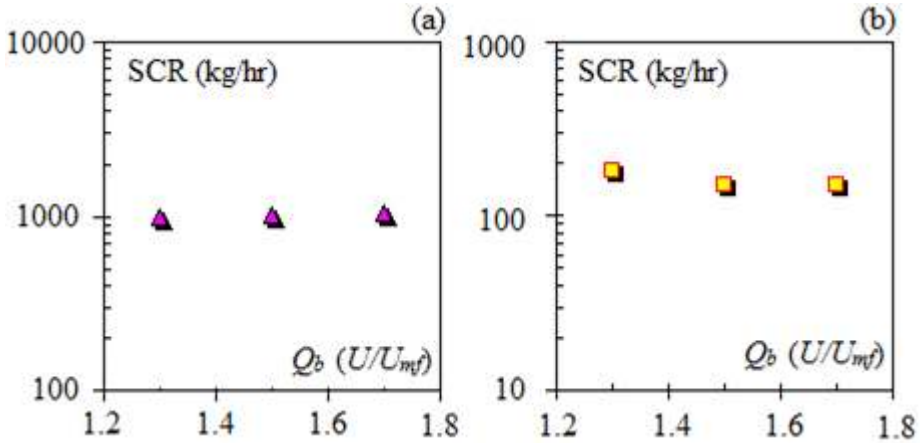

Figure 5-6: Solid circulation rate (SCR) versus main bed aeration; (a) H_b = 0.4 m, Q_v = 5 U/U_{mf}, Q_r = 8 U/U_{mf} , (b) H_b = 0.2 m, Q_v = 5 U/U_{mf}, Q_r = 12 U/U_{mf}.

This is in contrast to the findings by He (1993) and Bhattacharya et al. (1999) where SCR increases with the main bed aeration as a result of the increase in gas leakage from the main compartment into the V-valve orifice.

It seems that the relatively low main bed aeration in the present study is a main factor responsible for minimizing the contribution of the gas leakage on the SCR.

Effect of Riser Aeration

The effect of the riser aeration on the SCR is depicted in Figure 5-7. It is noted that the SCR initially increases then decreases with the increase in the riser aeration.

Firstly, an increase in the SCR with higher riser aeration can be expected, due to the higher entrainment rate. However, further increase of the riser aeration may increase the frictional and acceleration pressure drop in the riser. This eventually results in a reduction in the solid circulation rate.

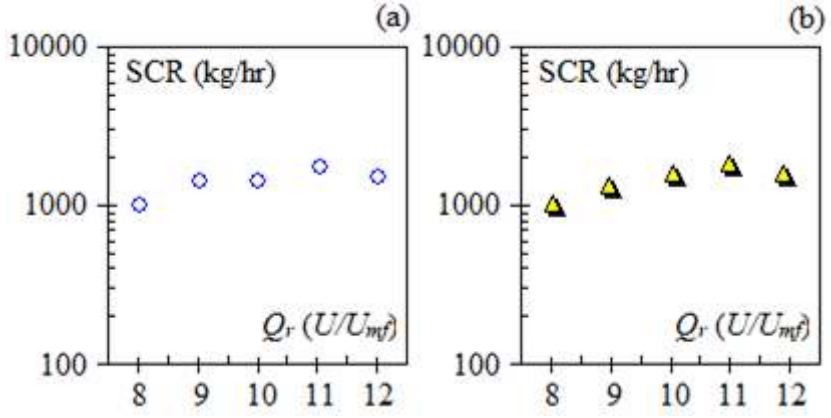

Figure 5-7: Solid circulation rate (SCR) versus riser aeration; (a) H_b = 0.4 m, Q_b = 1.7 U/U_{mf}, Q_v = 9 U/U_{mf}, and (b) H_b = 0.4 m, Q_b = 1.3 U/U_{mf}, Q_v = 5 U/U_{mf}.

This trend is consistent with the results reported by Bhattacharya et al. (1991).

Effect of V-valve Aeration

The effects of the V-valve aerations on the solid circulation rate (SCR) are shown in Figure 5-8. On one hand, Figure 5-8(a) shows that an increase in the V-valve aeration has no significant effect on the SCR. On the other hand, Figure 5-8(b) shows the SCR increases then decreases with the increase in the V-valve aeration.

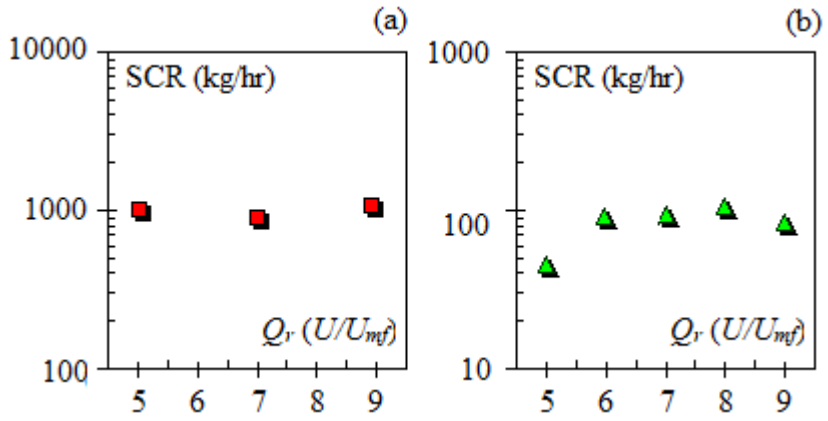

Figure 5-8: Solid circulation rate (SCR) versus V-valve aeration; (a) H_b = 0.4 m, Q_b = 1.7 U/U_{mf}, Q_r = 8 U/U_{mf}; and (b) H_b = 0.2 m, Q_b = 1.3 U/U_{mf}, Q_r = 8 U/U_{mf}.

Aeration through the V-valve induces a low pressure region that creates a pumping effect. Thus, it can be expected that higher aeration through the V-valve leads to greater pumping effect but at the same time, it increases the resistance across the V-valve-to-riser orifice (intermediate solid and gas passage). The contributions of the two opposing effects of the V-valve aeration determine the SCR trend.

To conclude, the solid circulation rate (SCR) increases with the increase in the bed height in CFBG. This is consistent to the findings by other authors in compartmented reactor design. Hence, the direct route to maximize the SCR is the increase of the static bed height. However, in CFBG, the maximum operating bed height is limited by the riser height.

Solid circulation rate remains almost unaffected by the main bed aeration since the bed pressure drop (the main driving force for the solid circulation) remains unchanged with further increase in the main bed aeration within the bubbling fluidization regime.

The V-valve or riser aeration may affect the solid circulation rate. Hence, in the next section, a factorial approach in combination with half normal plot and steepest ascent method is presented as a tool to determine the V-valve and riser aerations that optimize the solid circulation rate (since the main bed aeration has no effect on the SCR). It is then implemented for the different sand mean particle sizes.

5.5 STATISTICAL ANALYSIS OF OPTIMUM SOLID CIRCULATION RATE

Factorial design using Yates' algorithm and analysis of variance, ANOVA analysis was implemented by Yan and Rudolph (1996) to identify the individual and interacting effects of the four operating variables above on the solid circulation rate in a compartmented reactor. We have developed this approach further by incorporating (i) half normal plot and (ii) steepest ascent method that can be utilized to determine the optimum solid circulation rate (SCR).

A half normal plot (Johnson, 2005) is introduced to assess the reference values selection (α or *F*-value) during the ANOVA analysis. It is a graphical representation indicating the most important/significant effects. In the half normal plot, any large estimated effects would deviate from the straight line pattern formed by the many small estimated effects. It allows the elimination of ambiguous reference value (α or *F*-value) selection that may alter the conclusion from the ANOVA analysis.

The steepest ascent method (Johnson, 2005) is used to configure subsequent experiments for determining the optimum response, i.e. the solid circulation rate (SCR). To implement the steepest ascent method, the most important effects are selected to generate the respective coefficients based on the classical linear regression analysis. Then, by using the coefficients for these effects (i.e. V-valve and riser aerations), the subsequent experiments are tailored specifically to locate the optimum SCR.

2^4 Full Factorial Design

Table 5-2 below shows the 2^4 full factorial design of experiments with high, low and base level. Other than bed height (H_b), all three aerations to main bed (Q_b), riser (Q_r) and V-valve (Q_v) are specified in dimensionless terms.

At the base level (0), 4 repetitive experiments are carried out producing consistent values with the average SCR at 511 kg/hr and standard deviation of about 21 kg/hr.

Table 5-2: 2^4 factorial design for solid circulation rate (SCR).

Variables	Unit	Code	Low level (-1)	Base level (0)	High level (1)
Q_b	U/U_{mf}	*A*	1.3	1.5	1.7
Q_r	U/U_{mf}	*B*	8	10	12
Q_v	U/U_{mf}	*C*	5	7	9
H_b	m	*D*	0.2	0.3	0.4

Table 5-3 shows the statistical analysis using Yates' algorithm and ANOVA with a total of 16 combinations of treatment condition consisting of a single-factor (e.g. *A*), two-factor (e.g. *AB*), three-factor (e.g. *ABC*), and four-factor interactions (e.g. *ABCD*). In each treatment condition, the experiment is performed with two replicates, i.e. R(I) and R(II). It is noted that although tabulated in the standard order, the experiments are carried out randomly to avoid systematic errors.

In order to be considered as statistically significant, the computed *f*-value (as shown in Table 5-3) must be larger than the standard *F*-value based on the selected α value. Table 5-4 shows the corresponding standard *F*-value based on the 4 significant levels (α) for 1 and 15 numerator and denominator degrees of freedoms respectively (Devore, 2004). For example, at $\alpha = 0.1$, there are 7 significant interactions namely, *B*, *C*, *D*, *BD*, *CD*, *ABC* and *ABCD*. This is reduced to 4 significant interactions i.e. *B*, *C*, *D* and *BD* for $\alpha = 0.001$. Such ambiguity in the reference value selection can be avoided with the half normal plot.

Table 5-3: Experimental results based on Yates's algorithm and ANOVA sum of square.

Treatment condition	Q_b	Q_r	Q_v	H_b	SCR (kg/hr) R(I)	SCR (kg/hr) R(II)	R(I)+R(II)	Yates' analysis I	Yates' analysis II	Yates' analysis III	Yates' analysis IV	ANOVA sum of squares	*f*-value
1	-1	-1	-1	-1	40	48	88	130	797	2024	22281	-	-
A	1	-1	-1	-1	14	29	42	666	1227	20257	-397	4925	1.44
B	-1	1	-1	-1	158	207	365	306	9578	-106	4335	587203	171.40
AB	1	1	-1	-1	160	141	301	921	10679	-291	-95	280	0.08
C	-1	-1	1	-1	86	71	157	4087	-109	1150	1532	73392	21.42
AC	1	-1	1	-1	65	84	149	5490	3	3185	476	7095	2.07
BC	-1	1	1	-1	236	219	455	4449	-328	2	457	6524	1.90
ABC	1	1	1	-1	243	224	466	6230	37	-97	833	21697	6.33
D	-1	-1	-1	1	954	1060	2014	-46	536	431	18233	10389048	3032.44
AD	1	-1	-1	1	1062	1011	2073	-63	615	1102	-185	1064	0.31
BD	-1	1	-1	1	1431	1508	2939	-8	1403	112	2034	129315	37.75
ABD	1	1	-1	1	1263	1289	2552	11	1781	364	-99	307	0.09
CD	-1	-1	1	1	1198	1104	2303	59	-18	79	671	14083	4.11
ACD	1	-1	1	1	1056	1090	2146	-387	20	378	252	1986	0.58
BCD	-1	1	1	1	1542	1477	3019	-156	-446	38	299	2796	0.82
ABCD	1	1	1	1	1739	1473	3212	193	349	796	758	17946	5.24

Table 5-4: Results for various α and *F*-value.

α	0.1	0.05	0.01	0.001
F-value	3.07	4.54	8.68	16.59
Significant Interactions	Single-factor *B* *C* *D* Two-factor *BD* *CD* Three-factor *ABC* Four-factor *ABCD*	*B* *C* *D* *BD* *ABC* *ABCD*	*B* *C* *D* *BD*	*B* *C* *D* *BD*

Half Normal Plot

From the half normal plot in Figure 5-9, contrary to *F*-value analysis at α = 0.1, it is obvious that only *B*, *C*, *D* and *BD* are the most important effects as they have deviated from the linear line formed by the many smaller effects in the 2^4 factorial analysis. The visual evidence of the other combined effects *CD*, *ABC* and *ABCD* are not very strong.

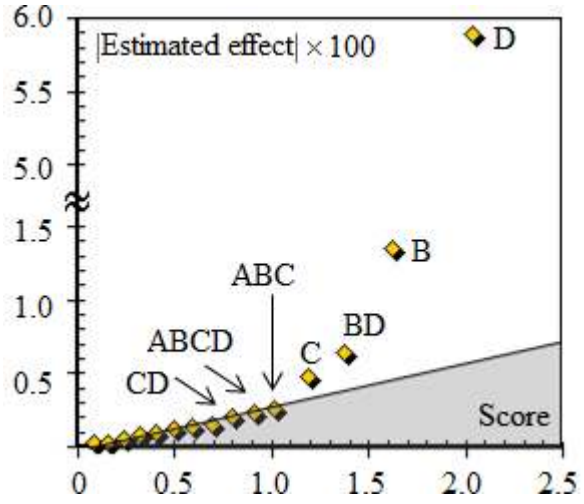

Figure 5-9: Half normal plot for 2^4 factorial analysis.

The statistical results are also consistent with the parametric studies of the four operating variables on SCR as discussed earlier. The half normal plot shows that the effect of bed height (*D*) on the solid circulation rate is the most significant; this is comparable to the trend observed in Figure 5-5. Besides that, the effect of the main bed aeration (*A*) on the SCR is statistically insignificant, similarly observed in Figure 5-6. The effect of the riser (*B*) and V-valve (*C*) aerations on the solid circulation rate respectively is found to be significant. This is consistent with the trends observed in Figures 5-7 and 5-8 respectively.

Steepest Ascent Method

In order to implement the steepest ascent method, 6 significant effects namely *B*, *C*, *D*, *BD*, *ABC* and *ABCD* are selected. Although the half normal plot shows that the three-factor and four-factor effects i.e. *ABC* and *ABCD* respectively are statistically insignificant, they are retained as they are able to quantify the interaction effects of the main bed aeration with the other variables on the rate of solid circulation as reported by Bhattacharya et al. (1991) and He (1993); the two effects provide additional aeration in the solid circulation loop. As it will be discussed in Chapter 6, this is also consistent with the observation where the steady solid circulation is achieved during palm shell gasification without aeration to the combustor V-valve due to the gas leakage from the gasifier into the combustor V-valve.

Table 5-5 below shows the respective coefficients generated based on the classical linear regression analysis performed on the 6 significant effects. The coefficients for riser (*B*) and V-valve (*C*) aerations are found to be -9.4 and 24.8 respectively.

Table 5-5: Coefficients for the 6 significant effects in classical linear regression analysis[1].

Effect	*B*	*C*	*D*	*BD*	*ABC*	*ABCD*	Intercept
Coefficient (Y)	-9.4	24.8	2516.3	259.6	-1.7	5.6	-910

Since the coefficient for the riser (*B*) aeration is negative while for the V-valve (*C*) aeration is positive, the subsequent optimization experiments are arranged based on

[1] Regression analysis is performed using Microsoft Excel®.

decreasing and increasing the aeration to riser (*B*) and V-valve (*C*) respectively. As shown in Table 5-6, SCR optimization is carried out using the normal steps of –0.76 and 2 respectively.

Table 5-6: Design of experiment for SCR optimization using steepest ascent method.

Variables	Unit	Riser aeration (*B*)	V-valve aeration (*C*)
Origin	U/U_{mf}	10	5
Increment (X)	U/U_{mf}	2	2
Coefficient (Y)	-	-9.4	24.8
X·Y	-	-18.8	49.6
Normal step[m]	U/U_{mf}	-0.76	2

Given that an increase in the bed height increases the solid circulation rate, the static bed height (*D*) is set at 0.4 m. As the main bed aeration (*A*) does not show any significant individual effect, it is kept at 1.7 U/U_{mf}. This is within the range of superficial velocity that can establish good overall mixing quality in both of the compartments as discussed in Chapter 4. Table 5-7 shows the optimum SCR value based on the steepest ascent method.

Table 5-7: Optimization of solid circulation rate; A = 1.7 U/U_{mf}, D = 0.4 m.

Riser Aeration, (*B*)	V-valve Aeration, (*C*)	Solid circulation rate (SCR)
U/U_{mf}	U/U_{mf}	kg/hr
9.24	7	2040
8.47	9	2011
7.71	11	2271
6.94	13	2319
6.18	15	1933
5.41	17	2157
4.65	19	2032

[m] The coefficient of V-valve (*C*) aeration, being larger than the coefficient of riser aeration is selected as the divisor to compute the normal step size.

It is found that the highest solid circulation rate is 2319 kg/hr. This occurred when the riser and V-valve aerations are set at 6.94 and 13 U/U_{mf} respectively.

This method is also implemented to assess the optimum SCR values for the different sand mean particle sizes of 196 and 272 μm. Figure 5-10 shows that the optimum SCR value increases with the increase in the sand mean particle size.

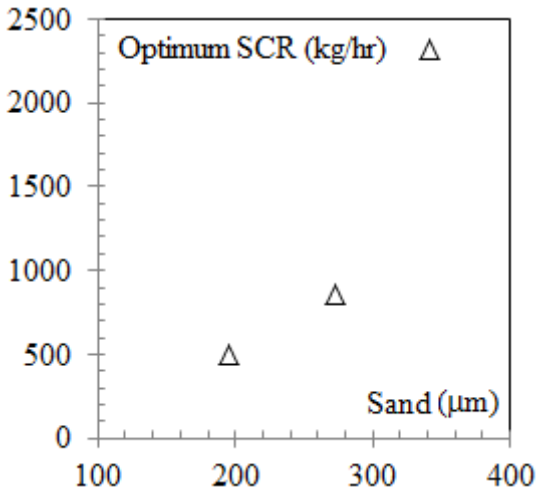

Figure 5-10: Optimum solid circulation rate (SCR) for different sand mean particle sizes; A = 1.7 U/U_{mf}, D = 0.4 m.

This tendency is supported by the findings from Sathiyamoorthy and Rudolph (1990) who reported that the SCR increases with the increase in particle's U_{mf}. It has been confirmed that U_{mf} increases with the increase in the sand mean particle size (refer to Table 3-3). This shows that the selection of larger inert mean particle size as the bed material offers greater magnitude of solid exchanged rate.

5.6 SUMMARY

The parametric study has demonstrated that the solid circulation rate is almost unaffected by the main bed aeration. This is consistent with the factorial analysis where this effect is found to be statistically insignificant.

One common finding obtained in the CFBG similar to the other compartmented reactor designs is that a higher static bed height always leads to a higher solid

circulation rate. However, the maximum operating height is limited by the riser height.

Factorial analysis in combination with the half normal plot and steepest ascent method allows the determination of optimum solid circulation rate by simultaneously adjusts the V-valve and riser aerations (at a fixed bed aeration and highest static bed height).

It is found that bigger sand mean particle size produces higher optimum SCR value. This suggests that the utilization of large sand mean particle size as a bed material in CFBG offers a higher and yet flexible solid circulation rate.

CHAPTER 6

CFBG PILOT PLANT PERFORMANCE TESTING

6.1 INTRODUCTION

In the preceding chapters, parametric and statistical studies have been conducted in a cold flow model to understand the behavior, main trends and tendencies on the hydrodynamics and solid circulation in the compartmented fluidized bed gasifier (CFBG), using palm shell and sand as the bed materials fluidized by air. This constitutes the first part of this thesis.

The feasibility studies of palm oil waste including palm shell as biomass gasification feedstock have been well reported in Kelly-Yong et al. (2007) and Shuit et al. (2009). The laboratory analysis on the physical and chemical characteristics has also been well documented by Guo and Lua (2001) and Yang et al. (2006) citing palm oil solid residual as an ideal choice for thermo-chemical conversion.

This chapter objective is to prove the concept of CFBG as a prospective technology for the gasification of palm shell in the pilot plant scale gasifier of 1 ton per day to produce medium calorific value fuel gas suitable for syngas production and power generation.

The full process of the palm shell gasification in the CFBG pilot plant is categorized in 7 basic operational stages from startup to the initial palm shell feeding, and then auto ignition and combustion process, followed by the solid circulation, air-to-steam switchover and finally, palm shell gasification process.

6.2 PILOT PLANT DESIGN

The essential works prior to the pilot plant performance testing are engineering design, procurement, construction, testing and commissioning as well as upgrading of the facility and utilities. The pilot plant facility is shown in Figure 6-1.

The piping and instrumentation diagram (P&ID) is depicted in Figure 6-2. A brief description of the main equipment, instrumentation and gas analysis system is given as below. The main equipment includes the air compressor system, air preheater, boiler system, steam superheater, CFBG reactor, screw feeder with lock hopper, cyclones and chimney. The tender documents containing the detailed specification of the pilot plant engineering design are included in the appendix.

Air Compressor System

As shown in Figure 6-2, the existing air compressor (denoted as '1') with air dryer (denoted as '2') is upgraded with the addition of a second air compressor unit to supply air up to 420 Nm^3/hr and 10 barg for the CFBG pilot plant.

Air Preheater

A 40 kW air preheater (indicated as '3') is used to heat up the air to 350°C. This temperature is sufficient to cause auto ignition of the palm shell during the initial palm shell loading as the startup fuel. It also supplements heat to the combustor during the gasification stage.

Boiler System

The boiler system consists of a boiler feed water tank (represented as '4'), boiler feed water pump (represented as '5') and boiler (represented as '6'). The electrical boiler, rated at 60 kW has a maximum steam capacity of 50 kg/hr at 7 barg. A downstream 25 kW electrical heater (represented as '3') is used to superheat the steam to about 250°C. The heater is also used to preheat the fluidizing air to the gasifier during the startup and initial combustion stage.

Figure 6-1: CFBG pilot plant facility (a) Overview (built-up area of 9 m x 15 m), and (b) CFBG reactor.

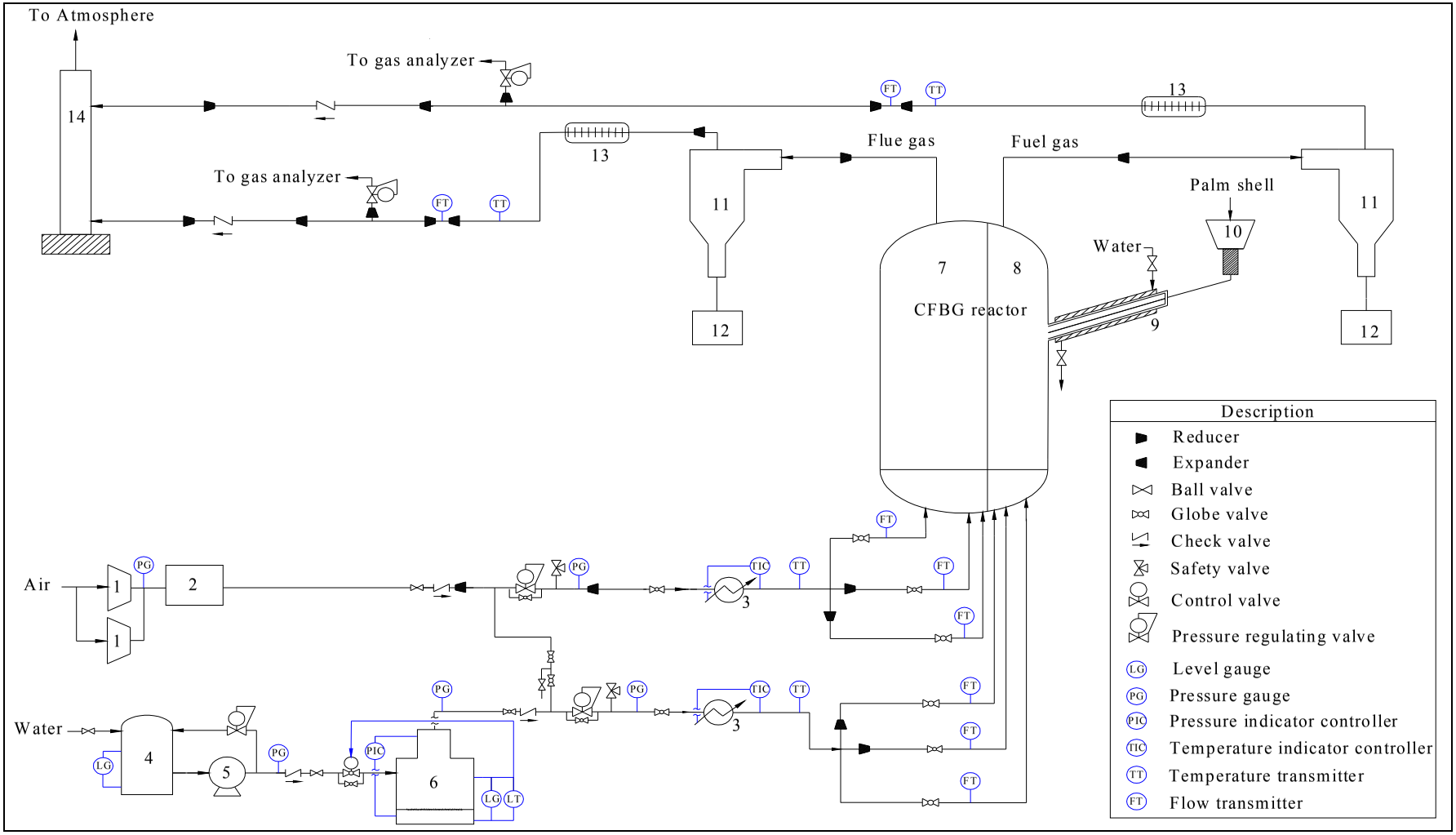

Figure 6-2: Piping and instrumentation diagram (P&ID) for CFBG pilot plant; 1: air compressor, 2: air dryer, 3: air/steam heater, 4: boiler feed water tank, 5: boiler feed water pump, 6: boiler, 7: combustor, 8: gasifier, 9: water cooler, 10: screw feeder with lock hopper, 11: cyclone, 12: water sealer, 13: air cooler, 14: chimney.

CFBG Reactor

The CFBG reactor is made of stainless steel with ID of 0.66 m. It is divided into two compartments by a vertical wall in 60:40 (based on 100%) cross-sectional area ratio. This corresponds to the effective bed diameters, D_e of 0.397 m and 0.290 m for the combustor (denoted as '7') and gasifier (denoted as '8') respectively. The effective bed diameter of the gasifier is slightly larger than the cold flow model following the findings in the preceding chapters and the study conducted by Wee et al., 2008. The total height of the reactor is 3.30 m (with plenum height of 0.20 m) to minimize carbon loss due to particle elutriation during the palm shell combustion and gasification. It is also thermally insulated. Similar to the cold flow model, perforated plate is selected as the distributor. The V-valve and riser pairs are also identical to the cold flow model. The isometric view of the CFBG pilot plant reactor is shown in Figure 6-3.

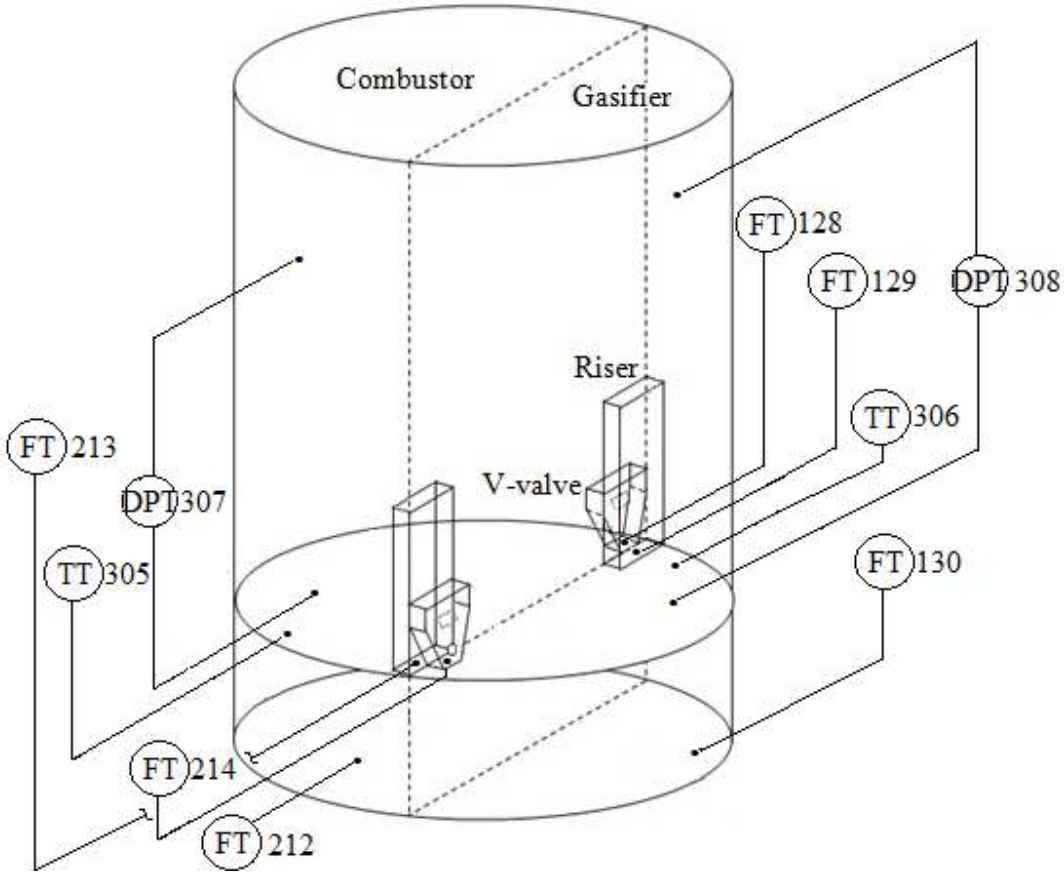

Figure 6-3: Isometric view of CFBG pilot plant reactor (TT: temperature transmitter, DPT = differential pressure transmitter and FT: flow transmitter).

Instrumentations

The instrumentations, namely the temperature transmitter (TT), differential pressure transmitter (DPT) and flow transmitters (FT) are connected to a data acquisition system for real time monitoring and data recording. The accuracy of the temperature measurement is ±10°C. Both the differential pressure and flow measurement have the accuracy of ±0.4%. Orifice plates for the flow transmitters are designed using the Yogokawa engineering software.

Screw Feeder

The biomass is fed using a screw feeder (indicated as '10') with lock hopper. Since the screw feeder is in contact with the gasifier, heat is conducted. Hence, a cooling water jacket (indicated as '9') is designed around the screw feeder placed close to the feeding point.

Cyclones

Two units of cyclones (represented as '11') are used in the pilot plant. As shown in Figure 6-2, one unit is for removing fine particles from the combustor flue gas, while the other unit is for the gasifier fuel gas. Both units are made from stainless steel. Water sealer (represented as '12') is placed at the bottom of each cyclone to collect any entrained fine particles.

Gas Analyzer System

Online and continuous gas analysis system[n] is utilized to measure the main gas constituents in the fuel gas, namely CH_4, O_2, CO, CO_2 and H_2 in dry basis during the palm shell gasification. The gas analyzer is also used to monitor O_2 and CO_2 in the combustor flue gas during the palm shell initial combustion stage. The gases from the respective compartments are cooled down using air coolers (denoted as '13') prior to sampling. The analyzers are calibrated with gas concentration accuracy of ±0.05%.

Chimney

Both the flue gas and fuel gas from the respective compartments are channelled to a common chimney (denoted at '14') to be discharged to the atmosphere at an elevated height.

[n] Teledyne 7600 is used to analyze CH_4, O_2, CO and CO_2 while Teledyne 2230 is used to analyze H_2.

6.3 OPERATIONAL CONSIDERATIONS

Palm Shell Properties

The physical properties of the palm shell from Malaysia have been described in Chapter 3. Its chemical properties in proximate and ultimate analysis are presented in Tables 6-1 and 6-2. These results are comparable with those reported in other countries e.g. Thailand and Columbia (Luangkiattikhun et al., 2007; Gomez et al., 2009).

Table 6-1: Proximate analysis of palm shell (as-received basis)

	Moisture	Ash	Volatile matter	Fixed carbon[o]	Gross heating value (MJ/kg)
wt%	7.73	4.10	74.77	13.40	20.40

Table 6-2: Ultimate analysis of palm shell (as-received basis)

	C	H	N	S	O[o]
wt%	43.70	5.40	0.36	0.42	38.28

Palm Shell Size Selection

The palm shell mean sieve size of 3.56 mm is selected as the startup fuel. This size has been determined in Chapter 3 as among the most abundantly available size in bulk supply obtained from the mill. Moreover, palm shell of this size can be loaded in large quantity, yet the characteristic fluidization velocities for the binary mixtures can be determined from its pure sand values if appropriate sand size is selected.

During the combustion and gasification stage, as-received palm shell (Equation (3-2) estimates it to be 4.24 mm) is fed continuously while keeping within the critical loading.

Sand Size Selection

It is reported in Chapter 3 that the palm shell critical loading increases with the increase in the sand mean particle size. Besides that, an increase in the sand mean particle size also increases the optimum solid circulation rate (refer to Chapter 5). Therefore, the largest sand mean particle size of 395 μm is selected as the main bed material.

[o] Fixed carbon and oxygen content are calculated based on difference.

Operating Bed Depth

In Chapter 5, it has been shown that higher bed height leads to greater solid circulation rate (SCR). This is expected to offer higher heat and mass transfer rate between the combustor and the gasifier. In addition, higher bed height permits greater amount of palm shell in the binary mixture within the critical loading.

However, the maximum operating bed height is limited by the riser height (60 cm). It is undesirable for the expanded bed height to exceed the riser height because of the risk of solid back flowing that may interrupt the solid circulation. To account for the bed expansion during fluidization and palm shell loading, the static bed height consisting of sand is set at 40 cm in both of the compartments. This corresponds to 110 kg and 77 kg in the combustor and gasifier respectively. Overall, the operating bed height is always below 55 cm.

Operating Superficial Velocity

It is reported in Chapter 4 that the sand-palm shell overall mixing quality (M) depends on the operating superficial velocity. Results indicate that a good mixing quality ($0.85 \leq M < 1.0$) can be established at the superficial velocity of 1.50÷2.50 U/U_{mf} and 1.43÷2.06 U/U_{mf} for the combustor and gasifier respectively. Thus, the air and steam flowrates to the combustor and gasifier respectively are configured based on these findings during the pilot plant performance testing. The U_{mf} value is estimated using the Equation (3-3) proposed in Chapter 3 and is accounted for the thermal variation based on the respective bed temperature.

Air Supply

The air flowrate to the combustor is controlled in the range of 20÷47 Nm^3/hr, with a typical value of 20.5 Nm^3/hr during the gasification stage. It is noted that the air flowrate required during the pilot plant performance testing is lower than that at ambient condition for the same superficial velocity due to the temperature effect. Air is supplied to the gasifier during the startup and combustion stages to elevate its bed temperature before switching over to steam for palm shell gasification. The air flowrate to the gasifier is controlled at about 12÷28 Nm^3/hr. The air is preheated to the range of 200÷350°C and is at atmospheric pressure in both compartments.

Steam Supply

The steam flowrate to the gasifier is controlled in the range of 7÷11 kg/hr, with an average value of 7.7 kg/hr during the gasification stage. The steam is superheated to 250°C and is at the atmospheric pressure.

Solid Circulation

In Chapter 5, apart from the main bed aeration, air was also supplied to the V-valve and riser in both compartments for solid to circulate (refer to Figure 5-2). Besides that, the operating superficial velocity for the combustor V-valve and riser pair was configured identical to that of gasifier V-valve and riser pair during the steady solid circulation.

During the gasification stage, instead of air, superheated steam is supplied to the gasifier V-valve and riser pair. As shown later, although preheated air is supplied to the combustor riser to provide the equivalent operating superficial velocity to that of the gasifier riser, no aeration is required for the combustor V-valve. This is probably due to the fluidizing gas from the gasifier that leaked into the combustor V-valve. Yan (1995) observed gas leakage during coal gasification in a compartmented reactor while He (1993) reported the same finding in a cold flow model.

Palm Shell Feeding Rate

The CFBG pilot plant capacity is of 1 ton palm shell per day. Palm shell feeding rate is controlled in the range of 12÷45 kg/hr, with an average value of 35 kg/hr during the gasification stage. It is noted that the palm shell is fed to both compartments during startup and combustion stages; during the gasification stage, palm shell is fed only to the gasifier.

Operating Temperature and Pressure

The operating bed temperatures for both the combustor and gasifier are controlled below ash sintering temperature or at least within the condition that minimizes the formation of ash agglomerates. During the pilot plant performance testing, the bed temperature is always below 700ºC for both compartments. The compartments are operated at atmospheric pressure.

6.4 CFBG PILOT PLANT GASIFICATION PROCESS

Generally, palm shell gasification process in the CFBG pilot plant can be categorized into 7 basic operational stages to reach a steady state production of fuel gas as shown in Figure 6-4, namely

(i) startup
(ii) palm shell feeding
(iii) auto ignition
(iv) heating up/combustion
(v) solid circulation
(vi) air-to-steam switchover, and
(vii) gasification

Each of the stages is illustrated in Figure 6-4 to give the pilot plant operational overview presented in terms of their characteristic bed temperature and duration. Each stage plays a role in ensuring a successful operation of the CFBG pilot plant. Although these stages are obtained by utilizing a specific reactor design, the process of the palm shell gasification is expected to be relevant if the compartmented reactor system is to be realized in the industrial scale.

From the startup, the bed temperature in both compartments is gradually increased to the maximum by the palm shell auto-ignition and combustion in both of the compartments. After that, solid circulation is initiated where the bed temperatures are initially reduced, then equalized before finally achieving the steady state values where the combustor temperature is higher than that of the gasifier.

In the following section, each operational stage is described using the respective historical profiles obtained from a complete experimental run. For the ease of interpretation, the bed temperature and bed pressure drop for the combustor and gasifier are colour coded in red and blue respectively.

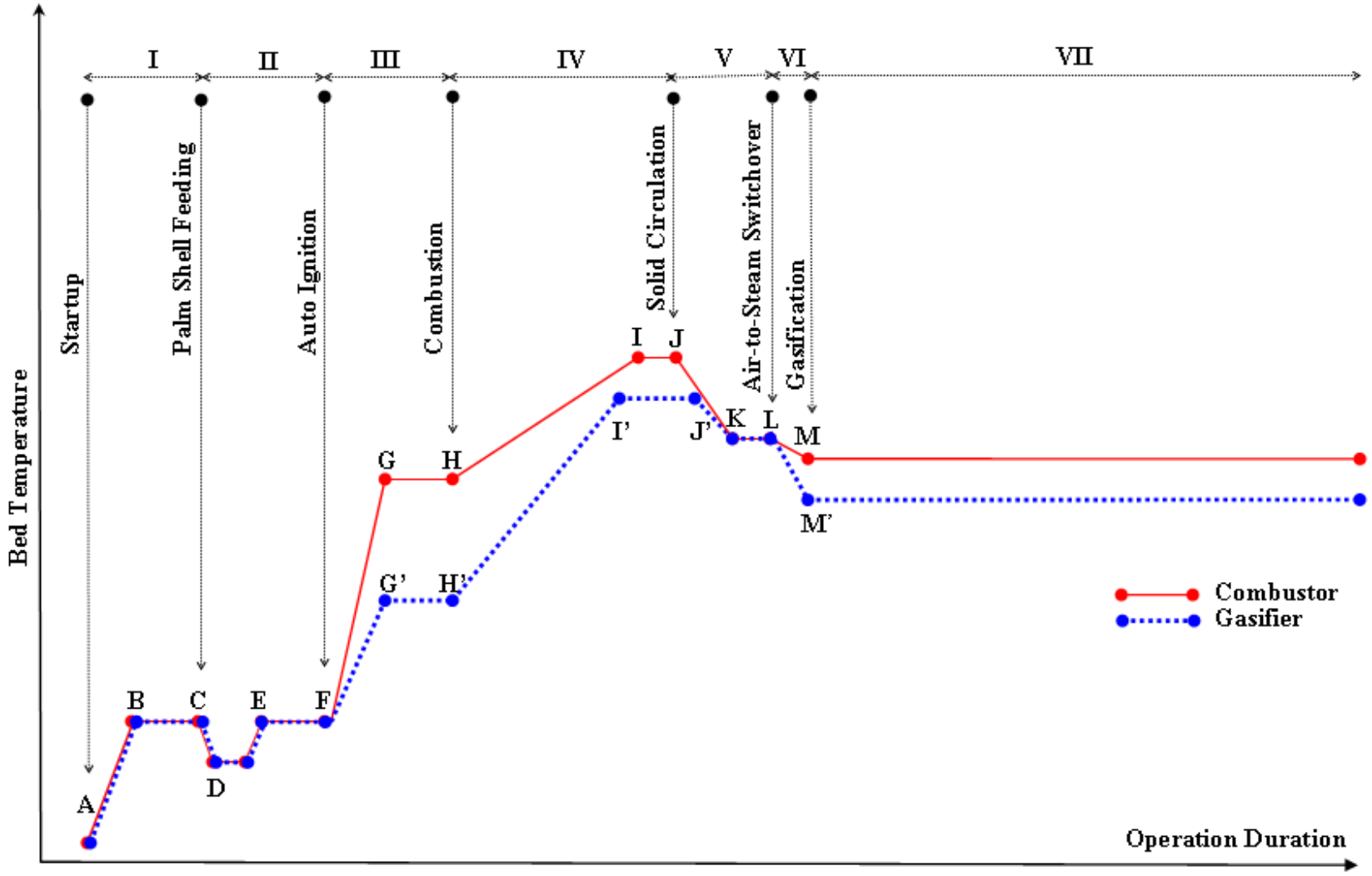

Figure 6-4: Typical bed temperature profiles for the combustor and gasifier.

Stage I: Startup

During CFBG pilot plant startup, preheated air is used to fluidize and heat up the sand in the combustor and gasifier where both bed temperatures (TT305 and TT306 respectively) gradually increased to about 200°C, as shown in Figure 6-5.

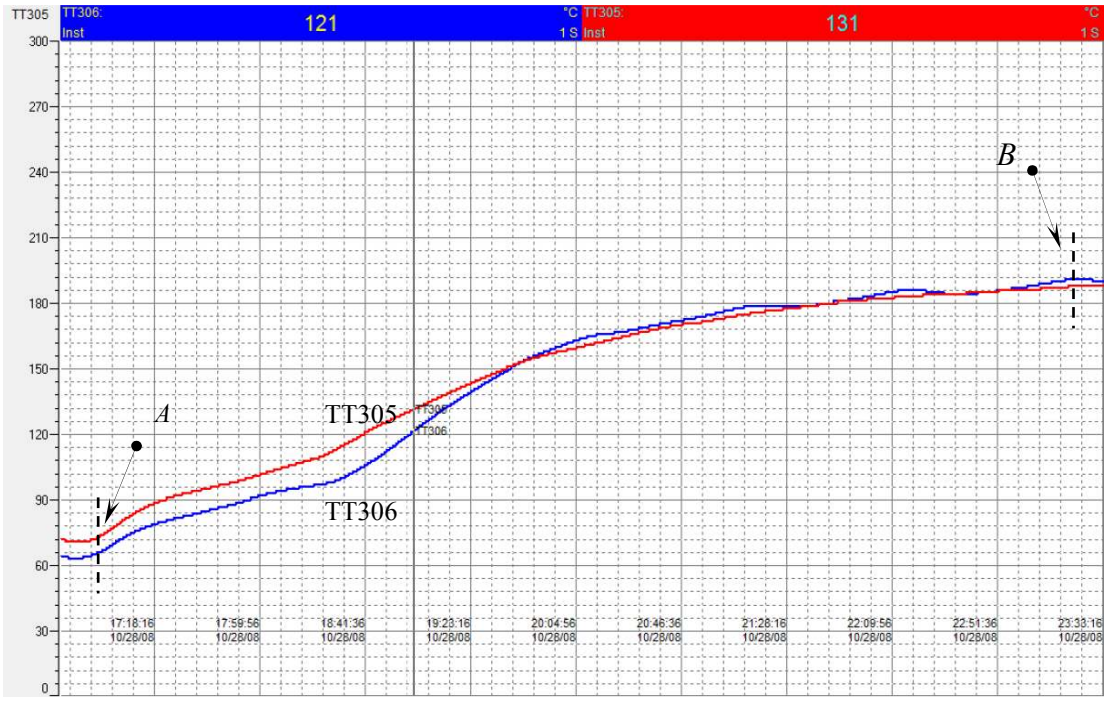

Figure 6-5: Bed temperature profiles in stage I; *'A'* and '*B'* indicate the initial and steady state bed temperatures.

Stage II: Palm Shell Feeding

Upon achieving the steady state bed temperature, palm shell mean sieve size of 3.56 mm is loaded to both the combustor and gasifier as the startup fuel. Figure 6-6 shows that the initial bed pressure drop, labelled as '*C'* for both the combustor and gasifier (DPT307 and DPT308 respectively) are at 50 mbar. When the palm shell is loaded, the bed pressure drop increased to 64 mbar and 56 mbar for both the combustor and gasifier respectively, denoted as '*D'* in Figure 6-6.

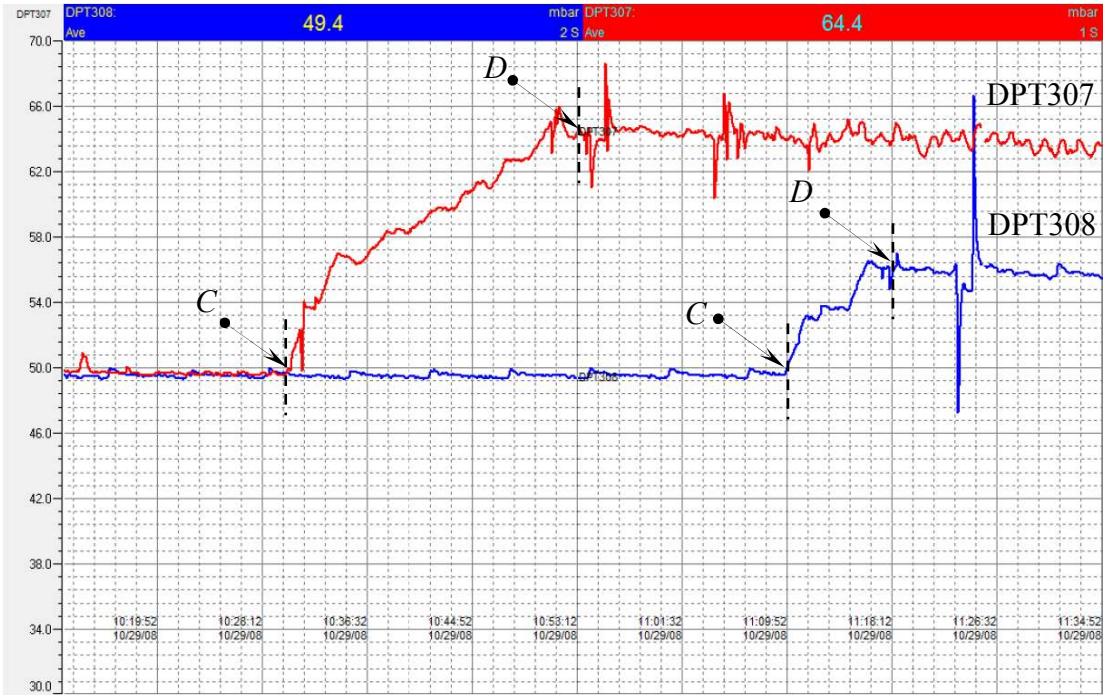

Figure 6-6: Bed pressure drop profiles in stage II; *'C'* and *'D'* indicate the starting and ending point of initial palm shell loading.

Once the palm shell is loaded, Figure 6-7 shows that the bed temperature in both compartments is slightly reduced (denoted as '*E*') by 10÷20°C due to the heat transfer, but it eventually recovers to 200°C (denoted as '*F*').

At this stage, the air flowrates (FT212 and FT130) to the combustor and gasifier are about 47 Nm^3/hr and 28 Nm^3/hr respectively. These correspond to the operating superficial velocities of about 2.05 and 1.87 U/U_{mf} for the combustor and gasifier respectively to promote good mixing in the sand-palm shell mixture.

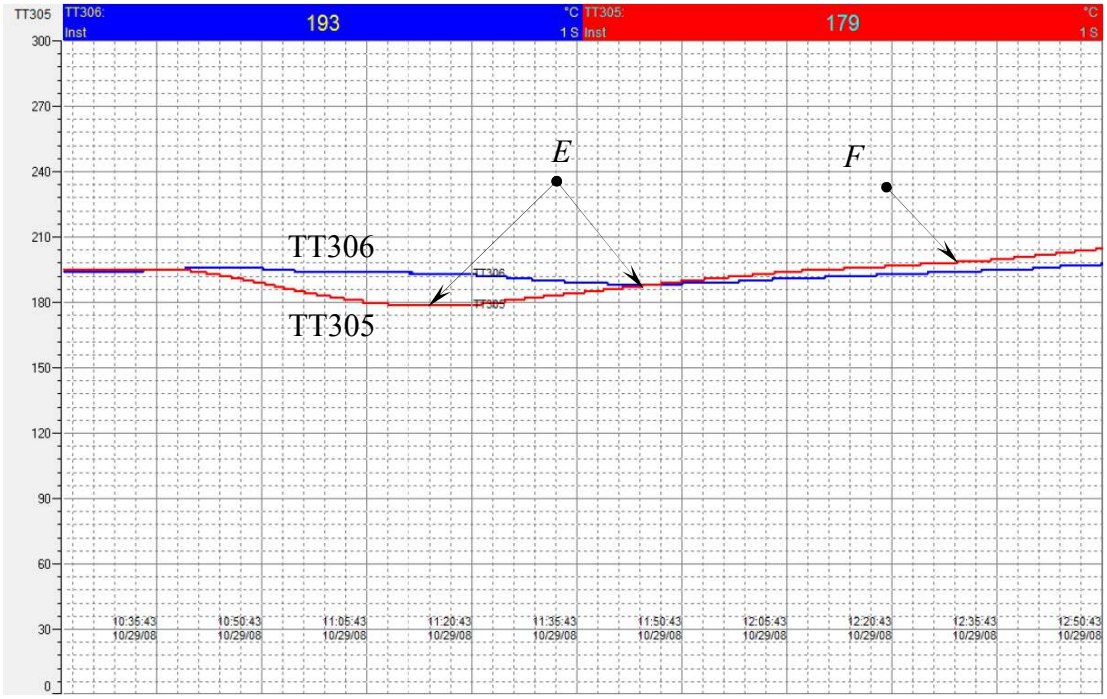

Figure 6-7: Bed temperature profiles in stage II; *'E'* and '*F'* indicate the lowest and the recovered bed temperature respectively after palm shell is loaded.

Stage III: Auto Ignition

At about 200°C, the palm shell started to combust leading to an increase in the bed temperature as depicted in Figure 6-8. The onset of palm shell combustion, indicated as '*G*', is found to be approximately equal to the typical starting temperature of palm shell devolatilization process of about 200÷220°C as reported by Yang et al. (2004), Shamsuddin and Williams (1992). This temperature is also very similar to the auto-ignition temperature of other biomass residual (220÷235°C) with high volatile (>70 wt%) such as wheat straw and poplar wood (Grotkjær et al., 2003).

Figure 6-9 shows that the onset of palm shell combustion, denoted as '*I*' is accompanied by a drop in the O_2 or increase in the CO_2 concentration in the flue gas. This process characteristic feature is typically observed during the startup of bubbling fluidized bed boiler (Combustion and Gasification in Fluidized Bed (2006)). The initial combustion process continued until the peak bed temperature (indicated as '*H*' in Figure 6-8) is achieved in the combustor and gasifier (of about 540°C and 450°C) while simultaneously, O_2 is restored to ambient air quality as shown in Figure 6-9 (indicated as *'J'*).

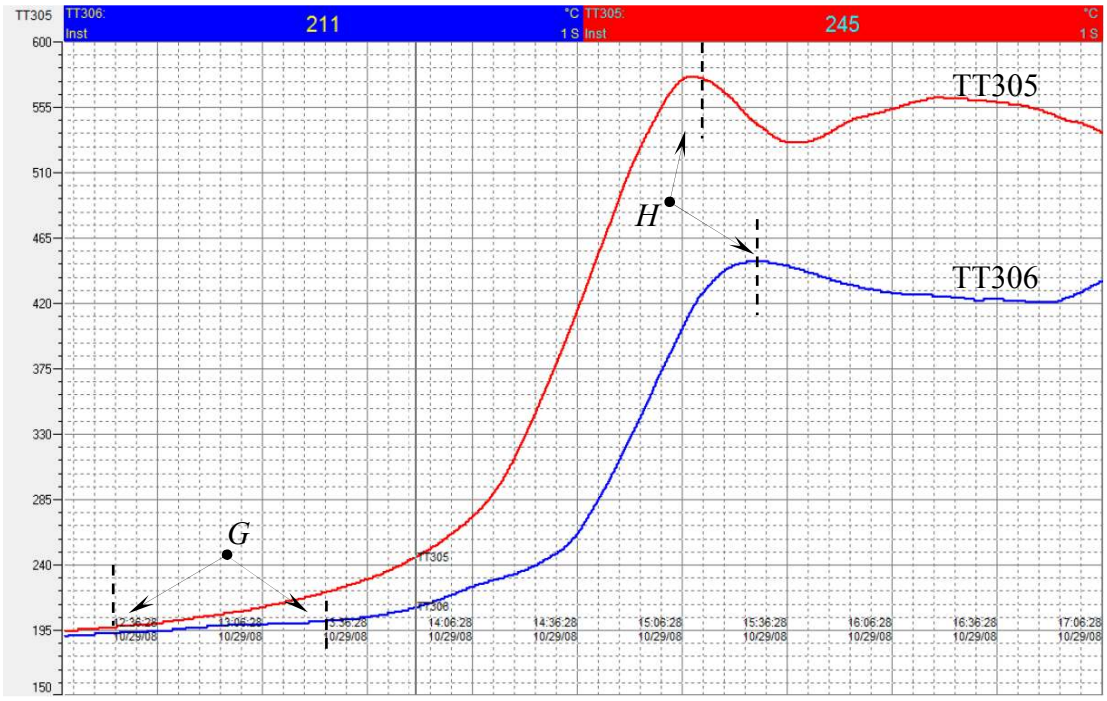

Figure 6-8: Bed temperature profiles in stage III; *'G'* and *'H'* indicate the palm shell auto ignition and maximum combustion temperature respectively.

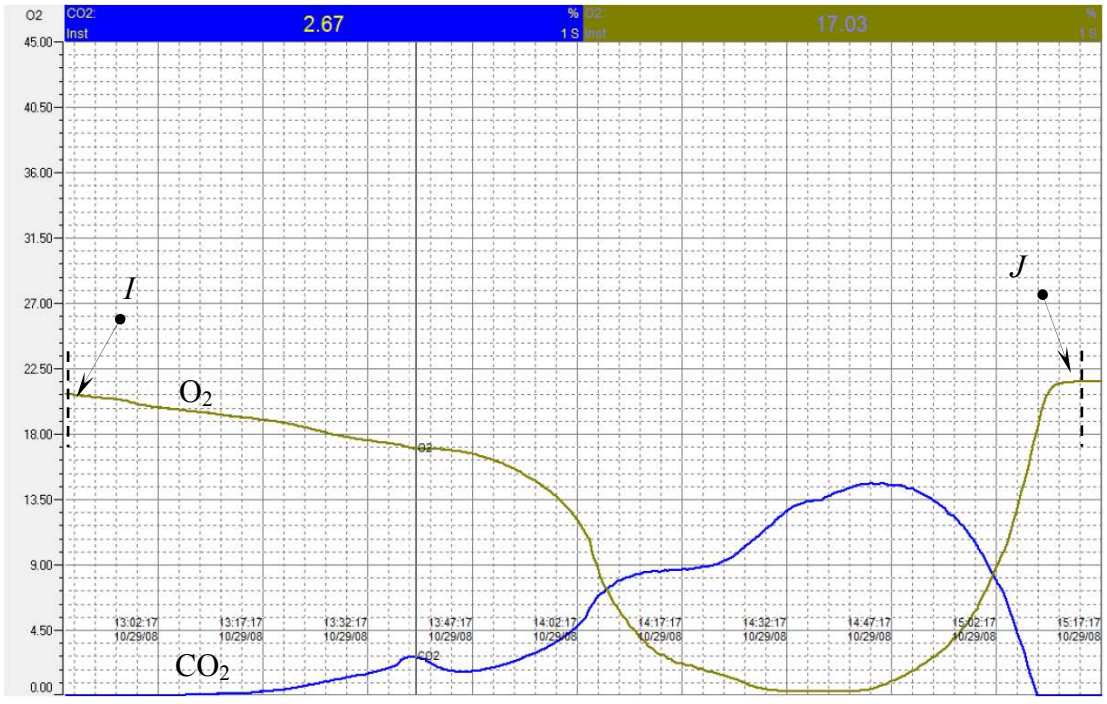

Figure 6-9: Flue gas profiles in stage III; *'I'* and '*J'* indicate the onset and completion of palm shell initial combustion.

Figure 6-10 shows that the bed pressure drop in stage II (denoted as '*K*') is gradually reduced to the startup bed pressure drop of 50 mbar (denoted as '*L*') for both the

combustor and gasifier (DPT307 and DPT308 respectively), thus confirming that the initial palm shell load had been fully combusted.

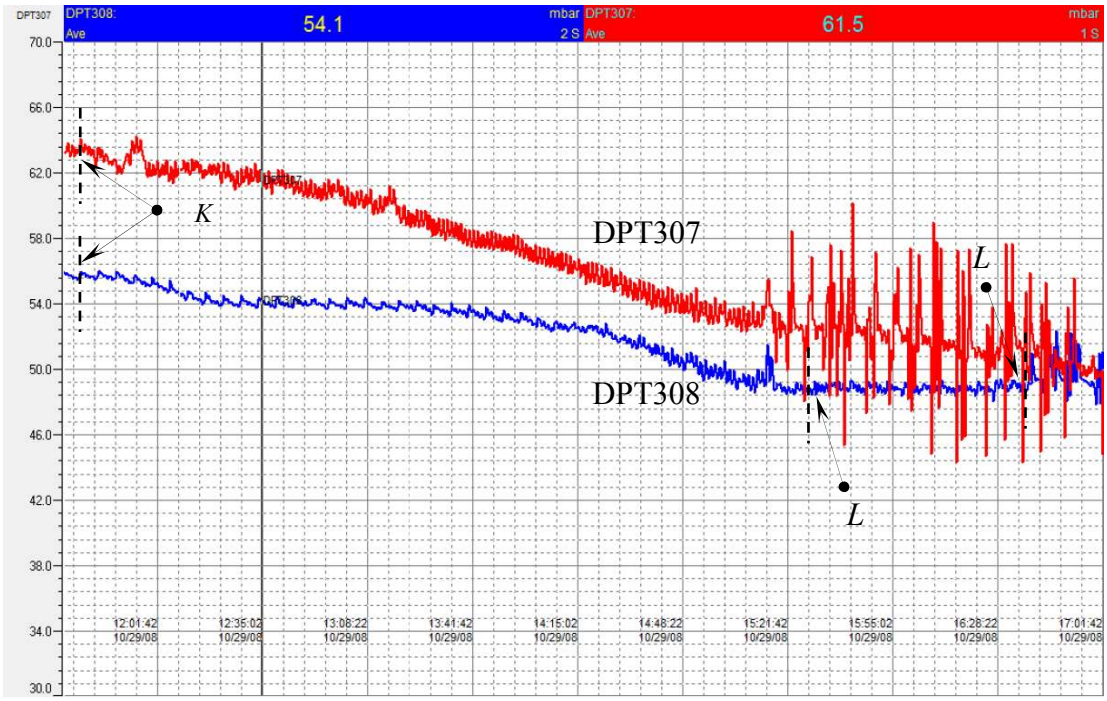

Figure 6-10: Bed pressure drop profiles in stage III; *'K'* and *'L'* indicate the bed pressure drop after palm shell is loaded and completion of palm shell combustion respectively.

Stage IV: Combustion

Once the initially loaded palm shell is fully combusted, the palm shell continuous feeding is started at the rate of about 9÷13 kg/hr, with a typical value of 12 kg/hr in both compartments[p]. To keep within the desirable state of fluidization at higher bed temperature, the air flowrate (FT212 and FT130) is gradually reduced to 23.5 Nm^3/hr and 12.5 Nm^3/hr for the combustor and gasifier respectively. These flowrates correspond to about 2.04 U/U_{mf} and 1.52 U/U_{mf}. The bed temperature (TT305 and TT306) in both compartments eventually reaches a steady value of about 500÷550°C as shown in Figure 6-11.

[p] Palm shell is manually fed into the combustor.

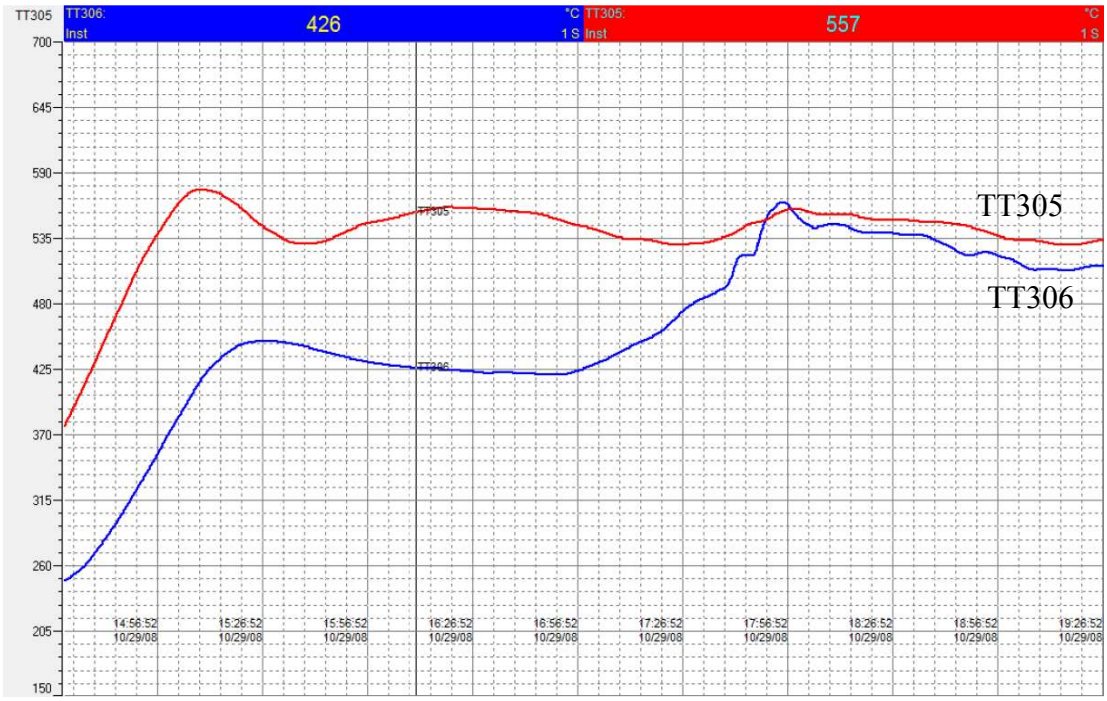

Figure 6-11: Bed temperature profiles in stage IV.

Until this stage, the combustor and the gasifier operate as an "individual" fluidized bed reactor since the internal solid circulation is only initiated in the subsequent stage.

Stage V: Solid Circulation

Upon achieving the stable bed temperature, solid circulation is initiated with the use of preheated air in the V-valve and riser pair in both the combustor and gasifier. The starting point is denoted as '*M'* in Figure 6-12. It can be observed that the bed pressure drop (DPT307 and DPT308) in the combustor and gasifier began to fluctuate in cyclic manner indicating the transfer of bed materials between the two compartments.

During the solid circulation, Figure 6-13 shows that the bed temperature in the two compartments quickly equalizes (at point '*N*'). This temperature gradually decreases and finally reaches a stable value indicated as '*O'*. The decrease in the bed temperature is probably due to the additional fine palm shell/chars that is entrained and combusted in the freeboard region, following the additional air supplied to the V-valves and risers.

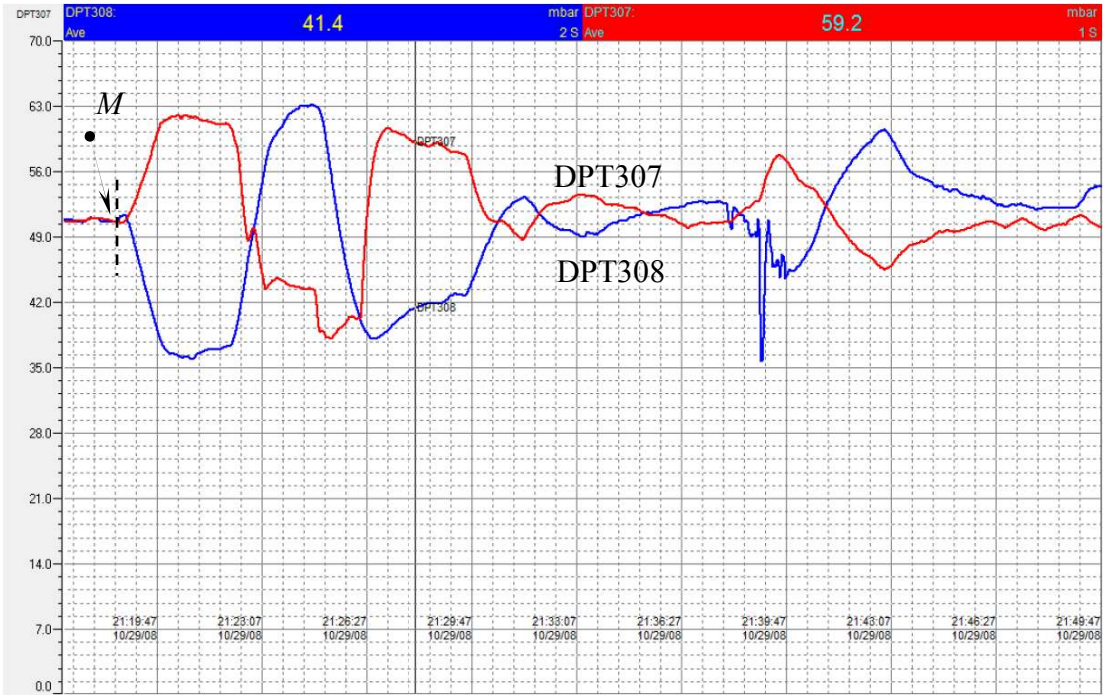

Figure 6-12: Bed pressure drop profiles in stage V; *J'* indicates the starting point for solid circulation using preheated air in both the combustor and gasifier V-valve and riser pair.

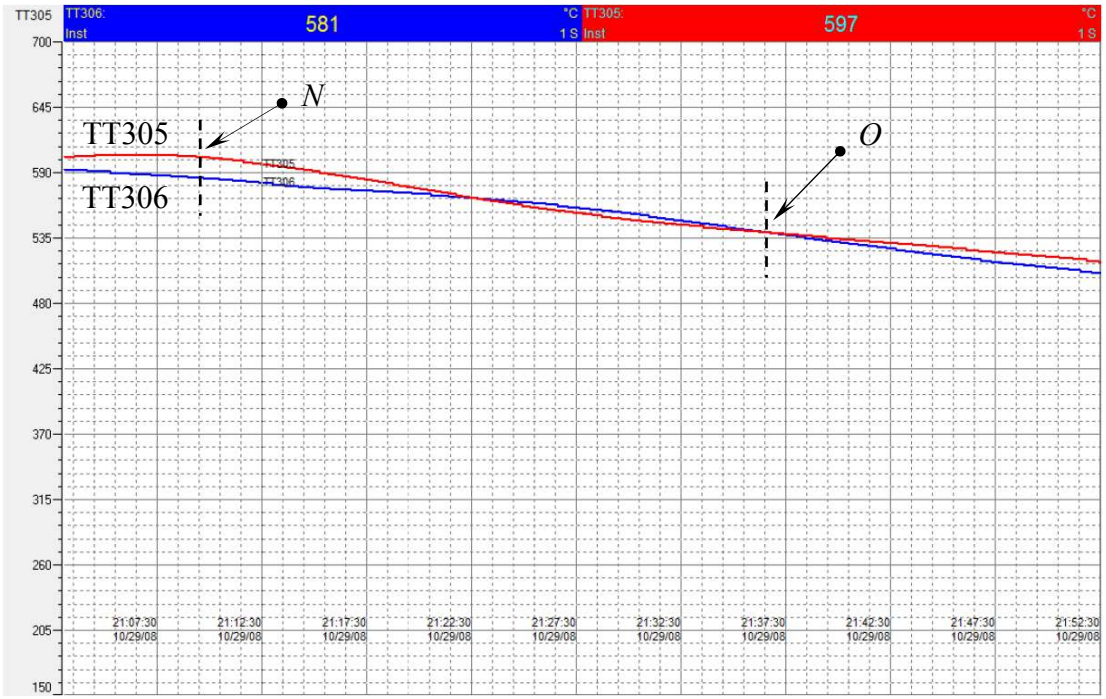

Figure 6-13: Bed temperature profiles in stage V; '*N*' and *'O'* indicate the point just after solid circulation is started and ended respectively using preheated air in both the combustor and gasifier V-valve and riser pair.

When the solid circulation is established, palm shell is continuously fed only to the gasifier at the feed rate of about 35÷45 kg/hr, with a typical value of 35 kg/hr.

Stage VI: Air-to-Steam Switchover

Once the bed temperature in both of the compartments has reached a steady state, the preheated air supplied to the gasifier and its V-valve and riser pair is switched over to superheated steam. This stage is performed in such a manner so that a steady solid circulation and bed temperature can be achieved in both compartments while the palm shell is continuously fed to the gasifier. This stage is the precursor for the palm shell gasification stage where the operational parameters are maintained until the completion of the pilot plant performance testing.

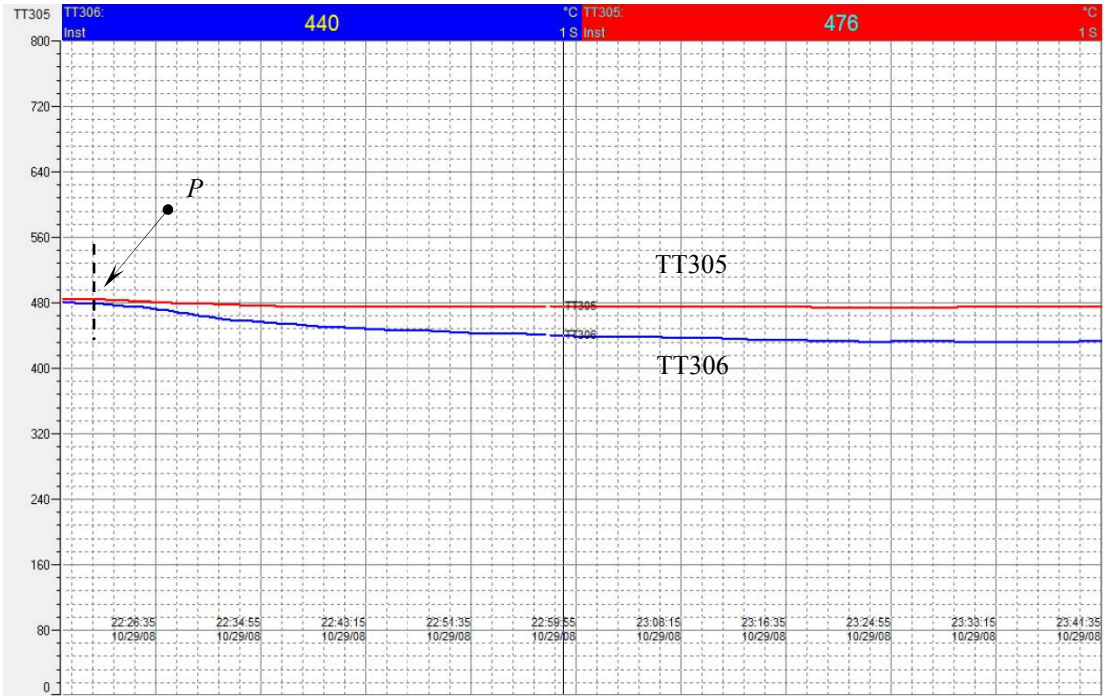

Figure 6-14: Bed temperature profiles in stage VI during air-to-steam switchover in the gasifier; *'P'* indicates the starting point of air-to-steam switchover.

Figure 6-14 shows the starting point "*P*" of utilizing superheated steam[q] in the gasifier and its V-valve and riser pair. The bed temperature in both the compartments decreased initially with greater reduction in the gasifier than in the combustor, before

[q] The orifices installed for preheated air flow measurement in the gasifier have been replaced with those orifices that are designed for superheated steam flow measurement.

gradually reaching the steady state values. The higher reduction of the bed temperature in the gasifier is due to the endothermic gasification reaction. It is worth mentioning that the steady state bed temperature difference of about 50°C between the combustor and gasifier.

Since the palm shell is only fed to the gasifier, the combustor bed temperature (TT305) that is maintained steadily at about 480°C is due to the in-bed combustion of the transported palm shell and/or chars from the gasifier via the solid circulation. Similarly, the gasifier bed temperature (TT306) that is maintained steadily at about 440°C, even under endothermic gasification reaction, is due to the indirect heat transferred via circulated hot solid from the combustor.

The preheated air[r] and superheated steam[s] flowrates (FT212 and FT130) to the combustor and gasifier are controlled at 20.5 Nm^3/hr and 7.7 kg/hr respectively. These correspond to operating superficial velocities of about 2.42 U/U_{mf} and 1.62 U/U_{mf}.

In the gasifier, the superheated steam flowrates (FT128 and FT129) to the V-valve and riser pair are about 5.1 kg/hr and 3.3 kg/hr respectively. These values correspond to 22.60 U/U_{mf} and 7.40 U/U_{mf}. Similarly, the preheated air flowrate (FT213) to the combustor riser is about 3.3 Nm^3/hr to give the same operating superficial velocity as configured in the gasifier riser. However, steady solid circulation is achieved during the gasification stage without aeration to the combustor V-valve (FT214). This is probably due to the leakage of fluidizing steam from the gasifier bed into the combustor V-valve, since solid circulation cannot occur if V-valve is not fluidized (He, 1993). It is assumed that the steam flowrate that leaked into the combustor V-valve is of 2.95 kg/hr[t] to give the above operating superficial velocity of the gasifier V-valve.

[r] Preheated air density is taken as 0.614 kg/m^3 at temperature of 300°C and in ambient pressure.

[s] Superheated steam density is taken as 0.421 kg/m^3 at temperature of 250°C and in ambient pressure.

[t] Superheated steam density is taken as 0.304 kg/m^3 at temperature of 440°C and in ambient pressure.

Stage VII: Gasification

The dry fuel gas composition in the gasifier during the palm shell gasification stage is shown in Figure 6-15. It can be seen that H_2 and CO composition are of about 15 and 35 vol% respectively, with lesser amount of CH_4 and CO_2 of about 12 and 14 vol% respectively. O_2 concentration is negligible. It is assumed that the remaining gas is N_2 of about 24 vol%. For comparison, the N_2 in fuel gas was 12÷22 vol% in coal gasification in the compartmented reactor (Yan, 1995). The heating value for the gas component can be found in Waldheim and Nilsson (2001).

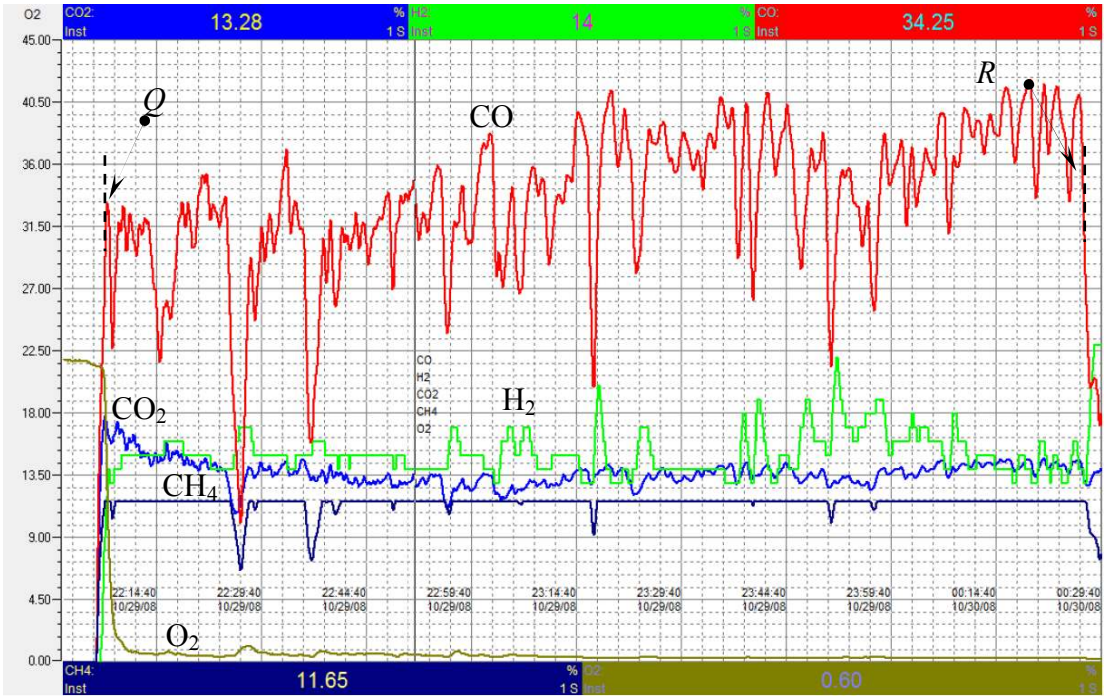

Figure 6-15: Dry fuel gas profiles in stage VII; *'Q'* and *'R'* indicate the start and end points in the gasification stage respectively.

Figure 6-16 shows the fuel gas flowrate[u] (FT401) of about 32 Nm^3/hr in wet basis. It is assumed that the moisture in the feedstock, steam supplied to the gasifier (after discounted for the steam leaked into the combustor V-valve described in stage VI), V-valve and riser pair are present in the fuel gas. The estimated moisture content in the fuel gas is about 60 vol%. Hence, the dry fuel gas flowrate is estimated to be about 12.8 Nm^3/hr.

[u] Fuel gas density is taken as 0.68 kg/m^3 at temperature of 100°C and in ambient pressure. The fuel gas flow transmitter (FT401) is located after the air cooler for the fuel gas from the gasifier (refer to Figure 6-2).

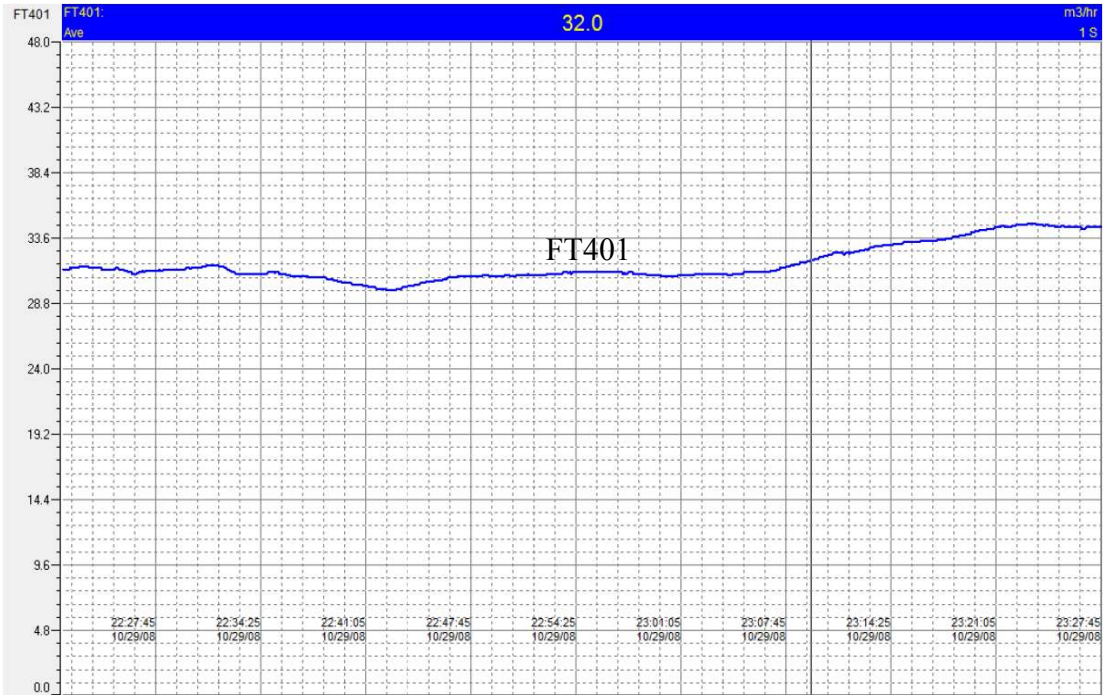

Figure 6-16: Fuel gas flowrate in stage VII.

Upon completion of the steady state data collection in the gasification stage, the solid circulation rate (SCR) is determined based on the procedures described in Chapter 5. The SCR is estimated to be of about 201 kg/hr. The main process parameters of the palm shell gasification are summarized in Table 6-3.

Table 6-3: Main process parameters of palm shell gasification

a)	Running time:		
	total:	16	(h)
	at steady state:	2	(h)
b)	Operating parameters:		
	1. Palm shell feeding rate	35	(kg/hr)
	2. Sand weights in bed		
	combustor	110	(kg)
	gasifier	77	(kg)

Table 6.3 *continued*

3. Palm shell mean particle size			
start up		3.56	(mm)
steady gasification		4.24	(mm)
4. Sand mean particle size		395[v]	(μm)
5. Solid circulation rate		201	(kg/hr)
6. Gas feed rates (273K, 1 atm)			
combustor (air)			
	main bed	20.5	(Nm^3/hr)
	V-valve	-	(Nm^3/hr)
	riser	3.3	(Nm^3/hr)
gasifier (steam)			
	main bed	7.7	(kg/hr)
	V-valve	5.1	(kg/hr)
	riser	3.3	(kg/hr)
7. Operating temperature (°C)			
		Combustor	Gasifier
air/steam		300	250
bed		480	440
8. Operating bed pressure drop			
combustor		50	(mbar)
gasifier		50	(mbar)

[v] Average sand mean particle size from stage II onwards is 350 μm. The lower sand mean particle size is due to particle attrition.

The fuel gas production flowrate, composition and higher heating value (HHV), as well as the gas yield are presented in Table 6-4 above in wet and dry basis. It can be seen that the fuel gas has a higher heating value in wet basis, HHV_w of 4.44 MJ/Nm^3 suitable to be used as town gas, for district heating and gas engines.

Table 6-4: Fuel gas of palm shell gasification

	Wet	Dry
1. Fuel gas production (Nm^3/hr)	32.0	12.8[w]
2. Higher heating value (MJ/Nm^3)	4.44	11.11
3. Fuel gas composition (vol%)		
H_2	6.0	15
CO	14.0	35
CH_4	4.8	12
CO_2	5.6	14
O_2	-	-
balance (N_2)	9.6	24[x]
balance (H_2O)	60.0	
4. Gas yield (Nm^3/kg feed)	0.91	0.37

If the steam is separated (via condensation) from the fuel gas, the higher heating value in dry basis, HHV_d is 11.11 MJ/Nm^3. The dry fuel gas quality is of medium calorific value. By standard comparison in terms of HHV_d and syngas (H_2 and CO) composition, CFBG pilot plant has significantly higher values than the existing bubbling fluidized bed (BFB) gasifier using air or air and steam as reported in the recent biomass gasification technologies survey by Ciferno and Marano (2002). Moreover, despite of the compact reactor feature, CFBG pilot plant can produce medium calorific value fuel gas that is comparable to the typically larger reactor column in circulating fluidized bed (CFB) reported in their work and other indirectly

[w] Moisture content and dry fuel gas flowrate are estimated based on the assumptions as discussed in stage VI and VII.

[x] N2 content in fuel gas is based on the assumption as discussed in stage VII.

heated gasification processes (Boerrigter & Rauch, 2006). Besides that, the H_2/CO ratio obtained in the CFBG pilot plant is of about 0.5, satisfying the recommended feed to Fischer-Tropsch process for synthetic gasoline and diesel production.

The calorific value of the dry fuel gas from the CFBG pilot plant can meet the gas turbine manufacturer requirement (Quaak et al., 1999). It is considered to be interchangeable with the conventional fossil fuel for industrial or utility applications (Marano & Ciferno, 2002). Integrating biomass gasifier with gas turbine and combined cycle (BIGCC) offers the highest electrical efficiency of about 50%, with higher figures expected within a decade because of the improved gas turbine (Williams & Larson, 1995). Such high efficiency is only attainable from medium and high calorific value fuel gas, which in turn requires lesser biomass consumption for electricity generation as compared to the producer gas quality.

According to Shuit et al. (2009), palm oil mills in Malaysia generate 5.92 million tonnes of palm shell waste annually. The availability of this biomass in Thailand and Columbia can be found in Arrieta et al. (2006). Correspondingly, by scaling up the performance data of CFBG pilot plant, 18 tonnes per hour of palm shell feed (144000 tonnes per annum or 2.5% consumption from the total availability in Malaysia annually) can generate 10MW_e of electricity to accommodate 10,000 houses[y].

6.5 SUMMARY

The performance testing of the CFBG pilot plant for the palm shell gasification has been successfully demonstrated. A steady state operation is achieved in the CFBG pilot plant using sand as the main fluidizing material and palm shell as the biomass feedstock with the capacity of 1 ton per day for the production of medium calorific value fuel gas (of 11.11 MJ/Nm^3 in dry basis) with H_2/CO ratio of 0.5 suitable for syngas and power generation.

It is worth emphasizing that the stable operation of CFBG pilot plant is realized using the operating ranges studied in the first part of this work.

[y] Electricity consumption for an average house is around 1 kW_e (Lim & Alimuddin, 2008).

CHAPTER 7

CONCLUSIONS AND RECOMMENDATIONS

This chapter summarizes the key findings on the fluidization behavior, mixing quality and solid circulation rate that were realized and identified in the CFBG cold flow model of a pilot plant scale, and the implementation of these findings to develop and operate CFBG pilot plant with particular reference to palm shell as a biomass feedstock. It also provides the recommendations for future research in this area.

Fluidization Characteristics

- The baseline study using common inert material, sand of 4 mean particle sizes i.e. 196, 272, 341 and 395 μm showed that the fluidization behaviour for a single component system in the compartmented reactor was similar to those observed in a cylindrical column with $U_{cf} > U_{mf}$, U_{mf} and U_{cf} increasing with the increase of sand mean particle size, and the characteristic fluidization velocities for the gasifier (of a smaller effective bed diameter) were larger than those of the combustor.

- The differences in the characteristic fluidization velocities between the compartments can be minimized by utilizing the larger sand mean particle size as a bed material, hence avoiding physical modification on the CFBG.

- The existing correlations were modified to predict satisfactorily the U_{mf} and U_{cf} for both the compartments.

- The sand-palm shell binary system fluidization study was performed using palm shell of 4 different mean sieve sizes i.e. 1.77, 3.56, 7.13 and 11.75 mm. The palm shell weight fractions were varied in 2, 5, 10 and 15 wt%. The findings are:
    - U_{mf} and U_{cf} for the gasifier are larger than those of the combustor.

- there is a tendency for the U_{mf} and U_{cf} to increase with the increase in the palm shell mean sieve size and weight percent.
- when a larger sand mean particle size was used in the binary mixture, analysis on $\left(\frac{U_{mf}}{U_{mf,sand}}\right)$ and $\left(\frac{U_{cf}}{U_{cf,sand}}\right)$ ratios revealed trends of reducing the ratios and approaching unity.

- The concept of critical loading was introduced to characterize the maximum palm shell content in the sand where the U_{mf} and U_{cf} for the binary mixture are determined principally by the sand. Within the critical loading, a single operational velocity can be set for the respective compartment based on the sand value and the proposed correlations developed from the sand can be used to estimate the U_{mf} and U_{cf} for the binary mixture.

- The critical loading was found to
  - increase with the sand mean particle size.
  - decrease with the increase of the palm shell mean sieve size.

Mixing Quality

- Palm shell vertical distribution was similar for both the compartments. The local mixing index is lower at the bed bottom as compared to the middle/upper bed sections.

- Palm shell lateral distribution was different for the two compartments. The local mixing index increased laterally (from the V-valve to riser) for the gasifier, but showed a decreasing trend for the combustor at higher superficial velocity.

- In spite of the local variation of the palm shell concentration, good overall mixing quality ($0.85 \leq M < 1.0$) can be established at the superficial velocity of 1.50÷2.50 and 1.43÷2.06 U/U_{mf} for the combustor and gasifier respectively.

- The study showed that the overall mixing quality
  - improves with the smaller palm shell mean sieve size.

- improves with the higher palm shell weight percent.
- for the combustor (of a larger effective bed diameter) is better than that for the gasifier.
- is not affected by the bed height.

Solid Circulation Rate

- From the parametric studies on the solid circulation rate, a common finding obtained in the CFBG similar to the other compartmented reactor designs is that a higher static bed height leads to a higher SCR. However, the maximum operating height is limited by the riser height.

- The main bed aeration shows no effect on the solid circulation rate. This is consistent with the statistical analysis.

- From factorial analysis in combination with the half normal plot and steepest ascent method, V-valve and riser aerations were simultaneously adjusted to determine the optimum solid circulation rate.

- It was found that a larger sand mean particle size produces a higher optimum SCR value. This suggests that the utilization of larger sand size as a bed material in the CFBG offers higher and yet flexible solid exchanged rate.

CFBG Pilot Plant Performance Testing

- A stable operation of CFBG pilot plant of 1 ton palm shell per day was realized using the operating ranges studied in the cold flow model where
  - air and steam flowrates were configured at 1.50÷2.50 U/U_{mf} and 1.43÷2.06 U/U_{mf} for the combustor and gasifier respectively. The U_{mf} was estimated using the proposed correlation and accounted for the thermal variation based on the respective bed temperature.
  - the sand mean particle size of 395 μm was loaded to a static bed height of 0.4 m in both compartments. The palm shell mean sieved size of 3.56 mm was selected as the startup fuel.

- Palm shell gasification process in the CFBG pilot plant was conceptually categorized into 7 basic operational stages to reach a steady state production of fuel gas.

- The fuel gas has a higher heating value in wet basis, HHV_w of 4.44 MJ/Nm^3 suitable to be used as town gas, for district heating and gas engines.

- The higher heating value in dry basis, HHV_d is 11.11 MJ/Nm^3. The dry fuel gas quality is of a medium calorific value suitable for gas turbine power generation. The H_2/CO ratio obtained is of about 0.5, satisfying the recommended feed for Fischer-Tropsch (FT) process.

Recommendations

Various new research perspectives have been identified during the course of this study leading to recommendations for future research as follows:

- Further investigation can be performed to determine the sand size that will give higher critical loading (e.g. 50 wt %). The findings may be used to increase the pilot plant throughput. The critical loading can also be developed for different bed materials (e.g. CaO) and other biomass (e.g. palm fibre).

- The mixing quality of the binary mixture was studied in a fixed sand mean particle size selected based on the overall highest U_{cf}/U_{mf} ratio. The experimental studies can be extended for a range of sand sizes.

- The effect of solid circulation (via aeration of V-valve and riser) on the mixing quality should be explored.

- A more extensive analysis of the fuel gas quality is recommended (e.g. tar analysis).

- The present work has successfully proved the concept of CFBG as a prospective technology for palm shell gasification. Further experimental and optimization study can be conducted particularly on increasing the bed temperatures that may improve the fuel gas yield and quality.

REFERENCES

Abdullah, M. Z., Hussain, Z. & Ying Pong, S. L. (2003). Analysis of cold flow fluidization test results for various biomass fuels, *Biomass and Bioenergy*, 24, 487-494.

Abdullah, S. S. & Yusup, S. (2010). Method of screening Malaysian biomass based on aggregated matrix for hydrogen production through gasification, *Journal of Applied Sciences*, 10, 3301-3306.

Adánez, J. & Abanades, J. C. (1991). Minimum fluidization velocities of fluidized-bed coal-combustion solids. *Powder Technology,* 67, 113-119.

Arrieta, F. R. P., Teixeiraa, F. N., Yáñez, E., Loraa, E. & Castilloc, E. (2007). Cogeneration potential in the Columbian palm oil industry: Three case studies, *Biomass and Bioenergy*, 31, 503-511.

Azali, A., Nasrin, A. B., Choo, Y. M. & Adam, N. M. (2005) Development of gasification system fuelled with oil palm fibres and shells, *American Journal of Applied Sciences (Special Issue),* 72-75.

Aznar, M. P., Gracia-Gorria, F. A. & Corella, J. (1992a). Minimum and maximum velocities for fluidization for mixtures of agricultural and forest residues with a second fluidized solid. I. Preliminary data and results with sand-sawdust mixtures, *International Chemical Engineering*, 32, 95-102.

Aznar, M. P., Gracia-Gorria, F. A. & Corella, J. (1992b). Experimental results for different mixtures, *International Chemical Engineering*, 32, 103-113.

Bhattacharya, B., Sathiyamoorthy, D., Govardhana Rao, V. & Mahajan, S. P. (1991). Solid circulation in a compartmented gas fluidized bed, *Powder Technology*, 101, 191-204.

Bhattacharya, B., Sathiyamoorthy, D., Govardhana Rao, V. & Mahajan, S. P. (1997). Intermixing of fluidizing gas streams in a compartmented circulating fluidized bed, *Chemical Engineering Technology*, 20, 522-532.

Bhattacharya, B., Sathiyamoorthy, D., Govardhana Rao, V. & Mahajan, S. P. (1999). Solid circulating in a compartmented gas fluidized bed, *Powder Technology*, 101, 191-204.

Boerrigter, H. & Rauch, R. (2006). Review of applications of gases from biomass gasification, *ECN Biomass, Coal & Environmental research*, 33.

Bourgeois, P. & Grenier, P. (1968). The ratio of terminal velocity to minimum fluidising velocity for spherical particles, *The Canadian Journal of Chemical Engineering*, 46, 325-328.

Bilbao, R., J. Lezaun, J. & Abanades, J. C. (1987). Fluidization velocities of sand/straw binary mixtures, *Powder Technology*, 52, 1-6.

Bilbao, R., Lezaun, J., Menendez, M. & J. C. Abanades, J. C. (1988). Model of mixing-segregation for straw/sand mixtures in fluidized beds, *Powder Technology*, 56, 149-155.

Bourgeois, P. Grenier, P. (1968). The ratio of terminal velocity to minimum fluidising velocity for spherical particles, *The Canadian Journal of Chemical Engineering*, 46, 325-328.

Buslik, D. (1950). Mixing and sampling with special reference to multisized granule material, ASTM Bulletin, 66, 165.

Carman, P. C. (1937). Fluid flow through granular beds. Transaction in Institution of Chemical Engineers, London, 15, 150-166.

Cheremisinoff, N. P (1993). *Encyclopaedia of Fluid Mechanics: Solid and gas-solid flows*, Houston, Gulf Publishing Company, 831-832.

Chiba, S., Chiba, T., Nienow, A.W. & Kobayashi, H. (1979). The minimum fluidization velocity, bed expansion and pressure-drop profile for binary particle mixtures, *Powder Technology*, 22, 255-269.

Chiba, S., Nienow, A. W., Chiba, T. & Kobayashi, H. (1980). Fluidized binary mixtures in which the denser components may be flotsam, *Powder Technology*, 26, 1-10.

Chyang, C. S, Kuo, C. C. & Chen, M. Y. (1989). Minimum fluidization velocity of binary mixtures, *The Canadian Journal Of Chemical Engineering*, 67, 344-347.

Ciferno, J.P. & Marano, J.J. (2002). *Benchmarking biomass gasification technologies for fuels, chemicals, and hydrogen production*, U.S DOE, National Energy Technology Laboratory.

Corella, J., Toledo, J. M. & Gregorio Molina, G. (2007). A review on dual fluidized-bed biomass gasifiers, *Industrial & Engineering Chemical Research*, 46, 6831-6839.

Cui, H. & Grace, J. R. (2007). Fluidization of biomass particles: A review of experimental multiphase flow aspects, *Chemical Engineering Science*, 62, 45-55.

Delebarre, A. B., Pavinato, A. & Leroy, J. C. (1994). Fluidization and mixing of solids distributed in size and density, *Powder Technology*, 80, 227-233.

Delebarre, A. B. (2002). Does the minimum fluidization exist*?, Journal of Fluids Engineering*, 124, 595-600.

Delebarre, A. B. (2004). Revisiting the Wen and Yu equations for minimum fluidization velocity prediction, *Chemical Engineering Research and Design*, 82, 587-590.

Devore, J.L. (2004). *Probability and Statistics for Engineering and the Sciences*, 6th Edition, Thomson, Brooks/Cole.

Ergun, S. (1952). Fluid flow through packed columns, *Chemical Process Engineering*, 48, 89.

Fauziah, M., Norazah, A. R., Nornizar, A., Azli Bahari, A. & Tajuddin, M. J. (2008). Cold flow binary fluidization of oil palm residues mixture in a gas-solid fluidized bed system, *Pertanika Journal of Science & Technology*, 16, 201-212.

Formisani, B., Cristofaro, G. D. & Girimonte, R. (2001). A fundamental approach to the phenomenology of fluidization of size segregating binary mixtures of solids. *Chemical Engineering Science*, 56, 109-119.

Formisani, B., Girimontea, R. & Longoa, T. (2008a). The fluidization pattern of density-segregating binary mixtures, *Chemical Engineering Research and Design*, 86, 344-348.

Formisani, B., Girimontea, R. & Longoa, T. (2008b). The fluidization process of binary mixtures of solids: Development of the approach based on the fluidization velocity interval, *Powder Technology*, 185, 97-108.

Fox, D., Molodtsof, Y., & Large, J. F. (1989). Control mechanisms of fluidized solids circulation between adjacent vessels, *AIChE Journal*, 35, pp. 1933-1941.

Frantz, J. F. (1966). Minimum fluidization velocities and pressure in fluidized beds, *Chemical Engineering Program Symposium Series*, 62, 21-31.

Gauthier, D., Zerguerras, S. & Flamant, G. (1999). Influence of the particle size distribution of powders on the velocities of minimum and complete fluidization, *Chemical Engineering Journal*, 74, 181-196.

Geldart, D. (1973). Types of gas fluidization, *Powder Technology*, 7, 5, 285.

Glicksman, L. R. & McAndrews, G. (1985). The effect of bed width on the hydrodynamics of large particle fluidized beds. *Powder Technology,* 42, 159-167.

Gómez, A., Rincón, S. & Klose, W. (2009). Oil palm shells conversion to higher value products, *PIPOC 2009 International Palm Oil Congress, Chemistry Process Technology & Bio Energy Conference*, Kuala Lumpur, Malaysia.

Goossens, W. R. A., Dumont, G. L. & Spaepen, G. L. (1971). Fluidization of binary mixtures in the laminar flow region, *AIChE Symposium Series,* 67, 38–45.

Gorin, A., Chok, V. S., Wee, S. K., Chua, H. B. & Yan, H. M. (2008). Hydrodynamics of binary mixture fluidization in a compartmented fluidized bed, *18th International Congress of Chemical and Process Engineering: CHISA 2008*, Prague, Czech Republic.

Grotkjær, T., Dam-Johansen, K., Jensen, A.D., Glarborg, P. (2003). An experimental study of biomass ignition, *Fuel* 82, 825–833.

Guo, J. & Lua, A. C. (2001). Kinetic study on pyrolytic process of oil-palm solid waste using two-step consecutive reaction model, *Biomass and Bioenergy* 20, 223-233.

He, Y. (1993). *Hydrodynamics of a compartmented dense phase circulating fluidised bed.* (Doctoral Dissertation). The University of Queensland, Australia.

He. Y, Rudolph, V., Nicklin, D.J. & Chong, Y.O. (1993). Circulating fluidized oil shale retort, *Fuel*, 72 (6), 879-883.

He, Y. & Rudolph, V. (1997). A model for a dense phase circulating fluidized bed, *Chemical Engineering Communications*, 161, 103-124.

Hilal, N., Ghannam, M. T. & Anabtawi, M. Z. (2001). Effect of bed diameter, distributor and inserts on minimum fluidization velocity, Chemical Engineering Technology, 2, 24, 161-165.

Husain, Z, Zainal, Z. A. & Abdullah, M. Z. (2003). Analysis of biomass-residue-based cogeneration system in palm oil mills, *Biomass and Bioenergy*, 24, 117-124.

Johnson, R. A. (2005). *Miller & Freund's Probability and Statistics for Engineers*, 7th Edition, Prentice Hall.

Kawser, J. M. & Nash, A. F. (2000), Oil palm shell as a source of phenol, *Journal of Oil Palm Research*, 12, 86-94.

Kelly-Yong, T. L., Lee, K. T. & Bhatia, S. (2007). Potential of hydrogen from oil palm biomass as a source of renewable energy worldwide, *Energy policy*, 35, 5692–5701.

Knoef, H. A. M. (2005). *Handbook on biomass gasification*, Netherlands, GasNet.

Kunii, D. & Levenspiel, O. (1991). *Fluidization Engineering*, 2nd edition, United States of America: Butterworth-Heinemann.

Lacey, P. M. C. (1954). Developments of the theory of particle mixing, *Journal of Applied Chemistry*, 4, 257-268.

Li, J. F., Yin, Y. F., Zhang, X. M., Liu, J. J. & Yan, R. (2009). Hydrogen-rich gas production by steam gasification of palm oil wastes over supported tri-metallic catalyst, *International Journal of Hydrogen Energy*, 34, 9108-9115.

Li, Z. Y., Kobayashi, N., Nishimura, A. & Hasatani, M. (2005). A Method to predict the minimum fluidization velocity of binary mixtures based on particle packing properties, *Chemical Engineering*, 192, 918-932.

Limtrakukl, S., Chalermwattanatai, A., Unggurawirote, K., Tsuji, Y., Kawagushi, T. & Tanthapanishakoon, W. (2003). Discrete particle simulation of solids motion in a gas-solid fluidized bed, *Chemical Engineering Science*, 58, 915-921.

Lin, C. L. (2002). The effect of particle size distribution on minimum fluidization velocity at high temperature, *Powder Technology*, 126, 297-301.

Liu, X. H., Xu, G. W. & Gao, S. Q. (2008). Micro fluidized beds: Wall effect and operability, *Chemical Engineering Journal*, 137, 302-307.

Luangkiattikhun, P., Tangsathitkulchai, C. & Tangsathitkulchai, M. (2008). Non-isothermal thermogravimetric analysis of oil-palm solid wastes, *Bioresource Technology*, 99, 986-997.

Lucas, A. Arnaldos, J., Casal, J. & Puigjaner, L. (1986). High temperature incipient fluidization in mono and polydisperse systems, *Chemical Engineering Communication*, 41, 121-132.

Mabrouk , R., Chaouki, J., Radmanesh, R. & Guy, C. (2005). Scale effects on fluidized bed hydrodynamics, *International Journal of Chemical Reactor*, 3, 1-9.

Mourad, M., Hemati, M. & Lagueris, C. (1994). Hydrodynamique d'un &choir B lit fluidis B flottation: Dktermination des vitesses caractkristiques de fluidisation de melanges de mak et de sable, Powder Technology, 80, 45-54.

Nienow, A. W., Rowe, P. N. & L.Y.-L. Cheung, L. Y. L. (1978). A quantitative analysis of the mixing of two segregating powders of different density in a gas-fluidised bed, *Powder Technology*, 20, 89-97.

Noda, K., Uchida, S., Makino, T. & Kamo, H. (1986). Minimum fluidization velocity of binary mixtures of particles with large size ratio, *Powder Technology*, 46, 149-154.

Pattipati, R. R. & C.Y. Wen, C. Y. (1981). Minimum fluidization velocity at high temperatures, *Industrial Engineering and Chemical Process Design and Development*, 20, 705-708.

Patumsawad, S. & Cliffe, K. R. (2002). Experimental study on fluidised bed combustion of high moisture municipal solid waste, *Energy Conversion and Management,* 43, 2329–2340.

Quaak, P., Knoef, H. & Stassen, H. (1999). *Energy from Biomass, A review of combustion and gasification technologies*, Washington DC. USA, World Bank Technical Paper No. 422, Energy Series, 34-38.

Ramli, M. & Rozaine, (1997). An Investigation of Particulate Emissions from Palm Oil Mill Boilers Using Solid Fuel. In the *CTCE'97*, National *Conference on Combustion Technologies for Cleaner Environment*, Kuala Lumpur, July 3.

Rao, T. R. & Ram. Bheemarasetti, J. V. (2001). Minimum fluidization velocity of mixtures of biomass and sands, *Energy*, 26, 633-644.

Rhodes, M (2008). *Introduction to Particle Technology*, 2nd edition, England: John Wiley & Son.

Rowe, P. N. & A.W. Nienow, A. W. (1976). Particle mixing and segregation in gas fluidised beds. A review, *Powder Technology*, 15, 141-147.

Rudolph, V., Rei, M.H. & Lin S.Y. (1985). Horizontally circulating fluid bed for catalytic reaction and regeneration: Transport phenomena in a cold test model, *Proceedings of 4th R.O.C. Symposium on Catalysis and Reaction Engineering*, Kaohsiung, Taiwan, 100.

Sahoo, A., & Roy, G. K. (2007). Artificial neural network approach to segregation characteristic of binary homogeneous mixtures in promoted gas–solid fluidized beds. *Powder Technology*, 171, 54-62.

Salam, F & B.M. Gibbs, B. M. (1987). Solid circulation between fluidized beds using jet pumps, *Powder Technology*, 52, 107-116.

Sathiyamoorthy, D. & Rudolph, V. (1990). Hydrodynamics of Compartmented Dense Phase Circulating Gas Fluidized Bed, *Proceeding of the 3rd International Conference in Circulating Fluidized Beds*, Japan, 505-510.

Scott, A. M & Bridgwater, J. (1975). Interparticle percolation: A fundamental solid mixing mechanism, *Industrial Engineering and Chemical Fundamental*, 14, 22-27.

Shamsuddin, A. H. & Williams, P. T. (1992). Kinetics of devolatilization of oil palm solid waste using thermo-gravimetric analysis, *Jurnal kejuruteraan*, 4, 35-42.

Shen, L. H., Xiao, J., Niklasson, F. & Johnsson, F. (2007). Biomass mixing in a fluidized bed biomass gasifier for hydrogen production, *Chemical Engineering Science*, 62, 636–646.

Shuit, S. H., Tan, K. T., Lee, K. T. & Kamaruddin, A. H. (2009). Oil palm biomass as a sustainable energy source: A Malaysian case study, *Energy*, 34, 1225-1235.

Sulaiman, F., Abdullah, N., Gerhauser, H & Shariff, A. (2011). An outlook of Malaysian energy, oil palm industry and its utilization of wastes as useful resources, *Biomass and Bioenergy*, 35, 3775-3786.

Sun, Q. Q., Lu, H. L., Liu, W. T., He, Y. R., Yang, L. D. & Gidaspow, D. (2005). Simulation and experiment of segregating/mixing of rice husk-sand mixtures in a bubbling fluidized bed, *Fuel*, 84, 1739-1748.

Thonglimp, V., Hiquily, N. & Laguerie, C. (1984). Minimum fluidization velocity and expansion of layers of mixtures of particulates solids fluidized by a gas, *Powder Technol*ogy, 39, 223-239.

Vaid, R. P. & Sen Gupta, P. (1978). Minimum fluidization velocities in beds of mixed solids, *The Canadian Journal of Chemical Engineering*, 56, 292-296.

Waldheim, L. & Nilsson T. (2001). *Heating value of gases from biomass gasification*, IEA Bioenergy agreement, Task 20: Thermal Gasification of Biomass. Retrieved http://128.131.132.12/app/webroot/files/file/publications/HeatingValue.pdf

Wen, C. Y & Yu, Y. H. (1966). A generalized method for predicting the minimum fluidization velocity. *AIChE Journal*, 12, 3, 610-612.

Wee, S. K., Chok, V. S., Srinivasakannan, C., Chua, H. B. & Yan, H. M. (2008). Fluidization quality study in a compartmented fluidized bed gasifier (CFBG), *Energy & Fuels*, 22, 61-66.

Wee, S. K., Chok, V. S., Gorin, A., Chua, H. B. & Yan, H. M. (2009). The effect of effective diameter on fluidization quality in compartmented fluidized bed gasifier, *Pertanika Journal Science & Technology*, 17, 2, 343-350.

Wen, C. Y. & Yu, Y. H. (1966). A generalized method for predicting the minimum fluidization velocity, *AIChE Journal*, 12, 610-612.

Werther, J. (1968). Influence of the bed diameter on the hydrodynamics of gas fluidized beds, *AIChE Symposium Series*, 141, 70, 53-62.

Williams, R. H. & Larson, E. D. (1995). Biomass gasifier gas turbine power generating technology, *Biomass and Bioenergy*, 10, 149-l66.

Wirsum, M., Fett, F., Iwanowa, N. & Lukjanow, G. (2001). Particle mixing in bubbling fluidized beds of binary particle systems, *Powder. Technology*, 120, 63-69.

Wu, S. Y. (1991). Effect of operating temperature on minimum fluidization velocity, *Powder Technology*, 67, 217-220.

Wu, S. Y. & Baeyans, J. (1998). Segregation by size difference in gas fluidized beds, *Powder Technology*, 98, 139-150.

Yan, H. M. (1995), *Development and modelling of coal combustion and gasification in a compartmented fluidised bed gasifier.* (Doctoral dissertation). Department of Chemical Engineering, The University of Queensland, Australia.

Yan, H. M. & Rudolph, V. (1996). A new method for measuring solid circulation rate in compartmented fluidised bed gasifier, *Chemical Engineering Communications*, 147, 133-144.

Yang, H. P, Yan, R., Chin, T., Liang, D. T., Chen, H. P. & Zheng, C. (2004), Thermogravimetric analysis-fourier transform infrared analysis of palm oil waste pyrolysis, *Energy & Fuels*, 18, 1814-182.

Yang, H. P., Yan, R., Chen, H. P., Lee, D. H., Liang, D. T. Liang & Zheng, C. (2006). Pyrolysis of palm oil wastes for enhanced production of hydrogen rich gases, *Fuel Processing Technology*, 87, 935-942.

Yusof, M. R. M. & Rozainee, M. (1993). Particulate emissions from a palm oil mill plant, a case study. *Jurnal Teknologi*, 22, 19-24.

Yusoff, S. (2006). Renewable energy from palm oil- innovation on effective utilization of waste, *Journal of Cleaner Production,* 14, 87-93

Zhang, Y., Jin, B. & Zhong, W. (2008). Fluidization, mixing and segregation of a biomass-sand mixture in a fluidized bed, *International Journal of Chemical Reactor Engineering,* 6, 1-29.

Zhong, W., Jin, B., Zhang, Y, Wang, X. & Xiao, R. (2008). Fluidization of biomass particles in a gas-solid fluidized bed, *Energy & Fuels*, 22, 4170-4176.

TENDER DOCUMENT

(Code Number: 02-99-08-0001-EA 001)

PROCUREMENT, DELIVERY, INSTALLATION, TESTING AND COMMISSIONING

OF

PILOT PLANT EQUIPMENT, INSTRUMENTATIONS AND DATA ACQUISITION SYSTEM

FOR

COMPARTMENTED FLUIDIZED BED GASIFIER

IN

CURTIN UNIVERSITY OF TECHNOLOGY
SARAWAK CAMPUS

Table of Content

List of Tables

List of Figures

1.0 DEFINITIONS

The scope of work as per the tender document 02-99-08-0001-EA 001 can be divided as a Total Package or two sub-packages, which are the Pilot Plant Package and Instrumentation Package. Further subdivision in package will NOT be considered.

Total Package consists of two sub-packages, which are Pilot Plant Package and Instrumentation Package.

Pilot Plant Package generally consists of but not limited to the procurement, delivery, installation, testing and commissioning of the pilot plant equipment, interconnecting piping and ducting, equipment integrated instrumentations and all mechanical, electrical and civil work that are required to necessitate the aforementioned. This also includes mobilization and demobilization of pilot plant equipment as well as mobilization and demobilization tools such as cranes, forklift, sky lift and man power for loading and unloading process as well as consumables that are required to necessitate the aforementioned scope of work.

The Instrumentation Package generally consists of but not limited to the procurement, delivery, installation, testing and commissioning of all the dedicated instrumentations and data acquisition system as well as ALL the electrical work and signal work that are required to necessitate the aforementioned scope of work.

The Main Contractor is a company that is responsible for the scope of work of the Total Package.

The Pilot Plant Sub-Contractor is a company that is responsible for the scope of work of the Pilot Plant Package. In addition, the Pilot Plant Sub-Contractor shall assist in communication and coordination with the Instrumentation Sub-Contractor to ensure that trial assembly can be conducted at the Pilot Plant Sub-Contractor site as well as final assembly can be conducted at the client site.

The Instrumentation Sub-Contractor is a company that is responsible for the scope of work of the Instrumentation Package. In addition, it is the responsibility of the Instrumentation Sub-Contractor to communicate and coordinate with the Pilot Plant Sub-Contractor to ensure that trial assembly can be conducted at the Pilot Plant Sub-Contractor site as well as final assembly can be conducted at the client site.

ALL installation, testing and commissioning MUST be done in the compound of Curtin Sarawak Miri (CSM) Campus. ALL testing and commissioning MUST be based on the operating conditions which includes operating temperature, pressure, flow rate and fluid medium whichever applicable and to be verified and endorsed by the client.

Final payment will ONLY be released AFTER all pilot plant equipment, instrumentations and data acquisition system as per the Pilot Plant Package and Instrumentation Package satisfy ALL testing and commissioning requirements.

2.0 PROCESS DESCRIPTION

Figure 1 shows the process flow diagram of CFBG process. Detailed process description is illustrated as below.

Air, Stream 1 is compressed by air compressor (C-101) and regulated to 1 barg at ambient temperature. It is (Stream 2) then preheated by electrical heater (E-102) in order to obtain preheated air at 1 barg and 600 ^{o}C. Before entering the compartmented reactor (R-101), the preheated air, Stream 3 is splitted to Stream 4, Stream 5 and Stream 6: Stream 4 flows into the combustion compartment of R-101, whereas Stream 5 and Stream 6 flow into the v-valve and riser of the combustion compartment of R-101.

On the other hand, soft water is pumped from water tank (V-101) to electrical boiler (E-101). The steam produced by E-101 is at 7 barg but regulated to 1 barg at saturated condition. It is (Stream 9) then heated up in the steam superheater (E-103) in order to obtain superheated steam at 250 ^{o}C and 1 barg. The superheated steam, Stream 10 from E-103 is branched into Stream 11, Stream 12 and Stream 13: Stream 11 is fed into the

gasification compartment of R-101, while Stream 12 and Stream 13 are fed into the v-valve and riser of the gasification compartment of R-101.

In addition, palm shell, Stream 15, is fed into R-101 through a hopper (H-101) and a water-jacketed screw feeder (SC-101) T 15-20 kg/hr. As the auto-ignition temperature of palm shell is believed to be lower than 600^{o}C, it will self-ignite in R-101 without implementation of any electrical heater on R-101.

In R-101, combustion process and gasification process takes place in combustion compartment and gasification compartment of R-101 respectively. The operating temperature of the combustor is 900°C and the complete combustion process can be represented by equation below:

$$C + O_2 \rightarrow CO_2 \text{ ----------(1)}$$

However, incomplete combustion might occur due to insufficient amount of oxygen. Equation (2) below shows the incomplete combustion reaction:

$$C + \tfrac{1}{2} O_2 \rightarrow CO \text{ ----------(2)}$$

Heat generated by incomplete combustion is less than the heat generated by complete combustion; hence it is a must to ensure complete combustion in R-101 by providing 10% of excess air.

The heat evolved from the combustion process is transferred to the endothermic gasification process by sand. The operating temperature is 850^{o}C and the main reaction occurred in the gasification compartment of R-101 can be represented by equation below:

$$C + H_2O \rightarrow H_2 + CO \text{ ----------(3)}$$

From Equation (3), it can be seen that the products from gasification compartment is H_2 and CO. Mixture of H_2 and CO is called synthesis gas or syngas. In reality, syngas is not the only product produced, pyrolysis will also take place and this process releases

the volatile components of palm shells at a temperature below 600°C via a set of complex reactions. The volatile vapors consist of hydrocarbon gases, hydrogen, carbon monoxide, carbon dioxide, tar and water vapor. Hydrogen sulphide is also one of the side products that are produced from R-101.

Both flue gas, Stream 7 and syngas, Stream 14 will pass through cyclones (CY-101 and CY-102) and the solids removed will be collected in the water sealer tank (W-101 and W -102). Gas sampling lines will be connected from the flue gas and syngas respectively for gas analysis purposes. The flue gas and syngas, which is free of solids, is then cooled and directed to flue stack (FS-101) before emitted to atmosphere.

Detailed process conditions for each stream are shown in Table 1.

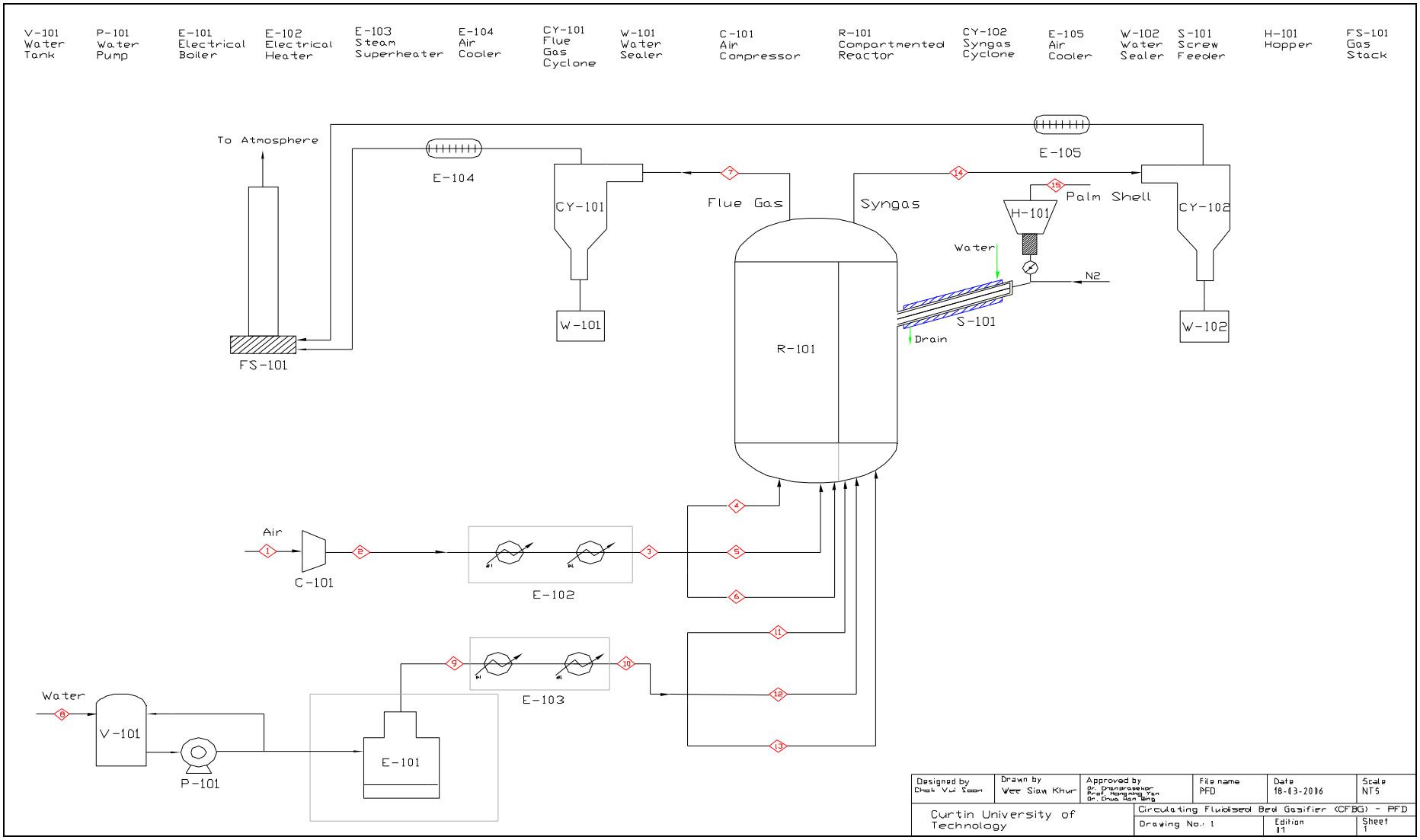

Figure 1: CFBG Process Flow Diagram (PFD); 1: air, 2: compressed air, 3: preheated air, 4: air to combustion compartment, 5: air to v-valve of combustion compartment, 6: air to riser of combustion compartment, 7: flue gas, 8: boiler feed water, 9: saturated steam, 10: superheated steam, 11: steam to gasification compartment, 12: steam to v-valve of gasification compartment, 13: steam to riser of gasification compartment, 14: syngas, 15: palm shell.

Table 1: Simulation Data Obtained from HYSYS

Stream	1	2	3	4	5	6	7	8	9	10	11	12	13	14	15
Vapor Fraction	1	1	1	1	1	1	1	0	1	1	1	1	1	1	0
Temperature (K)	298-303	298-303	473-873	473-873	473-873	473-873	1073-1173	298-303	393.5	473-523	473-523	473-523	473-523	1023-1123	298-303
Pressure (kPag)	0	100	100	100	100	100	100	0	100	100	100	100	100	100	100
Mole Flow (kmol/hr)	2.0-5.1	2.0-5.1	2.0-5.1	1.6-4.3	0.3-0.4	0.3-0.4	2.0-4.7	1.0-2.8	1.0-2.8	1.0-2.8	0.8-2.2	0.2-0.3	0.2-0.3	1.1-2.6	-
Mass Flow (kg/hr)	55-146	55-146	55-146	46-125	9.0-10.0	11.0-12.0	60-140	20-50	20-50	20-50	15-40	4.0-5.0	4.0-5.0	20-45	15-20
Vol. Flow (Nm^3/hr)	45-120	45-120	45-120	38-102	7.0-8.0	9.0-10.0	46-110	26-66	26-66	26-66	20-53	5.0-7.0	5.0-7.0	27-62	-
Component Mole Flow															
Carbon	0	0	0	0	0	0	0	0	0	0	0	0	0	0	0
Oxygen	0.21	0.21	0.21	0.21	0.21	0.21	0.16	0	0	0	0	0	0	0	0
CO_2	0	0	0	0	0	0	0.05	0	0	0	0	0	0	0	0
H_2O	0	0	0	0	0	0	0	1	1	1	1	1	1	0.79	0
CO	0	0	0	0	0	0	0	0	0	0	0	0	0	0.1	0
Hydrogen	0	0	0	0	0	0	0	0	0	0	0	0	0	0.1	0
Nitrogen	0.79	0.79	0.79	0.79	0.79	0.79	0.79	0	0	0	0	0	0	0	0
Palm Shell	0	0	0	0	0	0	0	0	0	0	0	0	0	0	1

3.0 TOTAL PACKAGE

Total Package consists of two sub-packages, which are Pilot Plant Package and Instrumentation Package.

Pilot Plant Package is defined in 4.0 Pilot Plant Package while the Instrumentation Package is defined in 5.0 Instrumentation Package.

The Main Contractor is a company that is responsible for the scope of work of the Total Package.

The Main Contractor is required to supply pilot plant equipment according to the specification listed in 4.1 Equipment Specifications and the interconnecting piping and ducting according to the specification listed in 4.2 Piping And Ducting Specifications.

In addition, the Main Contractor is also required to supply instrumentation according to the specification listed in 5.1 Instrumentation Specifications and data acquisition system according to the specification listed in 5.2 Data Acquisition System Specifications.

4.0 PILOT PLANT PACKAGE

Pilot Plant Package generally consists of but not limited to the procurement, delivery, installation, testing and commissioning of the pilot plant equipment and interconnecting piping and ducting and equipment integrated instrumentations as well as ALL mechanical, electrical and civil work that are required to necessitate the aforementioned.

ALL mechanical work includes but not limited to skids, pilot plant equipment support structure, piping and ducting support structure as well as insulations with aluminum cladding.

ALL electrical work includes but not limited to equipment and piping specific instrumentations, equipment and instrumentations power panels as well as electrical and signal wiring.

ALL civil work includes but not limited to drainage, base and base mounting.

In addition, ALL installation, testing and commissioning MUST be done in the compound of Curtin Sarawak Miri (CSM) Campus.

The installation part includes mobilization and demobilization of pilot plant equipment, interconnecting piping and ducting as well as mobilization and demobilization tools such as cranes, forklift, sky lift and man power as well as consumables that are required to necessitate the aforementioned scope of work.

The testing and commissioning part includes mobilization and demobilization testing and commissioning equipment such as cranes, forklift, sky lift and manpower as well as consumables that are required to necessitate the aforementioned scope of work.

ALL testing and commissioning MUST be based on the operating conditions which includes operating temperature, pressure, flow rate and fluid medium whichever applicable and to be verified and endorsed by the client.

Pilot Plant Sub-Contractor is responsible for the scope of work in the Pilot Plant Package. Pilot Plant Sub-Contractor is required to provide ALL the equipment fabrication drawings and to be verified and endorsed by the client EXCEPT for Reactor (Compartmented Fluidized Bed Gasifier).

Pilot Plant Sub-Contractor is required to supply pilot plant equipment according to the specification listed in 4.1 Equipment Specifications and the interconnecting piping and ducting according to the specification listed in 4.2 Piping and Ducting Specifications.

However, the Pilot Plant Sub-Contractor shall assist in communication and coordination with the Instrumentation Sub-Contractor to ensure that trial assembly can be conducted at the Pilot Plant Sub-Contractor site as well as final assembly can be conducted at the client site.

In addition, the Pilot Plant Sub-Contractor is required to supply the mechanical works on piping and ducting for the installation of instrumentations and data acquisition system as well as materials which includes but not limited to cutting, welding, flanges, gaskets, plugs, reducers, space allowance, instrumentations and data acquisition system support structure in order to assist the Instrumentation Sub-Contractor in executing their scope of work at both trial and final assembly.

Final payment will ONLY be released AFTER all pilot plant equipment, instrumentations and data acquisition system as per the Pilot Plant Package and Instrumentation Package satisfy ALL testing and commissioning requirements.

4.1 Equipment Specifications

Equipment specifications as shown in Table 2 lists down all the major and minor equipment with the preferred types, operating conditions, material selections, dimensions, auxiliaries, fabrication methods, insulations and consumables.

Table 2: Equipment Summary

No	Items	Specification	Quantity
1	Feeder	Type: Screw (With Water Jacketed Cooler) Function: Palm Shell Feeder Solid: Palm Shell Capacity: 15-50 kg/hr Pressure: 1-2 Barg Operating Temperature: 30-100 ^{o}C Material of Construction: Stainless Steel 304 Joint Preparation: Electrical Arc Welded Surface Preparation: Chemical Cleaned on Welded Surfaces Paintwork: - End Connection: Flanged Insulation: Required Remarks: (i) Feed Flowrate Calibration is to be Included. (ii) Water Jacketed Cooler is a Double Pipe Heat Exchanger. (iii) Water Jacketed Cooler Must be Located Closest Possible to the Palm Shell Feed Inlet. (iv) Water Jacketed Cooler Must be able to Maintain Screw Feeder Surface Temperature < 100 ^{o}C. (v) Equipment Power Panel (Eq-03) is to be included. (vi) Instrumentation Power Panel (Inst-03) is under the Instrumentation Supplier Scope of Work. (vii) Wiring between Eq-03 and Inst-03 to Feeder is to be Included.	1
2	Hopper	Type: Square Top Reducing Taper Gear or Equivalent Function: Palm Shell Storage to Feeder Solid: Palm Shell (Approx. 1.2 cm diameter) Capacity: 60 kg Pressure: Ambient Operating Temperature: Ambient Material of Construction: Galvanized Steel Joint Preparation: Electrical Arc Welded Surface Preparation: Copper Wire Brushed on Welded Surface Paintwork: Required End Connection: Flanged Insulation: -	1

3	Reactor	Type: Compartmented Fluidized Bed Gasifier Function: Combustion and Gasification Solid: Palm Shell, Sand, Char, Ash Fluid: Steam, Air Pressure: 1-2 Barg Operating Temperature: 850-1000 ^{o}C Material of Construction: Stainless Steel 316 Joint Preparation: TIG Welding for H2 environment Surface Preparation: Chemical Cleaned on Welded Surfaces Paintwork: - End Connection: Flanged Insulation: Double Layer External Insulations Remarks: (i) Mechanical Design Drawing is Provided (ii) All Mountings and Support Structure are to be Included. (iii) J3000 Reinforced Graphite Gasket or Equivalent High Temperature Gasket are to be Included.	1
4	Electrical Boiler	Type: Fulton or Simon or Equivalent Function: Steam Feedstock Solid: - Fluid: Soft Water Capacity: 20 – 50 kg/hr Pressure: 7 Barg Operating Temperature: Inlet Temperature, 25 ^{o}C Material of Construction: - Joint Preparation: - Surface Preparation: - Paintwork: - End Connection: Flanged Insulation: Required Remarks: (i) Automated Pressure Control, Water Level and Feed Water Control is to be Included. (ii) Equipment Power Panel (Eq-01) and Instrumentation Power Panel (Inst-01) is to be Included. (iii) Wiring between Item 4 to Eq-01 and Inst-01 is to be Included. (iv) To be Integrated with Item 5, 6, 7, 8 and 9 as a Complete Boiler Package with Integrated Piping. (v) Boiler Operation Training is Required. (vi) JKKP Certification is Required.	1

5	Water Softening	Type: Resin for Ions Exchange or Equivalent Function: To Provide Soft Water for item 4 Solid: - Fluid: Raw Water (Jabatan Bekalan Air) Capacity: 0.05 m^3/hr (Operates > 4000 hours Before Regeneration) Pressure: 2 Barg Operating Temperature: Ambient Material of Construction: To Suit Boiler Requirement Joint Preparation: To Suit Boiler Requirement Surface Preparation: To Suit Boiler Requirement Paintwork: To Suit Boiler Requirement End Connection: To Suit Boiler Requirement Insulation: To Suit Boiler Requirement Remarks: (i) To be Integrated with Item 4,6,7 and 8. (ii) Regeneration Training is Required.	1
6	Pump	Type: Centrifugal Function: Boiler Feed Water Pump Solid: - Fluid: Soft Water Pressure: > 10 Barg (To Suit Boiler Requirement) Capacity: 20 – 50 kg/hr Operating Temperature: Ambient Material of Construction: To Suit Boiler Requirement Joint Preparation: To Suit Boiler Requirement Surface Preparation: To Suit Boiler Requirement Paintwork: To Suit Boiler Requirement End Connection: To Suit Boiler Requirement Insulation: To Suit Boiler Requirement Remarks: (i) To be Integrated with Item 4,5,7,8 and 9.	1

7	Pump	Type: Positive Displacement (With Chemical Tanks) Function: Chemicals Dosing Pump Solid: - Fluid: Chemicals Pressure: To Suit Boiler Requirement Capacity: To Suit Boiler Requirement Operating Temperature: Ambient Material of Construction: To Suit Boiler Requirement Joint Preparation: To Suit Boiler Requirement Surface Preparation: To Suit Boiler Requirement Paintwork: To Suit Boiler Requirement End Connection: To Suit Boiler Requirement Insulation: To Suit Boiler Requirement Remarks: (i) To be Integrated with Item 4,5,6, 8 and 9. (ii) Chemicals, which are O_2 Scavenger, pH Booster and Discaler are to be Included for > 4000 Hours of Boiler Full Operation. (iii) 3 Chemical Tanks are to be Included.	3
8	Water Tank	Type: Galvanized Steel or Polymer Function: Boiler Feed Water Tank Solid: - Fluid: Water Pressure: To Suit Boiler Requirement Capacity: > 0.2 m^3 Operating Temperature: To Suit Boiler Requirement Material of Construction: To Suit Boiler Requirement Joint Preparation: To Suit Boiler Requirement Surface Preparation: To Suit Boiler Requirement Paintwork: To Suit Boiler Requirement End Connection: To Suit Boiler Requirement Insulation: To Suit Boiler Requirement Remarks: (i) To be Integrated with Item 4,5,6,7 and 9.	1
9	Blowdown Tank	Type: Galvanized Steel or Equivalent Function: Blowdown Receiver Tank Solid: - Fluid: Saturated Water Pressure: To Suit Boiler Requirement Capacity: To Suit Boiler Requirement Operating Temperature: To Suit Boiler Requirement Material of Construction: To Suit Boiler Requirement Joint Preparation: To Suit Boiler Requirement Surface Preparation: To Suit Boiler Requirement Paintwork: To Suit Boiler Requirement End Connection: To Suit Boiler Requirement Insulation: To Suit Boiler Requirement Remarks: (i) To be Integrated with Item 4,5,6,7 and 8.	1

10	Air Preheater	Type: Sylvania or Direct Heating Fin Coil or Equivalent Function: Preheating Feed Air Solid: - Fluid: Compressed Air (25 ^{o}C) Pressure: 2 Barg (Inlet) Capacity: > 210 Nm^3/hr (3500 l/min) Operating Temperature: 200-600 ^{o}C Material of Construction: Stainless Steel 304 Joint Preparation: Electrical Arc Welded Surface Preparation: Chemical Cleaned on Welded Surfaces Paintwork: - End Connection: Flanged Insulation: Required Remarks: (i) Two Internal Thermocouples for Temperature Control and Safeguard. (ii) Equipment Power Panel (Eq-02) and Instrumentation Power Panel (Inst-02) is to be Included. (iii) Wiring between Item 11 to Eq-02 and Inst-02 is to be Included. (iv) The electrical power and instrumentation wiring for TI208 and TI124 to Inst-02 is to be under Instrumentation Supplier Scope of Work.	1
11	Steam Superheater	Type: Electrical Direct Heating or Conduction or Equivalent Function: Superheating Feed Steam Solid: - Fluid: Saturated Steam Pressure: 2 Barg (Inlet) Capacity: 20 – 50 kg/hr Operating Temperature: 250 ^{o}C Material of Construction: Stainless Steel 304 Joint Preparation: Electrical Arc Welded Surface Preparation: Chemical Cleaned on Welded Surfaces Paintwork: - End Connection: Flanged Insulation: Required Remarks: (i) Two Internal Thermocouples for Temperature Control and Safeguard. (ii) Equipment Power Panel (Eq-02) and Instrumentation Power Panel (Inst-02) is to be Included (iii) Wiring between Item 12 to Eq-02 and Inst-02 is to be Included.	1

12	Cyclone	Type: Vortex Flow or Equivalent Function: Particulate-Gas Separation Fluid: Syngas (H_2, CO) with CH_4, H_2O (g), Air and Flue Gas Solid: Sand, Palm Shell, Char, Ash Pressure: 2 Barg (Inlet) Capacity: 62 Nm^3/hr (Syngas) and 110 Nm^3/hr (Flue Gas) Operating Temperature: 800-900 ^oC Material of Construction: Stainless Steel 304 Joint Preparation: Electrical Arc Welded Surface Preparation: Chemical Cleaned on Welded Surfaces Paintwork: - End Connection: Flanged Insulation: Required Remarks: (i) Mechanical Design Drawings will be Provided. (ii) All Mounting and Supporting Structure are to be Included.	2
13	Water Sealer	Type: Rectangular or Cylindrical Water Container Function: Collect Solids from Cyclones Fluid: Water Solid: Sand, palm shell, char, ash Pressure: 2 Barg (Inlet) Capacity: > 0.04 m^3 Operating Temperature: 800-900 ^oC Material of Construction: Stainless Steel 304 Joint Preparation: Electrical Arc Welded Surface Preparation: Chemical Cleaned on Welded Surfaces Paintwork: High Temperature Paint End Connection: Flanged Insulation: Required	2
14	Ambient Air Cooler	Type: Longitudinal Fins (4 on each cooler) Function: Air Cooler Fluid: Syngas and Flue Gas Solid: - Pressure: Ambient Capacity: - Operating Temperature: 800-900 ^oC Material of Construction: Stainless Steel 304 Joint Preparation: Electrical Arc Welded Surface Preparation: Chemical Cleaned on Welded Surfaces Paintwork: - End Connection: Welded Insulation: - Remarks: (i) Ambient Air Cooler Must be Located Closest Possible to the Cyclone Outlet. (ii) Minimum Fin Length = 3.0 m (iii) Minimum Fin Width = 0.15 m	2

15	Flue Stack	Type: Carbon Steel SS400 Function: Venting Stack Fluid: Syngas and Flue Gas Combined Solid: - Pressure: 2 Barg (Inlet) Capacity: > 700 actual m^3/hr Operating Temperature: 400-600 ^oC Material of Construction: Carbon Steel SS 400 Joint Preparation: Electrical Arc Welded Surface Preparation: Copper Wire Brushed on Welded Surface Paintwork: - End Connection: Flanged Insulation: Required Remarks: (i) Minimum Height = 10 m From Ground. (ii) Minimum Diameter = 250 mm.	1

4.2 Piping and Ducting Specifications

Piping and Ducting Specifications includes all the piping and ducting material selections, sizing and interconnections with pilot plant equipment and instrumentations as shown in Figure 2.

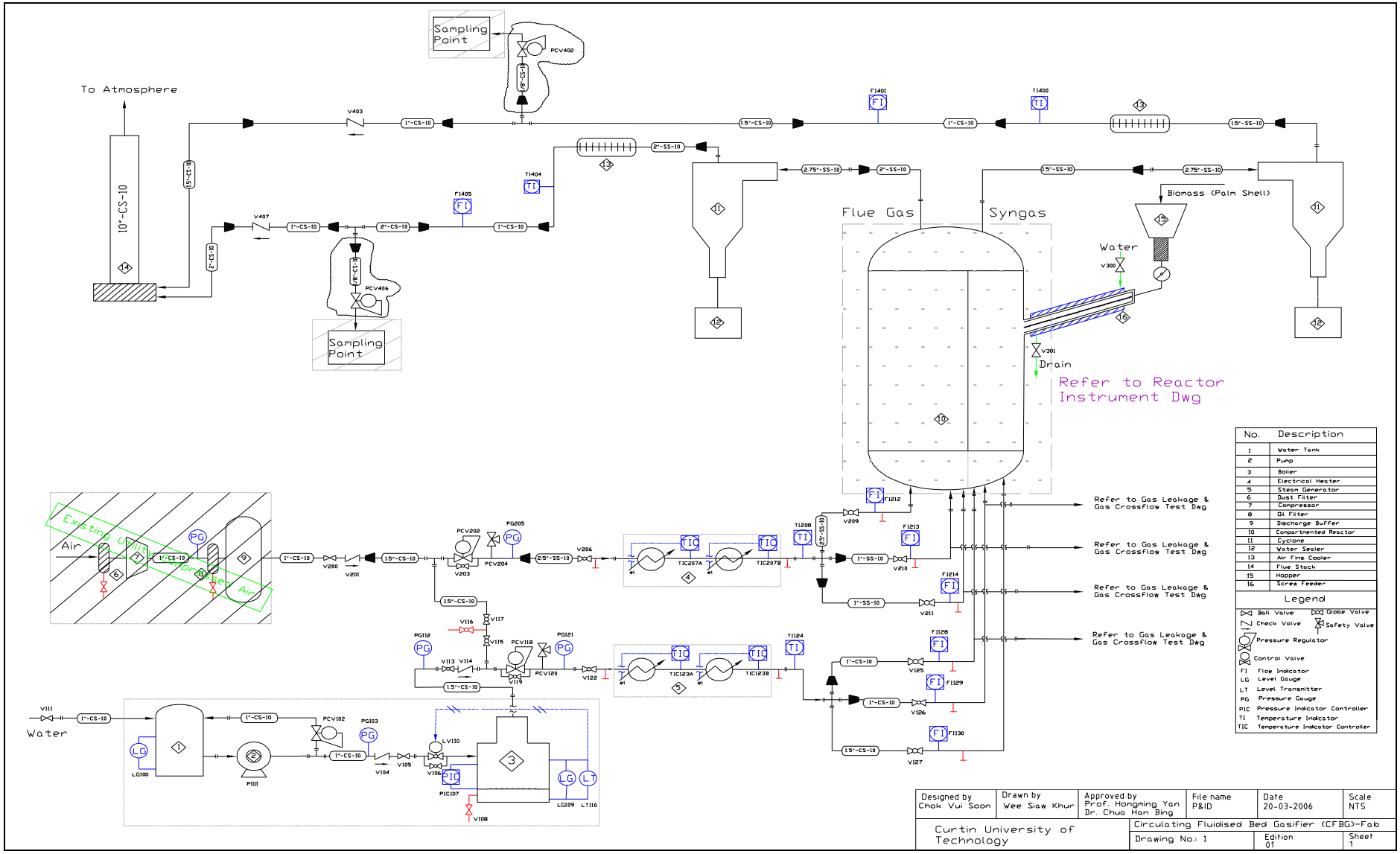

Figure 2: CFBG Process & Instrumentations Diagram (P&ID)

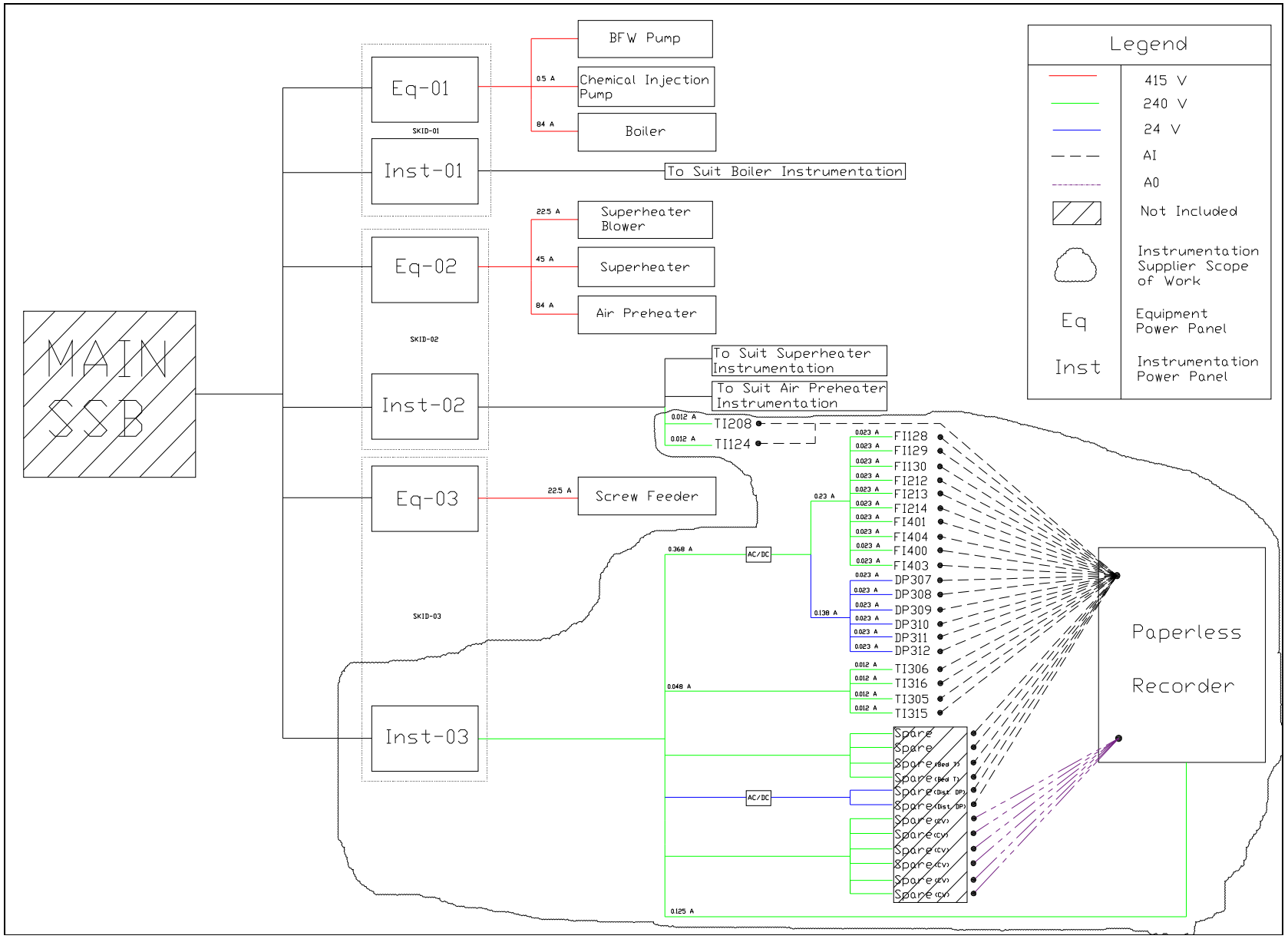

Figure 3: CFBG Electrical Drawing

NOTE: ALL pilot plant equipment electrical power and signal cablings MUST follow as specified in Figure 3 (unclouded zone).

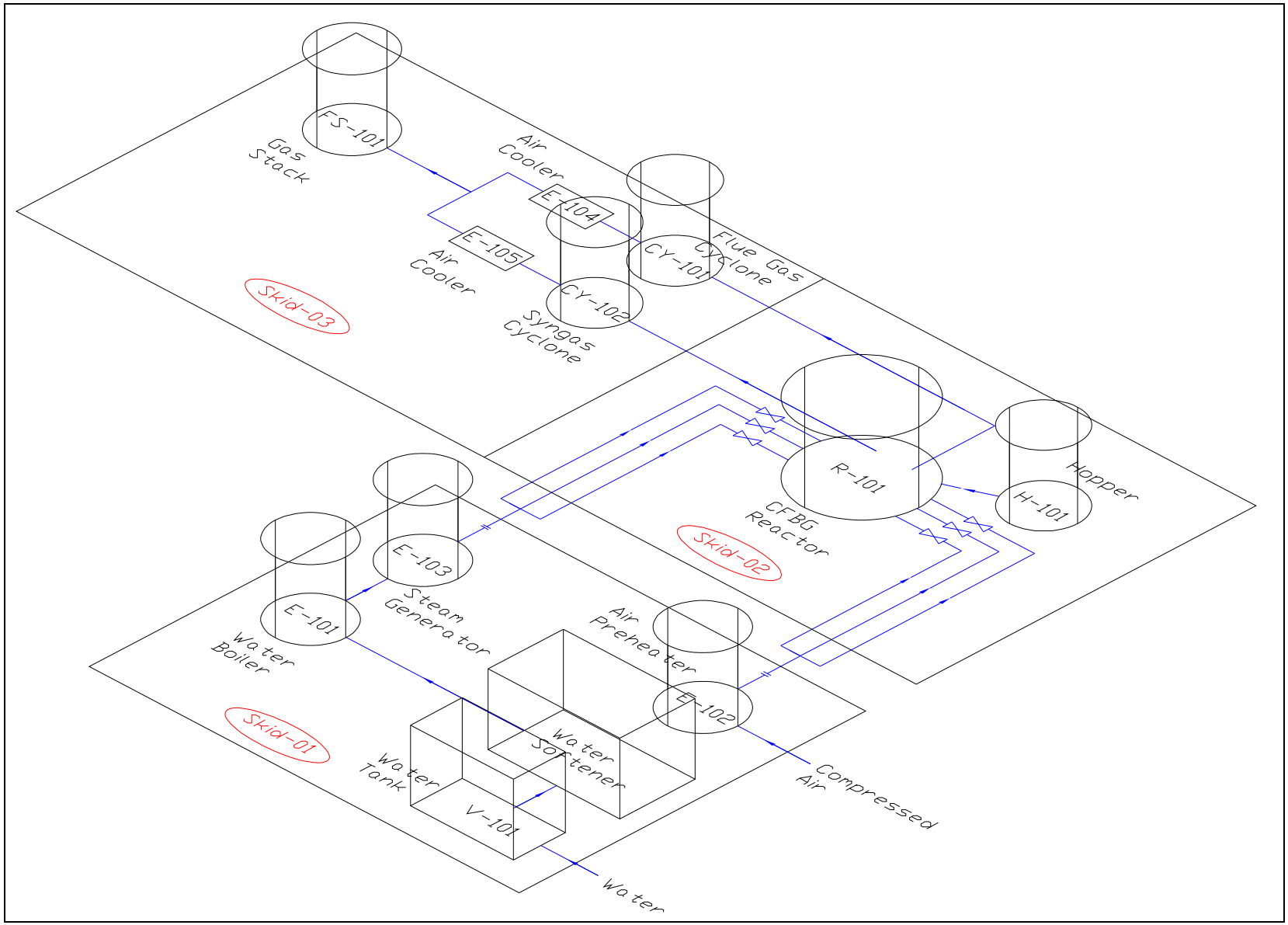

Figure 4: CFBG Pilot Plant Equipment Layout

NOTE: ALL pilot plant equipment MUST orient within THREE (3) skids as specified in Figure 4.

5.0 INSTRUMENTATION PACKAGE

Instrumentation Package generally consists of but not limited to the procurement, delivery, installation, testing and commissioning of the dedicated instrumentations and data acquisition system as well as ALL electrical and signal work that are required to necessitate the aforementioned.

ALL electrical work includes but not limited to electrical power cabling for instrumentations and data acquisition system.

ALL signal work includes but not limited to signal cabling from instrumentations to the data acquisition system.

ALL mechanical and civil work are EXCLUDED from Instrumentation Package

In addition, ALL installation, testing and commissioning MUST be done in the compound of Curtin Sarawak Miri (CSM) Campus.

ALL testing and commissioning MUST be based on the operating conditions which includes operating temperature, pressure, flow rate and fluid medium whichever applicable and to be verified and endorsed by the client.

Instrumentation Sub-Contractor is responsible for the scope of work in the Instrumentation Package.

Instrumentation Sub-Contractor is required to provide ALL the instrumentations and data acquisition system specification sheets, instrumentations and data acquisition outline and interconnection diagrams, and to be verified and endorsed by the client.

Instrumentation Sub-Contractor is required to supply instrumentations according to the specification listed in 5.1 Instrumentation Specifications and the data acquisition system according to the specification listed in 5.2 Data Acquisition System Specifications.

However, the Instrumentation Sub-Contractor is responsible in communicating and coordinating with the Pilot Plant Sub-Contractor to ensure that trial assembly can be conducted at the Pilot Plant Sub-Contractor site as well as final assembly can be conducted at the client site.

Final payment will ONLY be released AFTER all pilot plant equipment, instrumentations and data acquisition system as per the Pilot Plant Package and Instrumentation Package satisfy ALL testing and commissioning requirements.

5.1 Instrumentation Specifications

Instrumentation Specifications includes all the instrumentations fluid medium, tagging, sizing, operating conditions, desired range and quantity as shown in Table 3 and Table 4. Please refer Figure 2-3 and Figure 5 for detailed pilot plant and reactor instrumentation locations respectively.

Table 3: Instrumentation Specifications (Pilot Plant)

No	Items	Medium/Phase	Tag	Line Size	Operating Condition	Desired Range	Quantity
	Manual Valves:						
1	Globe Valve	Steam	V113 V119 V122	1.5"	<10 Barg ; <150 °C	-	3
		Steam (V-valve/Riser)	V125 V126	1"	<2 Barg ; <250 °C	-	2
		Steam (Main)	V127	1.5"	<2 Barg ; <250 °C	-	1
		Steam/Air (Bypass)	V115 V116 V117	1.5"	<10 Barg ; <150 °C	-	3
		Air	V200	1"	<10 Barg ; 25 °C		1
		Air (V-valve/Riser)	V210 V211	1"	<2 Barg ; 600 °C	-	2
		Air (Main)	V209	2.5"	<2 Barg ; 600 °C		1
		Air	V203	1.5"	<10 Barg ;150 °C	-	1
		Air	V206	2.5"	<2 Barg ; 150 °C	-	1
						Subtotal	15
2	Check Valve	Steam	V114	1.5"	<10 Barg ; 150 °C	-	1
		Air	V201	1"	<10 Barg ; 150°C	-	1
		Flue Gas	V405	1"	<2 Barg ; 600 °C	-	1
		Syngas	V402	1"	<2 Barg ; 600°C	-	1
						Subtotal	4

	Regulator:						
3	Pressure Regulator	Steam	PCV118	1.5"	2 Barg ; 150 °C	0-5 Barg	1
		Air	PCV202	1.5"	2 Barg ; 150 °C	0-5 Barg	1
						Subtotal	2
	Gauges:						
4	Pressure Gauge	Steam	PG112	1.5"	5 Barg ; 150 °C	0-10 Barg	1
		Steam	PG121	1.5"	2 Barg ; 150 °C	0-5 Barg	1
		Air	PG205	1.5"	2 Barg ; 150 °C	0-5 Barg	1
						Subtotal	3
5	Flow Indicator (Element)	Preheated Air (Riser)	FI214	1"	2 Barg ; 600 °C ; 10 Nm^3/hr	-	1
		Preheated Air (Main Bed)	FI212	2.5"	2 Barg ; 600 °C ; 126 Nm^3/hr	-	1
		Flue gas	FI404	1"	<2 Barg ; 600 °C ; 110 Nm^3/hr	-	1
		Syngas	FI401	1"	<2 Barg ; 600 °C ; 62 Nm^3/hr	-	1
						Subtotal	4
6	Temperature Indicator (Element)	Superheated Steam	TI124	1.5"	<2 Barg ; 250 °C	0-500 °C	1
		Preheated Air	TI208	2.5"	<2 Barg ; 600 °C	0-1000 °C	1
		Flue Gas	TI403	1"	<2 Barg ; 600 °C	0-1000 °C	1
		Syngas	TI400	1"	<2 Barg ; 600 °C	0-1000 °C	1
						Subtotal	4
	Others:						
7	Safety Valve	Steam	PCV120	1.5"	2.2 Barg ; 150 °C ; 60 act m^3/hr ; 50 kg/hr	0-5 Barg	1
		Air	PCV204	1.5"	2.2 Barg ; 150 °C ; 144 Nm^3/hr ;	0-5 Barg	1
						Subtotal	2
	Transmitter						
8	Flow Indicator (Element)	Superheated Steam (V-valve)	FI128	1"	2 Barg ; 250 °C ; 6 act m^3/hr ; 5 kg/hr	-	1
		Superheated Steam (Riser)	FI129	1"	2 Barg ; 250 °C ; 6 act m^3/hr ; 5 kg/hr	-	1
		Superheated Steam (Main)	FI130	1.5"	2 Barg ; 250 °C ; 48 act m^3/hr ; 40 kg/hr	-	1
		Preheated Air (V-valve)	FI213	1"	2 Barg ; 600 °C ; 8 Nm^3/hr	-	1
						Subtotal	4

Table 4: Instrumentation Specifications (Reactor)

No	Items	Medium/Phase	Tag	Line Size	Operating Condition	Desired Range	Quantity
	Manual Valves:						
9	Globe Valve	Combustor	V313	1"	2 barg ; 900 ^{o}C	-	1
		Gasifier	V314	1"	2 barg ; 900 ^{o}C	-	1
		Cooling Water (In)	V300	1"	1 barg ; 60 ^{o}C		1
		Cooling Water (Out)	V301	1"	1 barg ; 60 ^{o}C		1
						Subtotal	4
	Gauges:						
10	Pressure Gauge	Combustor	PG303 PG317	1"	2 Barg ; 600 ^{o}C	0-2 Barg	2
		Gasifier	PG304 PG318	1"	2 Barg ; 900 ^{o}C	0-2 Barg	2
						Subtotal	4
	Others:						
11	Safety Valve	Combustor	PCV319	1.5"	2.2 Barg ; 900 ^{o}C ; 110 Nm^{3}/hr	0-5 Barg	1
		Gasifier	PCV320	1.5"	2.2 Barg ; 900 ^{o}C ; 62 Nm^{3}/hr	0-5 Barg	1
						Subtotal	2
	Transmitter:						
12	Temp Indicator (Element)	Combustor	TI305 TI315	1"	2 Barg ; 900^{o}C		2
		Gasifier	TI306 TI316	1"	2 Barg ; 900 ^{o}C		2
						Subtotal	4
13	DP Indicator (Element)	Combustor/Gasifier	DP307 DP308	1"	2 Barg ; 900^{o}C ; Min Detection 500 Pa	0-5000Pa	2
		V-valves/Risers	DP309 DP310 DP311 DP312	1/4"	2 Barg ; 900 ^{o}C ; Min Detection 100 Pa	0-2000	4
						Subtotal	6

NOTE: ALL instrumentations listed in Table 3 and Table 4 MUST be metal-tagged.

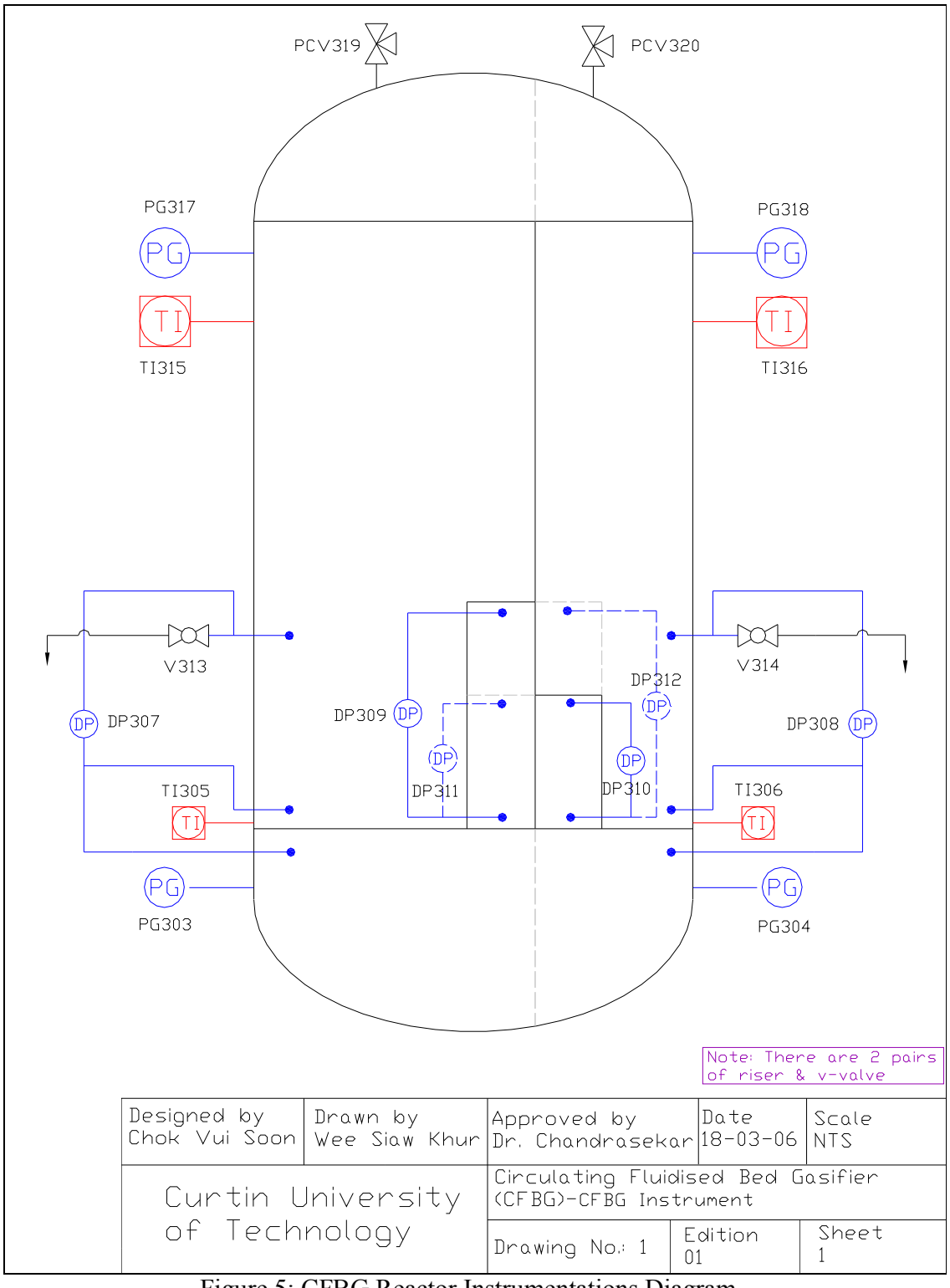

Figure 5: CFBG Reactor Instrumentations Diagram

5.2 Data Acquisition System Specifications

Data Acquisition System Specifications includes display resolution, maximum analog and digital input and output channels, graphical and statistical display formats, power input, internal memory and computer communication capability as shown in VR18 Paperless Recorder Specifications.

The client preferred data acquisition system is Brainchild VR-18 Paperless Recorder with 15 channels (quantity of 2) or equivalent.